

**NEW SAMPLING AND DETECTION APPROACHES
FOR COMPRESSED SENSING AND THEIR
APPLICATION TO ULTRA WIDEBAND
COMMUNICATIONS**

by

Zhongmin Wang

A dissertation submitted to the Faculty of the University of Delaware in partial fulfillment of the requirements for the degree of Doctor of Philosophy in Electrical and Computer Engineering

January, 2010

© 2010 Zhongmin Wang
All Rights Reserved

**NEW SAMPLING AND DETECTION APPROACHES
FOR COMPRESSED SENSING AND THEIR
APPLICATION TO ULTRA WIDEBAND
COMMUNICATIONS**

by

Zhongmin Wang

Approved: _____

Kenneth E. Barner, Ph.D.

Chair of the Department of Electrical and Computer Engineering

Approved: _____

Michael J. Chajes, Ph.D.

Dean of the College of Engineering of the University of Delaware

Approved: _____

Debra Hess Norris, M.S.

Vice Provost for Graduate and Professional Education

I certify that I have read this dissertation and that in my opinion it meets the academic and professional standard required by the University as a dissertation for the degree of Doctor of Philosophy.

Signed: _____

Gonzalo R. Arce, Ph.D.
Professor in charge of dissertation

I certify that I have read this dissertation and that in my opinion it meets the academic and professional standard required by the University as a dissertation for the degree of Doctor of Philosophy.

Signed: _____

Javier Garcia-Frias, Ph.D.
Member of dissertation committee

I certify that I have read this dissertation and that in my opinion it meets the academic and professional standard required by the University as a dissertation for the degree of Doctor of Philosophy.

Signed: _____

Jose L. Paredes, Ph.D.
Member of dissertation committee

I certify that I have read this dissertation and that in my opinion it meets the academic and professional standard required by the University as a dissertation for the degree of Doctor of Philosophy.

Signed: _____

Brian M. Sadler, Ph.D.
Member of dissertation committee

I certify that I have read this dissertation and that in my opinion it meets the academic and professional standard required by the University as a dissertation for the degree of Doctor of Philosophy.

Signed: _____

Xianggen Xia, Ph.D.
Member of dissertation committee

ACKNOWLEDGEMENTS

First and foremost I would like to thank my Ph.D advisor, Dr. Gonzalo R. Arce, for his guidance and support throughout my Ph.D program. His wealth of ideas, clarity of thought, enthusiasm and energy have made working with him an exceptional experience for me. I am grateful to my thesis committee members, Dr. Brian M. Sadler, Dr Jose L. Paredes, Dr Javier Garcia-Frias and Dr Xianggen Xia, for giving me valuable feedback and supports. I would also like to thank Dr Sebastian Hoyos, Dr. Kenneth E. Barner, Dr Giovanni D. Crescenzo, Dr. Xiaoming Li and Dr Takashi Buma for their academic support. Financial support for my research in part through collaborative participation in the Communications and Networks Consortium sponsored by the U. S. Army Research Laboratory under the Collaborative Technology Alliance Program, Cooperative Agreement DAAD19-1-2-0011, and in part by the National Science Foundation (NSF) under EECS-0725422 and CIF-0915800 is also gratefully acknowledged.

I would like to thank my wife, Hong Xu, my daughter, Gloria, and my parents, my brother and sisters for their support and encouragement during my studies. My special thanks go to my colleagues Dr. Jan Bacca Rodríguez, Dr. Lu Zhang, Dr InKoo Kang, Dr Yu Yuan, Dr. Bo Gui, Dr. Xu Ma, Dr. Peng Wang, Ms. Peng Ye, Mr. Xiantao Sun, Mr. Yuehao Hu and many others for their fruitful discussion and suggestions, and for creating a nice working environment.

I dedicate this thesis to my family and to my friends in my life.

TABLE OF CONTENTS

| | |
|----------------------------------|-------------|
| LIST OF FIGURES | viii |
| LIST OF TABLES | xi |
| ABSTRACT | xii |

Chapter

| | |
|---|-----------|
| 1 INTRODUCTION | 1 |
| 1.1 Compressed Sensing | 1 |
| 1.1.1 Sparse Signal | 1 |
| 1.1.2 Compressive Measurements | 2 |
| 1.1.3 Sparse signal recovery | 5 |
| 1.2 Variable Density Compressed Image Sampling | 7 |
| 1.3 Adaptive Subspace Compressive Detection for Sparse Signals | 9 |
| 1.4 Adaptive Compressive Detection for Pilot Assisted Ultra-Wideband Impulse Radio | 12 |
| 2 VARIABLE DENSITY COMPRESSED IMAGE SAMPLING | 16 |
| 2.1 Incoherent Fourier Sampling of Sparse Wavelet Subbands | 16 |
| 2.2 Variable Density Sampling in the Fourier Domain | 17 |
| 2.2.1 Variable Density Sampling Functions | 17 |
| 2.2.2 Variable Density Sampling Spiral for MRI | 21 |
| 2.3 Sampling in the ordered DHT domain | 22 |
| 2.4 Evaluation of incoherence sampling | 23 |
| 2.5 Simulations | 26 |

| | | |
|----------|---|-----------|
| 3 | ADAPTIVE SUBSPACE COMPRESSIVE DETECTION FOR SPARSE SIGNALS | 39 |
| 3.1 | Motivation | 39 |
| 3.2 | Detection of Unknown Sparse Signal | 46 |
| 3.2.1 | Subspace Compressive Detection | 46 |
| 3.2.2 | Compressive Detection | 48 |
| 3.3 | Detection with Narrowband interference | 50 |
| 3.3.1 | Subspace Compressive Detection | 50 |
| 3.3.2 | Compressive Detection | 52 |
| 3.4 | Discussion | 54 |
| 3.4.1 | Signal Subspace Estimation using Compressive Measurements | 54 |
| 3.4.2 | Optimal Quantization for the Subspace Projection | 57 |
| 3.5 | Simulations | 59 |
| 4 | ADAPTIVE COMPRESSIVE DETECTION FOR PILOT ASSISTED ULTRA-WIDEBAND IMPULSE RADIO | 68 |
| 4.1 | System Design | 68 |
| 4.1.1 | Model of Received UWB Signal | 68 |
| 4.1.2 | Receiver Structure | 70 |
| 4.2 | Design of subspace measurement operator | 73 |
| 4.2.1 | Sparsity Dictionary | 73 |
| 4.2.2 | Estimation of Signal Subspace | 74 |
| 4.2.3 | Design of Subspace Compressive Measurement Matrices | 77 |
| 4.3 | Symbol Demodulation | 79 |
| 4.3.1 | Test Statistic for Compressive UWB Signal Detection | 79 |

| | | |
|----------|---|------------|
| 4.3.2 | Performance Evaluation | 81 |
| 4.4 | Discussion | 82 |
| 4.4.1 | Parameter Selection and Hardware Implementation | 82 |
| 4.4.2 | Comparison with Other Receivers | 84 |
| 4.5 | Simulations | 87 |
| 4.5.1 | UWB Subspace Estimation | 88 |
| 4.5.2 | Symbol Detection with Binary Measurement Waveform | 89 |
| 4.5.3 | Circuit Nonideality | 94 |
| 5 | SUMMARY | 98 |
| 5.1 | Variable Density Sampling | 98 |
| 5.2 | Compressive Detection for Sparse Signal | 100 |
| 5.3 | Compressive Detection for Impulse Ultra-wideband | 101 |
| | BIBLIOGRAPHY | 103 |

LIST OF FIGURES

| | | |
|------------|---|----|
| 2.1 | Ordered DHT and DCT spectra of Daubechies-4 wavelets. (a) at scale 4; (b) at scale 3; (c) at scale 2; (d) at scale 1. | 24 |
| 2.2 | The original MRI images: (a) <i>Brain</i> ; (b) <i>Angiography</i> . (c) Proposed single-shot spiral sampling pattern. (d) Proposed variable density sampling pattern. Each sampling pattern has a 22.9% undersampling ratio. | 31 |
| 2.3 | Part of the reconstructed image with (a) proposed spiral sampling pattern; (b) proposed variable density sampling pattern; See Table 2.1 for corresponding PSNR. | 32 |
| 2.4 | (a) Radial sampling pattern. (b) Logarithmic spiral pattern. (c) Random phase-encodes undersampling pattern. Each sampling pattern has a 22.9% undersampling ratio. | 33 |
| 2.5 | Reconstruction of (a) radial sampling pattern; (b) logarithmic spiral pattern. (c) random phase-encodes undersampling pattern. See Table 2.1 for corresponding PSNR. | 34 |
| 2.6 | (a) The original image <i>Boat</i> . (b) Proposed variable density sampling pattern. (c) Radial sampling pattern. (d) Logarithmic spiral sampling pattern. Each sampling pattern has a 30.5% undersampling ratio. | 35 |
| 2.7 | Part of the reconstructed image with (a) proposed variable density sampling pattern; (b) radial sampling pattern; (c) logarithmic spiral pattern; (d) SBHE. See Table 2.2 for corresponding PSNR. | 36 |
| 2.8 | Reconstruction results of images from proposed sampling patterns generated by different a_H with 20000 number of measurements. | 38 |

| | | |
|------------|--|----|
| 2.9 | Reconstruction results for image “ <i>Boat</i> ” using min-TV algorithm with quadratic constraints. | 38 |
| 3.1 | Test signal: (a) Doppler, (b) Bumps, (c) HeaviSine. They are sparse in the Daubechies-8, Haar and Daubechies-8 wavelet basis, respectively. The length of the signals is 1024. | 58 |
| 3.2 | Detection of unknown Doppler signal with known subspace. The simulation parameters are set as: $N = 1024$, $K = 111$, $M_s = 77$, $M_c = 512$, $\text{ENR} = 15$ dB. | 60 |
| 3.3 | Detection of unknown Doppler signal with known subspace. The simulation parameters are set as: $N = 1024$, $K = 111$, $M_s = 77$, $M_c = 512$, $P_f = 10^{-4}$ | 61 |
| 3.4 | Ratio of $\mathbf{x}^T \mathbf{P}_{\hat{\mathbf{G}}} \mathbf{x}$ over $\mathbf{x}^T \mathbf{x}$ for different realization of \mathbf{G} | 62 |
| 3.5 | Performance of subspace compressive GLRT detector with interference rejection. The number of measurements are $M_s = 54$ and $M_c = 512$ | 63 |
| 3.6 | Signal subspace estimation and signal reconstruction by modified BPDN algorithm. P_r is the ratio of the signal energy residing in the estimated signal subspace over the total signal energy; P_c is the probability of perfect reconstruction. | 64 |
| 3.7 | Performance of BPDN + subspace compressive GLRT detector. In one method, signal subspace with dimension 49 is estimated; In another case, signal subspace with dimension 33 is estimated. . . . | 65 |
| 3.8 | Quantization on the detection performance. | 66 |
| 4.1 | Proposed I-UWB Receiver for subspace compressive detection. . . . | 71 |
| 4.2 | A channel realization of CM-7 sparse in the time domain [1]. | 87 |
| 4.3 | Performance of UWB subspace estimation algorithm with different number of measurements. | 88 |

| | | |
|------|--|----|
| 4.4 | Performance of subspace compressive GLRT UWB detectors. “Sub” is the proposed receiver; “Sub-q” is the proposed receiver with binary measurement waveform; “Nyquist” is the full-resolution digital receiver; “Approximation” is the Gaussian approximation; “Transform-q” is the transform based receiver with quantized binary measurement waveform. | 90 |
| 4.5 | Comparison with different receivers. “SRake” is the SRake receiver; “SRake-q” is the SRake receiver with binary measurement waveform; “Compressive” is the compressive receiver; “TR” is the transmitted reference receiver. | 91 |
| 4.6 | Performance of subspace compressive GLRT UWB detector with $T_i = 16$ ns and $T_i = 32$ ns. | 93 |
| 4.7 | Performance of subspace compressive GLRT UWB detector with different number of measurements. | 94 |
| 4.8 | Measurement waveform with different delay time. No delay is assumed for the ideal waveform. | 95 |
| 4.9 | Performance of subspace compressive GLRT UWB detector with delayed measurement waveforms. | 96 |
| 4.10 | Performance of subspace compressive GLRT UWB detector under timing error and measurement waveforms delay. | 97 |

LIST OF TABLES

| | | |
|------------|--|----|
| 2.1 | Reconstruction of MRI images. The performance is measured by PSNR (dB). “P. VD” is the proposed variable density sampling; “P. SS” is the proposed single-shot spiral sampling; “P-E U.” is the phase-encodes undersampling. | 26 |
| 2.2 | Reconstruction of images in ordered DHT domain. The performance is measured by PSNR (dB). “P. VD” is the proposed variable density sampling. | 37 |

ABSTRACT

Compressed sensing (CS) provides an efficient way to acquire and reconstruct sparse signals from a limited number of linear projection measurements leading to sub-Nyquist sampling rates. The advantages of compressed sensing include simpler hardware design, faster acquisition time, and less power consumption. In this thesis, several important applications of compressed sensing are addressed and better performance than that of existing solutions is obtained by exploiting the theory of compressed sensing.

Firstly, we focus on designing efficient sampling methods for image acquisition based on CS. A key to the success of CS is the design of the measurement ensemble. A novel variable density sampling strategy is designed, where the *a priori* information of the statistical distributions that natural images exhibit in the wavelet domain is exploited. The proposed variable density sampling has the following advantages: 1) the generation of the measurement ensemble is computationally efficient and requires less memory; 2) the necessary number of measurements for image reconstruction is reduced; 3) the proposed sampling method can be applied to several transform domains and leads to simple implementations. The application of our proposed method to magnetic resonance imaging (MRI) is also provided in this thesis.

Secondly, we address the detection of sparse signals within the CS domain. A new family of detectors called subspace compressive detectors are developed for the detection of sparse signals based on the theory of compressed sensing. The proposed detectors reduce the number of measurements needed for a given detection

performance by exploiting the fact that the sparse signal resides in a low dimension subspace. By designing random projection operators tailored to the subspace where the signal-of-interest lies, the signal energy can be captured more efficiently leading to better detection performance. The information of the signal subspace can be learned from compressive measurements of training signals and the detectors are adaptive to the signal structure. Within the compressed sensing framework, it is shown that very limited random measurements of training signals can suffice to provide valuable information of the signal subspace for detection purposes. The performance of the proposed subspace compressive detectors is analyzed and implementation issues including the waveform quantization are discussed. Subspace compressive detection under narrowband interference is also considered in this thesis.

In the last part of this dissertation, the theory of compressed sensing is exploited in the design of a new type of suboptimal impulse ultra-wideband (I-UWB) receivers where only sub-Nyquist sampling of the received UWB signal is required. However, the proposed I-UWB receivers have simple hardware implementations and, at the same time, shares the flexibility in data processing with full-resolution digital receivers based on Nyquist sampling. An improved symbol detection method is proposed for I-UWB communications by exploiting the sparsity of the received UWB signals, where the sparsity is mainly due to the multipath diversity introduced by I-UWB channels. A compressive pilot assisted time-hopping spread-spectrum signaling is introduced and performance analysis of the proposed receivers is provided. Compared with other suboptimal I-UWB receivers, satisfactory detection performance is achieved with simple hardware implementation.

Chapter 1

INTRODUCTION

1.1 Compressed Sensing

To reconstruct a band-limited signal, traditional signal processing approaches sample the signal uniformly at a rate which is at least twice the bandwidth of the underlying signal. Such sampling strategy creates difficulties in the acquisition of wideband signals where the required sampling rate exceeds the current limit of state-of-art commercial analog to digital converters (ADC) [2]. Sampling the signals directly at or above the Nyquist rate may also lead to costly hardware implementations, such as in the design of high resolution infrared imaging cameras [3]. Traditional sampling methods also demand large storage space to save the measurements, and most often a waste of resources occurs since in many practical applications, measurements are simply discarded after signal compression. The theory of compressed sensing (CS) emerged to overcome the difficulties associated with tradition sampling methods. By exploiting the fact that many natural signals are sparse or compressible, CS provides a new framework to jointly measure and compress signals that allows less sampling and storage resources than traditional approaches based on Nyquist sampling.

1.1.1 Sparse Signal

A signal $\mathbf{x} \in \mathcal{R}^N$ is said to be S -sparse on some basis $\Psi = [\underline{\psi}_1, \underline{\psi}_2, \dots, \underline{\psi}_N]$ if \mathbf{x} can be represented by a linear combination of S vectors from Ψ with $S \ll N$.

That is:

$$\mathbf{x} = \Psi \underline{\theta}, \quad (1.1)$$

where $\underline{\theta}$ is the $N \times 1$ coefficient vector with only S non-zero entries. Many real signals are not strictly sparse but compressible on some basis in that most of the entries of their coefficient vectors $\underline{\theta}$ are non-zeros but very small. Furthermore, the magnitudes of the entries in $\underline{\theta}$ decay following a power law [4]. Since only a few coefficients dominate, compressible signals can be adequately approximated by a S -sparse signal model by keeping the S largest coefficients [5].

1.1.2 Compressive Measurements

Within the compressed sensing framework, measurements are taken not by directly sampling the sparse signal but by measuring a few of linear projections of the underlying signal. The linear measurements can be modeled as:

$$\mathbf{y} = \Phi \mathbf{x}, \quad (1.2)$$

where Φ is an $M \times N$ projection matrix where the number of measurements M is far less than the signal dimension N . Let the measurements be $\mathbf{y} = [y_1, y_2, \dots, y_m]^T$ and Φ be $\Phi = [\underline{\phi}_1, \underline{\phi}_2, \dots, \underline{\phi}_M]^T$, then one measurement includes projecting the signal \mathbf{x} onto $\underline{\phi}_i$ and then measuring the inner product

$$y_i = \langle \mathbf{x}, \underline{\phi}_i \rangle, \quad (1.3)$$

where $i \in \{1, 2, \dots, M\}$. If the inner product is implemented in the analog domain, then a reduced sampling rate is achieved.

Given the linear measurements \mathbf{y} , the sparse signal \mathbf{x} can be reconstructed from \mathbf{y} via nonlinear optimization by exploiting the *a priori* information that \mathbf{x} is sparse on some basis Ψ . However, to successfully reconstruct the signal with high probability, the projection matrix Φ has to satisfy a set of properties. A key factor for the successful reconstruction of \mathbf{x} is that the measurement ensemble Φ

and the sparsity basis Ψ should be incoherent with each other. That is, $\underline{\phi}_i$ does not have a compact representation on Ψ and likewise, $\underline{\psi}_i$ does not have a compact representation on Φ [6]. A quantitative measure of incoherence is given by [7]:

$$\mu(\Phi, \Psi) = \sup\{|\langle \underline{\phi}_i, \underline{\psi}_j \rangle| : \underline{\phi}_i \in \Phi, \underline{\psi}_j \in \Psi\}. \quad (1.4)$$

If $\underline{\phi}_i$ and $\underline{\psi}_j$ both have unit energy, then it follows that $\mu \in [1, \sqrt{N}]$. Note that if Φ is constructed such that each entry of Φ is taken from an independent and identically distributed (i.i.d.) random distribution, then with high probability, Φ is incoherent with any fixed basis Ψ and $\mu(\Phi, \Psi)$ is close to 1 rather than \sqrt{N} [6]. Frequently employed random distributions include the Gaussian distribution and the Bernoulli distribution.

A guideline to construct a measurement matrix Φ that leads to robust reconstruction of a S -sparse signal is based on the the restricted isometry property (RIP) of a matrix. For each integer $S = 1, 2, \dots, N$, the isometry constant δ_S of a matrix Φ is defined as the smallest number such that

$$(1 - \delta_S)\|\mathbf{x}\|_2^2 \leq \|\Phi\mathbf{x}\|_2^2 \leq (1 + \delta_S)\|\mathbf{x}\|_2^2, \quad (1.5)$$

holds for all S -sparse signal \mathbf{x} [6, 8]. Φ obeys the RIP of order S if δ_S is significantly smaller than 1. Obeying the RIP indicates that any subset of columns of Φ with cardinality less than S behaves like an orthonormal system, which implies that \mathbf{x} does not exist in the null space of Φ . If δ_{2S} is also sufficiently small, then for any two S -sparse signals \mathbf{x}_1 and \mathbf{x}_2 , the following holds:

$$(1 - \delta_{2S})\|\mathbf{x}_1 - \mathbf{x}_2\|_2^2 \leq \|\Phi(\mathbf{x}_1 - \mathbf{x}_2)\|_2^2 \leq (1 + \delta_{2S})\|\mathbf{x}_1 - \mathbf{x}_2\|_2^2. \quad (1.6)$$

It means that RIP preserves the distance of any pair of S -sparse signals in the measurement domain, which guarantees the robust recovery of a S -sparse signal from its compressive measurements [6]. The measurement matrix Φ can be constructed such that each entry of Φ is taken from an i.i.d. zero-mean Gaussian distribution

with variance $1/M$ or a Bernoulli distribution with amplitude $1/\sqrt{M}$. It is observed that Φ obeys the RIP with high probability for robust sparse signal recovery if the number of measurements M satisfies $M = CK \log N \ll N$ where $C \geq 1$ is the oversampling factor [9].

The observation that a sensing matrix constructed from a random distribution is suitable for compressed sensing can also be explained by the well-developed Johnson-Lindenstrauss (JL) lemma in the dimensionality-reduction area [10]. The JL lemma basically states that if Φ is constructed from a random distribution and each row of Φ has been normalized to $\sqrt{N/M}$, then the following holds with high probability:

$$(1 - \epsilon)\|\mathbf{x}_1 - \mathbf{x}_2\|_2^2 \leq \|\Phi(\mathbf{x}_1 - \mathbf{x}_2)\|_2^2 \leq (1 + \epsilon)\|\mathbf{x}_1 - \mathbf{x}_2\|_2^2, \quad (1.7)$$

where ϵ is sufficiently small and \mathbf{x}_1 and \mathbf{x}_2 are S -sparse signals. What is revealed in (1.7) is that a random matrix is a stable embedding of the geometry of the sparse signal in the measurement domain. Technically, the RIP can be viewed as a straightforward consequence of the JL lemma [11].

Another way to obtain compressive measurements is random sampling in a transform domain Υ which enables fast computation if there exists fast transform algorithms for Υ and Ψ , respectively. To obtain the sparse signal information, we acquire a small set of transform coefficients of \mathbf{x} in Υ . The measurements can also be represented as $\mathbf{y} = \Phi\mathbf{x}$, where Φ here is also an $M \times N$ matrix with $M \ll N$. Here, however, each row of Φ , $\underline{\phi}_i$, is taken from a subset of the atoms of Υ . If Ψ and Υ are incoherent with each other and $\underline{\phi}_i$ is randomly chosen, then \mathbf{x} can be recovered from \mathbf{y} with high probability. It is found that the low coherence property holds for many pairs of bases (Ψ, Υ) [7].

1.1.3 Sparse signal recovery

It is well known that a practical way to recover the sparse signal is to solve the following l_1 -norm minimization problem:

$$\min \|\underline{\theta}\|_1 \quad \text{subject to} \quad \Phi\Psi\underline{\theta} = \mathbf{y}, \quad (1.8)$$

where $\|\underline{\theta}\|_1 = \sum_i |\theta_i|$. The solution $\hat{\underline{\theta}}$ leads to the reconstructed sparse signal $\mathbf{x}^* = \Psi\hat{\underline{\theta}}$. By minimizing the l_1 -norm, the solution to (1.8) gives a sparse representation of the signal that satisfies the compressive measurements. This reconstruction method is called Basis Pursuit [12, 13]. Basis pursuit is a computationally efficient algorithm and can be implemented by linear programming.

The following theorem derived in [14] links the RIP of a sensing matrix to the success of the sparse signal reconstruction.

Theorem 1.1.1 ([14]) *Assume that \mathbf{x} is S -sparse and suppose that the isometry constants δ_{2S} and δ_{3S} satisfy $\delta_{2S} + \delta_{3S} < 1$, then the solution \mathbf{x}^* to (1.8) is exact, i.e., $\mathbf{x}^* = \mathbf{x}$*

Note that if there are fast algorithms associated with Φ and Ψ , then the BP algorithm can be implemented using fast transform algorithms, which make sparse signal recovery feasible for large-dimension data. Iterative greedy algorithms, such as matching pursuit (MP) [15], Orthogonal Matching Pursuit (OMP) [16] and tree matching pursuit (TMP) [17], can also be employed to recover the sparse signal. However, to obtain the same results, slightly more measurements are needed.

In practice, the linear projection measurements are contaminated with noise and the measurements can be modeled by

$$\mathbf{y}_n = \Phi\Psi\underline{\theta} + \mathbf{n}, \quad (1.9)$$

where \mathbf{n} is zero-mean white Gaussian noise. A recovery algorithm that explicitly considers the noise effect is needed. The sparse signal can be reconstructed from \mathbf{y}_n by using Basis Pursuit Denoising (BPDN) as follows [13] :

$$\min \|\Phi\Psi\theta - \mathbf{y}_n\|_2^2 + \lambda\|\theta\|_1 \quad \text{s. t.} \quad \mathbf{y}_n = \Phi\Psi\theta + \mathbf{n}, \quad (1.10)$$

where $\lambda > 0$ depends on the noise level. Here λ balances the tasks of minimizing the l_2 norm of the noise and the minimization of the l_1 norm of the sparse signal. Here λ has to be carefully chosen so that the reconstructed signal keeps a high fidelity of the original signal. Again, if there are fast algorithms associated with Φ and Ψ , then a fast reconstruction algorithm can be implemented for signal reconstruction [8, 18, 19].

For robust reconstruction of the sparse signal, the l_1 -norm minimization with noisy measurement can also be formulated as a LASSO problem. That is [6]:

$$\min \|\theta\|_1 \quad \text{s. t.} \quad \|\Phi\Psi\theta - \mathbf{y}\| \leq \epsilon, \quad (1.11)$$

where ϵ limits the noise power in the measurements. Problem (1.11) is also a convex problem and efficient algorithms can be developed to solve (1.11). The theorem listed below shows how accurate the solution of (1.11) is expected.

Theorem 1.1.2 ([8]) *Assume that $\delta_{2S} < \sqrt{2} - 1$, then the solution \mathbf{x}^* to (1.11) obeys:*

$$\|\mathbf{x}^* - \mathbf{x}\|_2 \leq C_0\|\mathbf{x} - \mathbf{x}_S\|_1\sqrt{S} + C_1\epsilon, \quad (1.12)$$

where C_0 and C_1 are positive constants and \mathbf{x}_S is an approximation of \mathbf{x} where all but the largest S components are set to 0.

Theorem (1.1.2) reveals that the reconstruction error is bounded by two terms. The first is the approximation error and the second is the measurement noise level. It is also shown that the constants C_0 and C_1 are typically small [6]. Thus, robust recovery of the sparse signal is achieved even with noisy measurements.

To reconstruct smooth and sparse signals like natural images, another algorithm that can be used is the minimization of total variation (min-TV) with quadratic constraints. Let $\mathbf{x}(i, j)$ be an $N \times N$ image, then min-TV with quadratic constraints aims to solve the following problem [8]:

$$\min_{\mathbf{x}} \|\mathbf{x}\|_{TV} \quad \text{s. t.} \quad \|\Phi\mathbf{x} - \mathbf{y}_n\| \leq \epsilon, \quad (1.13)$$

where $\|\mathbf{x}\|_{TV} = \sum_{i,j} \sqrt{[x(i+1, j) - x(i, j)]^2 + [x(i, j+1) - x(i, j)]^2}$ is the total variation and $\epsilon > 0$ is again a constant depending on the noise level. Min-TV with quadratic constraints usually provides better quality of image reconstruction at the cost of more computation than BPDN.

In this thesis, we focus on three topics based on compressed sensing. Firstly, we derived strategies for random sampling in a transformed domain for image acquisition, which reduces the number of measurements for a given reconstruction performance. Secondly, by exploring the sparse signal structure, we have proposed a set of adaptive subspace compressive detectors based on compressive measurements. At last, we have applied compressed sensing and adaptive subspace compressive detection to ultra wide-band communications, which leads to simple hardware implementations with satisfactory detection performance.

1.2 Variable Density Compressed Image Sampling

By exploiting the sparsity of natural images, compressed sensing has shown that it is feasible to acquire and reconstruct natural images from a limited number of linear projection measurements at sub-Nyquist sampling rates [9, 12]. A key to the success of CS is the design of the measurement ensemble, which is based on the evaluation of the incoherence between the measurement ensemble and the sparsity basis. Due to the large scale nature of images, the generation of the measurement ensemble should also be both computationally and memory efficient. Furthermore, the sampling scheme should enable fast algorithms to perform image reconstruction.

Measurement matrices where each entry is an independent and identically distributed (i.i.d.) random variable obeying Gaussian or Bernoulli distribution have been proposed for compressed image sampling [9, 12]. Recently, it has been shown that the performance of CS sampling can be improved if the random measurement matrices are suitably optimized [20]. These methods lead to optimized but unstructured measurement matrices and thus large memory space and computation demanding resources are needed, making them prohibitively expensive for implementation. A more desirable way to obtain linear measurements is by incoherent sampling in a transform domain that is equipped with fast transform algorithms [19]. Measurement ensembles in the transform domain that enable fast computations include partial Fourier ensemble, scrambled Fourier ensemble (SFE), scrambled block Hadamard ensemble (SBHE), and Noiselets. These have been shown to obtain good performance in CS applications [12, 19, 21]. With the exception of signal sparsity on a given basis, however, the formulation of these sampling approaches does not exploit any *a priori* information of natural images that could lead to improved CS performance [22, 23].

We propose a method to effectively exploit such *a priori* information in the design of efficient CS measurement ensemble by using the inherent statistical distributions that natural images exhibit in the sparse wavelet domain. A novel family of variable density sampling patterns are designed in the frequency transform domain, which is applicable to the Discrete Fourier Transform (DFT), Discrete Cosine Transform (DCT) and ordered discrete Hadamard transform (DHT) [24]. To design the proposed measurement matrices, the widely used generalized Gaussian distribution (GGD) model is adopted to statistically describe the distribution of image wavelet coefficients. The method of incoherent Fourier sampling of subband wavelets proposed in [19] provides an efficient way to acquire sparse subband wavelets in the DFT domain. The Fourier coefficients in the band where significant energy of the

wavelet exists are sampled randomly to minimize the coherence between the sparse wavelets and the measurement Fourier atoms. Based on such incoherent Fourier sub-band sampling strategy, we derive a variable density sampling function $p(m, n)$ in the frequency transform domain according to the adopted statistical wavelet model. Here $p(m, n)$ indicates the probability that the (m, n) th coefficient is sampled. The design of the variable density sampling function is then further improved so that not only the distribution of significant wavelet coefficients are considered, but also their rapid magnitude decay from coarse scales to fine scales. The sampling patterns in the frequency transform domain are generated randomly according to the underlying probability function.

Equipped with fast transform algorithms, the proposed sampling processes are simple, fast and can be easily implemented. By exploiting the *a priori* information of natural images, the CS performance obtained with the proposed sampling method is significantly improved. Compared with other sampling patterns, such as radial sampling pattern and variable density spiral that also exploit some *a priori* information of the images [12, 23], the proposed sampling patterns are not heuristically constructed, but are based on reliable statistical models of wavelet coefficients and thus the proposed sampling patterns are analytically justified.

1.3 Adaptive Subspace Compressive Detection for Sparse Signals

Compressed sensing has provided a new framework to jointly measure and compress sparse signals that allows less sampling resources than traditional approaches based on Nyquist sampling. Besides signal reconstruction, the CS framework also provides a measurement approach for sparse signal detection and classification [15, 25, 26, 27, 28]. A reduced number of random measurements could suffice to provide sufficient signal statistics for signal detection or classification without even reconstructing the signal. Based on such compressive measurements, the compressive detector proposed in [25] provides a systematic way to perform sparse signal

detection and estimation for applications where only a reduced number of measurements are available. However, unlike signal reconstruction, compressive signal detection suffers from performance degradation due to the fact that random measurements are less distinguishable to random noise than the original sparse signals. Thus, the compressive measurement scheme [25], which is independent of the sparse signal structure, leads to detection performance inferior to traditional detectors relying on Nyquist sampling [29].

In this thesis, a set of subspace compressive detectors are proposed for sparse signal detection by exploiting the fact that a sparse signal resides in a low dimension subspace and, therefore, one can capture most of the signal energy with a few measurements just by projecting the underlying signal into its own subspace [30]. More precisely, by designing a measurement projection matrix tailored to the subspace where the signal-of-interest lies, the signal energy can be captured more efficiently, and at the same time, the effect of noise and interference is greatly mitigated. In turn, improvement on detection performance can be achieved with fewer random measurements [31]. The proposed subspace compressive detectors are suitable for situations where only very limited measurements, even less than the signal sparsity K , are available. Note that reducing the number of measurements needed is always an important goal within the CS framework since it leads to simpler hardware requirements.

The information of the signal subspace can be obtained *a priori*. More specifically, natural images, for instance, always reside in subspaces expanded by coarse scale wavelets, and orthogonal frequency-division multiplexing (OFDM) signals reside in frequency bands known to the receiver [32, 33]. More importantly, the subspace information can be obtained from a reduced set of compressive measurements from the training data [2]. The complete recovery of the signal sparsity pattern would require the number of measurements on the same order of magnitude as that

needed for the complete recovery of the signal itself. However, in signal detection we are only interested in partial sparsity recovery [34, 35]. That is, we are interested in searching for the subspace components that contain a large fraction of the signal energy. By employing signal recovery algorithms such as orthogonal matching pursuit (OMP) or basis pursuit denoising algorithm (BPDN), simulation results in this thesis show that we can always achieve partial sparsity recovery from a reduced set of compressive measurements which is far fewer than that required for signal reconstruction [13, 16]. The estimated signal subspace, either coarse or accurate, would lead to significant improvements on sparse signal detection.

Although we motivate the design of the subspace compressive detector for applications where the detection of a known sparse signal is desired, the main focus is on the design of adaptive subspace compressive detectors for the detection of an unknown sparse signal where a simple solution such as a matched filter is not available. Furthermore, signal subspace estimation is also addressed in the compressed sensing domain. Estimated signal subspace is learned from the compressive measurements and employed in the design of proposed subspace compressive detectors. The performance of the proposed detectors is analyzed in detail and compared to Nyquist sampling-rate based subspace detection. As in CS applications, we only assume that the sparsity basis Ψ is known *a priori*. The designed detectors are adaptive to the signal structure learned from compressive measurements gained from training signals. This approach can be naturally extended to sparse signal detection with narrowband interference (NBI) mitigation [36]. Simulation results are provided to validate the theoretical performance predictions. For implementation purposes, discussion on the performance loss due to the measurement waveform quantization is also provided.

The subspace compressive detector differs from traditional matched subspace detector in that for optimal detection performance, the Nyquist sampled full-length

received signal is not needed [29]. The received signal, in its analog form, is projected onto analog measurement waveforms and only the small set of projected results are sampled and digitized. Note that the signal detection based on the classes of linear transforms also exploits the signal subspace. However, such method requires the number of measurements at least the dimension of the signal subspace [37]. The proposed subspace compressive detection provides a more flexible measurement scheme in that the number of measurements is adjustable and more measurements lead to better detection performance. Since additional signal subspace information is exploited, the proposed subspace compressive detector can achieve the same detection performance with fewer measurements than that of compressive detectors proposed in [25]. Although the subspace compressive detector does not provide universality for signal detection w.r.t all signals in the \mathcal{R}^N space, it does provides universality for signal detection w.r.t all signals in a specific subspace.

1.4 Adaptive Compressive Detection for Pilot Assisted Ultra-Wideband Impulse Radio

The concepts developed in compressive subspace detection are then applied to the design of ultra-wideband receivers. Impulse ultra-wideband (I-UWB) communications convey information by transmitting ultra-short pulses [38]. The large bandwidth of I-UWB signals enables fine time resolution, precise localization and robustness to multipath environments [38, 39, 40]. Furthermore, the low power spectral density and the use of ultra-short waveforms not only enable I-UWB systems to coexist with existing communication systems, but also provide low probability of intercept (LPI) [38]. Despite the vast research efforts devoted to I-UWB communications, challenges still exist for the implementation of I-UWB receivers due to the large signal bandwidth, low power spectrum and the rich multipath diversity introduced by the UWB channel. The tradeoff between the receiver complexity and performance has to be carefully evaluated.

A full-resolution digital I-UWB receiver can provide considerable flexibility in downstream data processing. However, it demands ultra-fast analog-to-digital converters (ADCs) that are complex and power-consuming [38]. At a reduced sampling rate, a Rake receiver with maximum ratio combining (MRC) can be employed in I-UWB communications to exploit the multipath diversity of the UWB channel [38]. However, the performance of Rake receivers relies on accurate UWB channel information which has been shown to be difficult to obtain [2, 41, 42]. Furthermore, the number of multipath components (MPCs) may be too large for practical hardware implementation of a Rake receiver. To reduce the hardware complexity, selective Rake (SRake) receivers and partial Rake (PRake) receivers have been proposed where only a subset of MPCs are exploited [43]. However, SRake receivers still require channel estimation and PRake receivers do not perform well for widely encountered sparse UWB channels.

One way to circumvent channel estimation is the use of autocorrelation receivers with preamble training pilots [44]. Autocorrelation receivers, such as the transmitted-reference receiver, exploit the multipath diversity of UWB channels by correlating the received signal with a previously received pilot signal [45]. Although the entire energy of the received signal can be captured at a reduced sampling rate, autocorrelation receivers suffer from performance deterioration since noisy pilot signals are used as correlation templates for demodulation [46]. Practical implementation of autocorrelation receivers is also constrained by the fact that a wideband analog delay line that is required for signal demodulation is hard to build in low-power circuits [47]. Efforts to remove the wideband delay line also introduce other disadvantages such as limited transmission rate, high peak-to-mean power ratio, or additional hardware needed to produce a well-tuned pulse shape [47, 48].

In this thesis, novel I-UWB receivers at sub-Nyquist sampling rate are proposed based on the emerging theory of compressed sensing (CS) leading to comparable detection performance and affordable hardware implementations. CS has provided a new framework to jointly measure and compress sparse signals that allows less sampling resources than traditional approaches based on Nyquist sampling. Besides signal reconstruction, the CS framework also provides a measurement scheme for sparse signal detection and classification [15, 26, 27]. A reduced set of random measurements can suffice to provide sufficient signal statistics for signal detection or classification without signal reconstruction. Recently, we have successfully applied CS to I-UWB channel estimation and symbol detection by exploiting the time sparsity of the multipath UWB channels [2, 49].

This thesis presents an improved design of the subspace compressive I-UWB receivers with joint channel estimation and symbol detection. The proposed UWB receivers lead to a simpler hardware implementation by exploiting both the sparsity of the received UWB signals and the repetitive structure of transmission signaling. In the proposed method, the received UWB signal can be sparsely represented by a suitably designed dictionary tailored to the signal characteristics. The design of the sparsity dictionary is based on the fact that the received signal is a linear combination of the delayed UWB pulses modulated by the UWB channel. Random measurements are obtained by the pilot UWB signals, where CS based approaches are used to estimate the sparse UWB channel and obtain an estimation of the UWB signal subspace. By exploiting the repetitive signaling, a sufficient number of measurements is obtained for signal subspace estimation even with severely constrained hardware. Using the estimated signal subspace, a subspace random projection operator that exploits the low-dimension signal subspace is designed, which is efficient at capturing the underlying signal energy and for noise mitigation. Thus, a reduced number of measurements are required by a generalized likelihood ratio test (GLRT)

detector for a desired detection performance.

For simplicity of hardware implementation, the projection operator is further proposed to be quantized to only binary levels since it is much easier to generate wideband binary waveforms than to generate arbitrary wideband waveforms [50]. To reduce the performance loss due to quantization, the well-known Lloyd-Max optimal bit allocation method is employed for waveform quantization [51]. In hardware, wideband binary measurement waveforms can be generated by high-speed shift registers with flip-flops [52]. The proposed hardware architecture is similar to the random modulation preintegration (RMPI) architecture proposed in [6, 53].

The proposed I-UWB receiver projects the received UWB signal onto random basis in the analog domain by drawing elements of the parallel mixed-signal architecture introduced in [54, 55, 56], while incorporating CS ideas. The received UWB signals are sampled at sub-Nyquist rate and no ultra-fast ADC is needed. It can be shown that the proposed subspace compressive I-UWB receivers has less complexity than SRake receivers [43]. Furthermore, no *a priori* information except the sparsity of the I-UWB channel is required and the detection algorithm is adaptive to the underlying UWB channel. Compared with the analog autocorrelation receivers, cumbersome wideband analog delay lines are not required [47]. Since the compressive measurements are presented digitally, it is easy to implement noise reduction by averaging the measurements over multiple signal frames without increasing the hardware complexity. Simulation study also shows that the proposed receivers are robust against circuit nonidealities.

Chapter 2

VARIABLE DENSITY COMPRESSED IMAGE SAMPLING

2.1 Incoherent Fourier Sampling of Sparse Wavelet Subbands

Wavelets have well defined spectral characteristics in the Fourier domain [57]. A coarse scale wavelet has its spectrum localized in the low frequency band whereas a fine scale wavelet has its spectrum widely spread out in the high frequency band. In [19], it is observed that if the signal to be acquired is restricted to a certain wavelet subband, a set of incoherent measurements can be obtained by selecting the Fourier coefficients from the corresponding frequency band where significant energy of the wavelet exists.

Let $k = 1, 2, \dots, K$ denote the scale of the 1D wavelets where $k = 1$ is the finest scale and $k = K$ is the coarsest scale. Without loss of generality, it is assumed that the wavelet has length $N = 2^K$. Let $\varphi_{k,l}$ denote the 1D wavelet at a scale k with a shift $l \in [0, N2^{-k} - 1]$, then the DFT spectrum of $\varphi_{k,l}$ is over the band $\mathcal{B}_k = [-N2^{-k}, -N2^{-k-1}] \cup [N2^{-k-1}, N2^{-k}]$. To reconstruct $\varphi_{k,l}$ from its DFT samples, the DFT atoms are randomly selected within the band \mathcal{B}_k [19]. Assume the number of significant wavelets over \mathcal{B}_k is S_k , then approximately $2S_k$ to $3S_k$ Fourier measurements are needed. The probability that a DFT atom is sampled depends on the size of \mathcal{B}_k and on the sparsity S_k . Since smooth signals have most of their significant wavelet components clustered in the coarse scales, incoherent

Fourier subband sampling implies that the low frequency Fourier coefficients, which contain much of the signal's energy, should be sampled with higher probability ¹.

The principle of Fourier sampling of wavelet subbands can be readily applied to 2D images. Assume the underlying image is of size $N \times N$. Let $\varphi_{k,i,j}^B$ denote the (i, j) th 2D wavelet at the k th scale of subband B where $B \in LH, HL, HH$, $i, j = 0, \dots, N_k - 1$ and $N_k = N/2^k$. Here LH subbands are low-pass in the horizontal direction and high-pass in the vertical direction; HL subbands are high-pass in the horizontal direction and low-pass in the vertical direction; HH subbands are high-pass in both directions. The DFT spectrum of all the wavelets at the k th scale can be characterized by $\bar{\mathcal{B}}_k = ([-N2^{-k}, -N2^{-k-1}] \cup [N2^{-k-1}, N2^{-k}]) \times ([-N2^{-k}, -N2^{-k-1}] \cup [N2^{-k-1}, N2^{-k}])$. Again, the probability that a 2D DFT atom within $\bar{\mathcal{B}}_k$ is sampled depends on the size and on the number of significant wavelets of $\bar{\mathcal{B}}_k$.

2.2 Variable Density Sampling in the Fourier Domain

2.2.1 Variable Density Sampling Functions

For 2D natural images, the significant wavelet components tend to cluster around coarse scales. Thus, according to the principle of Fourier sampling of wavelet subbands, the Fourier coefficients to be measured should also cluster over low frequency bands. Obviously, by placing the samples selectively but still in a random manner, we can achieve better quality of image reconstruction than if those measurements are chosen uniformly random. In the following, we discuss how the sampling probability of the Fourier samples should change over different frequency bands.

¹ Results in [19] do not directly imply that if multiple subbands contain nonzero elements and the corresponding frequency intervals are sampled proportionally to their occupancy, the signal can still be recovered with high probability. Thus, splitting the signal into various wavelet subbands and then performing incoherent sampling is suggested.

For natural images, it is well-known that the distribution of wavelet subband coefficients can be adequately described by GGD models [58]. Let $w_{i,j,k}^B$ denote the (i, j) th wavelet coefficient in the k th scale. For ease of analysis, we assume that $w_{i,j,k}^B$, for $B \in LH, HL, HH$, belongs to the same GGD with the probability density function given by:

$$f(x; \sigma_k, \beta_k) = \eta(\sigma_k, \beta) \exp\{-[|x|/d(\sigma_k, \beta_k)]^{\beta_k}\}, \quad (2.1)$$

where $d(\sigma_k, \beta_k) = \sigma_k \sqrt{\frac{\Gamma(1/\beta_k)}{\Gamma(3/\beta_k)}}$, $\eta(\sigma_k, \beta_k) = \frac{\beta_k}{2\Gamma(\frac{1}{\beta_k})d(\sigma_k, \beta_k)}$ and $\Gamma(z) = \int_0^\infty t^{-1+z} e^{-t} dt$ is the Gamma function. The parameters σ_k and β_k are the standard deviation and the shape parameter of the k th scale, respectively. Typical values of β_k for natural images falls in the range $[0.5, 1]$ [58]. The variance of the k th scale wavelet coefficients is given by σ_k^2 which is assumed to decrease exponentially from coarse scales to fine scales [59]:

$$\sigma_k^2 = 2^{-a(K-k)}, \quad (2.2)$$

where $a > 0$. It was shown in [59] that a can range from 2.25 to 3.1 based on the inference from empirical studies. Equation (2.2) also reveals the fact that the magnitude of wavelet coefficient decays rapidly from coarse scales to fine scales. Here the coarsest scaling coefficient of the image is assumed to belong to a uniform distribution $U(0, 1)$.

We first discuss how the sampling probability of DFT atoms should change according to the incoherent sampling of wavelet subbands. Here we define the significant wavelet coefficients as the wavelet coefficients whose magnitudes are larger than a threshold $\mu > 0$. Since the number of wavelet coefficients at scale k is $3(4^{K-k})$, the mean of the number of significant wavelet coefficients at scale k is:

$$\lambda_k = 6(4^{K-k}) \int_\mu^\infty f(x; \sigma_k, \beta_k) dx. \quad (2.3)$$

Consider the (m, n) th DFT atom within the band $\bar{\mathcal{B}}_k$ corresponding to the wavelet scale $k = K - \lfloor \log_2(2s) \rfloor$ where $s = \max\{|m|, |n|\}$ and $-N/2 \leq m, n < N/2$. It is

clear that the number of DFT atoms within $\bar{\mathcal{B}}_k$ satisfies: $\varsigma_k \propto 4^{K-k}$. Thus, based on the incoherent Fourier subband sampling method, the probability that the (m, n) th DFT atom is selected also satisfies:

$$\tilde{p}(m, n) \propto \frac{\lambda_k}{\varsigma_k} \propto \int_{\mu}^{\infty} f(x; \sigma_k, \beta_k) dx. \quad (2.4)$$

Before examining $\tilde{p}(m, n)$ in the general case it is insightful to consider a special case of the GGD: the Laplacian ($\beta_k = 1$). The Laplacian distribution is of particular importance for the following two reasons: 1) it is analytically more tractable; 2) the empirical distribution of subband wavelets for many natural images are close to Laplacian [58]. With $\beta_k = 1$ and $d(\alpha_k, \beta_k) = \sigma_k/\sqrt{2}$, it can be shown that:

$$\int_{\mu}^{\infty} f(x; \sigma_k, \beta_k) dx = \frac{1}{2} \exp\left(-\frac{\sqrt{2}\mu}{\sigma_k}\right). \quad (2.5)$$

Thus, $\tilde{p}(m, n)$ can be approximated as:

$$\tilde{p}(m, n) \propto \exp[-(2^{\frac{a+1}{2}} \mu s^{\frac{a}{2}})]. \quad (2.6)$$

It is clear that $\tilde{p}(m, n)$ decays exponentially along with the atom coordinates s and the decay rate depends on the image characteristic parameter a . Analysis based on the Laplacian distribution indicates that in the general case, $\tilde{p}(m, n)$ should also decay exponentially with its atom coordinates. For the random selection of DFT atoms, it is convenient to construct a sampling density function in the DFT domain and generate a sampling pattern according to the sampling density function. Designing a sampling density function following (2.6) would require image dependent parameter a , β_k and μ . However, in reality, only the number of measurements J is known. A method which does not require image dependent information to design an effective sampling density function is more desirable.

To conform to the decaying behavior of the sampling probability with increasing coordinates while keeping a simple form, we propose a new family of sampling

density functions containing only exponential terms. Assuming the size of the underlying image is $M \times N$, the probability that the (m, n) th coefficient is sampled is given by:

$$p_F(m, n) = \exp \left[-\frac{\left(\sqrt{\left(\frac{m}{N}\right)^2 + \left(\frac{n}{N}\right)^2}\right)^{a_F}}{\sigma_F^2} \right], \quad (2.7)$$

where $-M/2 \leq m < M/2$ and $-N/2 \leq n < N/2$. $a_F > 0$ is a parameter characterizing the decay of the sampling probability. $\sigma_F > 0$ is a parameter tuned to obtain the desired number of samples. Since $0 < p_F(m, n) < 1$, $p_F(m, n)$ is suitable as a probability function. Furthermore, the proposed sampling density function is flexible to accommodate various decaying rates and different number of measurements by tuning the parameters a_F and σ_F . Given a_F , the sampling ratio defined as J/MN is a monotonically increasing function of σ_F . Thus, the search of σ_F for a desired number of measurements is straightforward. Furthermore, σ_F can also be found by numerically solving the following problem:

$$\int_{-\frac{1}{2}}^{\frac{1}{2}} \int_{-\frac{1}{2}}^{\frac{1}{2}} \exp \left[-\frac{\left(\sqrt{x^2 + y^2}\right)^{a_F}}{\sigma_F^2} \right] dx dy = \frac{J}{M \times N}. \quad (2.8)$$

The sampling patterns generated from the sampling density function are binary where 1 at (m, n) indicates a sampling point and 0 means no measurement on that point is made. With a probability given by $p_F(m, n)$, 1 will be generated at (m, n) ; otherwise, 0 will be generated.

Based on the observation from the case of the Laplacian distribution, it is reasonable to set $a_F = \frac{1}{2}a\bar{\beta}$, where $\bar{\beta}$ is defined as the averaged value of several coarsest scale shape parameters. However, it should be noted that the above analysis based on the incoherent Fourier subband sampling principle only provides approximately equal probability of reconstruction for significant wavelet components both at coarse scales and at fine scales. For image reconstruction, the contribution of an individual significant wavelet component to the image quality should be considered. Equation (2.2), along with empirical data analysis, reveals that a significant wavelet coefficient at a coarse scale usually has much larger magnitude than that of a significant

wavelet coefficient at a fine scale. Thus, probabilistically, a coarse scale wavelet has much more contribution to the reconstructed image quality than that of a fine scale wavelet. Consequently, to achieve good reconstructed image quality, it is desirable to give more preference to the reconstruction of coarse scale wavelet components. Such intuitive analysis shows that an effective sampling density function should decay faster than predicted by $a_F = \frac{1}{2}a\bar{\beta}$ and it is desirable to increase the decaying parameter a_F away from $\frac{1}{2}a\bar{\beta}$. Simulation results show that $a_F \approx 1.3 a$ leads to good image reconstruction, as will be illustrated in Sec. 3.5. It is also observed that the quality of the reconstructed image is robust to variations of a_F if a_F is sufficiently large. If an estimation of a is not available, then setting $a_F = 3.5$ is recommended since this value leads to robust and satisfactory CS performance.

2.2.2 Variable Density Sampling Spiral for MRI

The variable density sampling pattern proposed in Sec. 2.2.1 can be applied to MRI in k -space, leading to a reduced set of measurements. However, this method does not necessarily reduce the total scan time. For MRI applications that have limited scan time, like functional MRI, a single-shot spiral pattern can effectively cover the k -space within one repetition time (T_R) period [60].

Based on the proposed variable density sampling function $p_F(m, n)$, a single-shot spiral sampling pattern is designed which involves two steps. In the first step, starting from the origin of the k -space, the proposed spiral samples all the points within radius γ on the sampling grid. For a given threshold $0 < t_h < 1$, γ is set such that $p_F(m, n) > t_h$ for $\sqrt{m^2 + n^2} < \gamma$. In the second step, where $\sqrt{m^2 + n^2} \geq \gamma$, the trajectory of the spiral is described by the polar equation:

$$r(t) = \exp(bt^{a_F}), \quad \left(\frac{\ln \gamma}{b}\right)^{\frac{1}{a_F}} \leq t \leq \left(\frac{\ln \frac{N}{2}}{b}\right)^{\frac{1}{a_F}}, \quad (2.9)$$

where $b > 0$ and N is the size of the sampling grid in the k -space. The parameter t is sampled sufficiently so that the sampling points are continuously located along

the spiral and b is adjusted to obtain a desired number of samples. It is shown that $t_h = 0.8$ leads to spirals whose performance approximates those patterns generated from $p_F(m, n)$. Here it is assumed that the MRI gradient hardware is designed such that the slew-rate and amplitude constraints allow the sampling trajectory to move from one sampling point to its neighboring points on the sampling grid without any difficulty [61].

2.3 Sampling in the ordered DHT domain

Sampling in the ordered Discrete Hadamard Transform (DHT) domain is suitable for image sampling with hardware capable of representing binary measurement matrices since the basis images of 2D ordered DHT are binary. Furthermore, ordered DHT has fast transform algorithms. In ordered DHT, the atoms are ordered by the number of sign changes (zero crossing) between consecutive entries in a Hadamard atom [24]. Thus, ordered DHT can be regarded as a generalized class of DFT and more specifically, a binarized version of DCT sharing thus many properties of DFT and DCT [62].

To design the incoherent sampling pattern in the ordered DHT domain, we need to exploit the fact that ordered DHT can be regarded as a binary approximation of the DCT. For illustrative purposes, we first describe the spectrum characteristics of 1D wavelets in the DCT domain. Let $v_{k,l}(m)$, $0 \leq m \leq N - 1$ be the DCT of a 1D wavelet $\varphi_{k,l}(n)$, $n = 0, 1, \dots, N - 1$. Define the averaged DCT spectrum of wavelets at scale k as:

$$V(m)_k = \sum_{l=0}^{N2^{-k}-1} |v_{k,l}(m)|. \quad (2.10)$$

It can be shown that the DCT spectrum of wavelets at scale k has approximately the same shape as their Fourier spectra. The DCT spectrum band $\tilde{\mathcal{B}}_k$ of wavelets at scale k is $\tilde{\mathcal{B}}_k \approx [N2^{-k}, N2^{-k+1}]$. Similar to incoherent subband sampling in the Fourier domain, to reconstruct $\varphi_{k,l}$ from its DCT samples, we need to select the

DCT atoms randomly within the band $\tilde{\mathcal{B}}_k$. Now consider the incoherent sampling in the ordered DHT domain. We can define the averaged ordered DHT spectrum of wavelets at scale k as:

$$H(m)_k = \sum_{l=0}^{N2^{-k}-1} |h_{k,l}(m)|, \quad (2.11)$$

where $h_{k,l}(m)$, $0 \leq m \leq N-1$, is the ordered DHT of $\varphi_{k,l}(n)$. Since ordered DHT is a binary approximation of the DCT, $H(m)_k$ can be approximated as: $H(m)_k \approx V(m)_k$. Figure 2.1 shows $H(m)_k$ for $k = 1$ to 4 where $N = 256$ and the underlying wavelets are Daubechies-4 wavelets. The corresponding DCT spectrum at scale k is also shown. It can be seen that the averaged ordered DHT spectrum and the averaged DCT spectrum are similar, which indicates that the principles of sampling in the DCT domain should be equally applied to the sampling in the ordered DHT domain. The above analysis can be readily applied to 2D cases. Following a similar procedure to that described in Sec. 2.2.1, the variable density sampling function in the 2D ordered DHT domain is designed as follows:

$$p_H(m, n) = \exp \left[-\frac{(\sqrt{(\frac{m}{M})^2 + (\frac{n}{N})^2})^{a_H}}{\sigma_H^2} \right], \quad (2.12)$$

where $0 \leq m \leq M-1$, $0 \leq n \leq N-1$. σ_H depends on the number of samples and a_H depends on the desired decay of the sampling probability. The sampling patterns are then obtained as realizations of $p_H(m, n)$. As sampling in the DFT domain, the sampling ratio is a monotonically increasing function of σ_H and searching of σ_H for a desired number of measurements is straightforward. Similar to (2.8), an initial guess of σ_H can also be found. As in Fourier sampling, simulation results show that $a_H \approx 1.3 a$ leads to good image reconstruction. If an estimation of a is not available, then setting $a_H = 3.5$ is also recommended.

2.4 Evaluation of incoherence sampling

Undersampling in the transform domain inevitably brings aliasing interference in signal reconstruction. However, if the sampling is incoherent, the aliasing

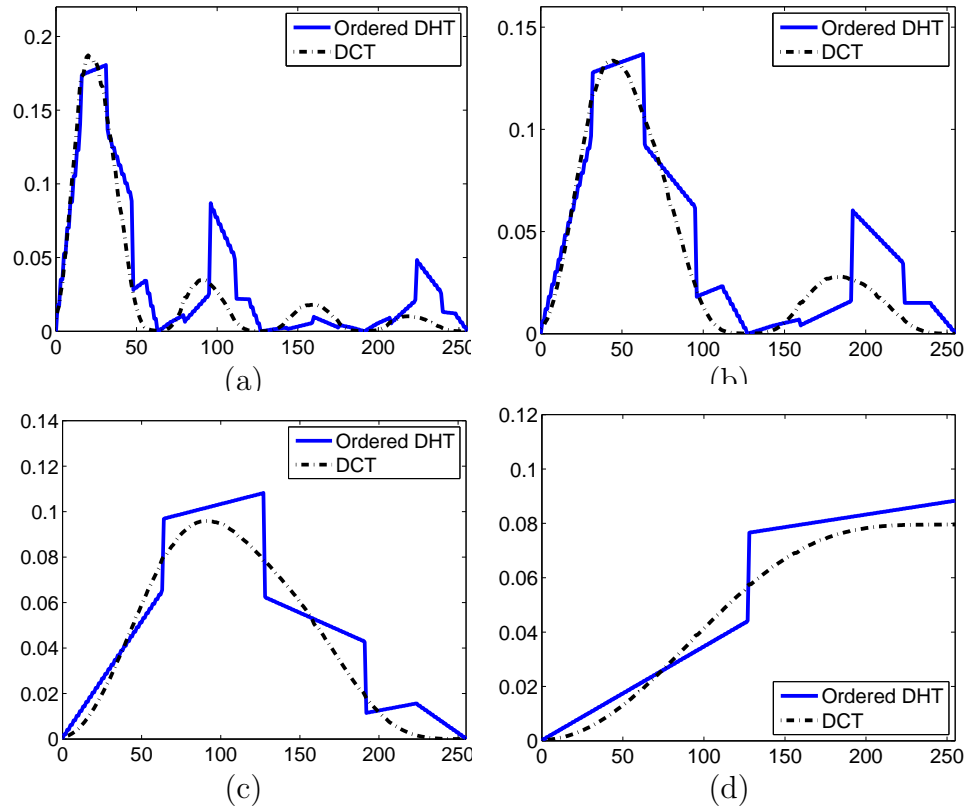


Figure 2.1: Ordered DHT and DCT spectra of Daubechies-4 wavelets. (a) at scale 4; (b) at scale 3; (c) at scale 2; (d) at scale 1.

interference has noise-like effect and can be removed by compressed sensing without degrading the image quality [22]. To evaluate the incoherent sampling patterns for natural images we consider the interference in the wavelet domain resulted from undersampling in the measurement transform domain Φ . To this end, we extend the TPSF analysis in [22] and incorporate the statistical model of signal distribution in the wavelet domain.

Let $w_{i,j}$, $(i,j) \in [0, N-1] \times [0, N-1]$, be the simplified notation of the (i,j) th 2D wavelet coefficient of a natural image that obeys the proposed model in Sec. 2.2. Incoherence is measured by the interference in the wavelet domain caused by the undersampling in Φ . Without loss of generality, let Φ_u be the undersampled ordered DHT operator and Φ_u^+ be the back-projection ordered DHT operator. Let Ψ be the sparse wavelet transform and $\Psi^{i,j}$ be the (i,j) th wavelet atom. For an image of size $N \times N$, we define a weighted TPSF as: $T_w^{i,j} = |w_{i,j}| \Psi \Phi_u^+ \Phi_u \Psi^{i,j}$. $T_w^{i,j}$ is the interference in the wavelet domain caused by the undersampling of $|w_{i,j}| \Psi^{i,j}$ in ordered DHT. $T_w^{i,j}$ is the distribution of the energy of $|w_{i,j}| \Psi^{i,j}$ to other wavelets through back-projection. A nonzero value of $T_w^{i,j}$ at $(m,n) \neq (i,j)$ means that the wavelet component at (m,n) suffers from the interference caused by the undersampling of the wavelet component at (i,j) . Note that if test image is available, $w_{i,j}$ can also be drawn from the test image directly. The incoherence of the sampling pattern can be evaluated by the following metric ξ defined as:

$$\xi = \frac{1}{N^2 \times N^2} \sum_{(i,j)} \sum_{(m,n)} |\tilde{T}_w^{i,j}(m,n)|^2, \quad (2.13)$$

where $\tilde{T}_w^{i,j}(m,n)$ is defined as: $\tilde{T}_w^{i,j}(m,n) = T_w^{i,j}(m,n)$ for $(m,n) \neq (i,j)$ and $\tilde{T}_w^{i,j}(m,n) = 0$ for $(m,n) = (i,j)$. ξ can effectively measure the strength of the aliasing interference. The smaller the ξ , the smaller the incoherent interference. As will be shown in the simulations, among several sampling patterns, ξ can be used to select the sampling pattern that yields the lowest incoherence interference.

2.5 Simulations

In this section, extensive simulations are provided to illustrate the effectiveness of the proposed methods. The selection of the design parameters are also discussed. In the simulations, all the images are assumed sparse in the Daubechies-8 wavelet domain and pixel values are within $[0, 1]$. It is also assumed that each measurement is corrupted by additive white Gaussian noise with variance $\sigma^2 = 1e^{-4}$. The BPDN algorithm is used for image reconstruction.

Table 2.1: Reconstruction of MRI images. The performance is measured by PSNR (dB). “P. VD” is the proposed variable density sampling; “P. SS” is the proposed single-shot spiral sampling; “P-E U.” is the phase-encodes undersampling.

| No. | P. VD | P. SS | Radial | Log-spiral | P-E U. |
|--------------------|--------------|-------|--------|------------|--------|
| <i>Brain</i> | | | | | |
| 5000 | 21.03 | 19.78 | 16.26 | 17.19 | 17.15 |
| 10000 | 23.86 | 22.45 | 19.55 | 20.58 | 20.46 |
| 15000 | 25.56 | 24.74 | 22.46 | 23.40 | 22.99 |
| 20000 | 27.23 | 26.51 | 24.68 | 25.97 | 24.73 |
| 25000 | 28.77 | 28.32 | 27.05 | 28.10 | 27.01 |
| <i>Angiography</i> | | | | | |
| 5000 | 23.68 | 22.32 | 19.87 | 20.34 | 21.27 |
| 10000 | 26.02 | 25.07 | 22.89 | 23.85 | 23.39 |
| 15000 | 27.85 | 27.38 | 25.30 | 26.10 | 25.70 |
| 20000 | 29.74 | 29.34 | 27.25 | 28.54 | 27.73 |
| 25000 | 31.34 | 31.09 | 29.18 | 30.39 | 29.61 |

In the first example, the proposed variable density sampling is applied to MRI image acquisition and reconstruction. The MRI images to be measured, *Brain* and *Angiography*, are of size 256×256 and are shown in Fig. 2.2(a) and Fig. 2.2(b), respectively. The estimated parameter a for each image is 2.32 and 2.47, respectively. The sampling patterns under investigation contains 15000 samples and there are 15000 real-valued measurements made along with each sampling pattern. Figure 2.2(c) shows the proposed single-shot spiral sampling pattern for fast MRI. The

parameters of the spiral trajectory is set as: $a_F = 3.5$, $t_h = 0.8$, $\gamma = 47$ and $b = 4.5 \times 10^{-11}$. To generate the spiral pattern with continuously located sampling points, the sampling interval along t is set as: $\Delta t = 0.007$. Figure 2.3(a) shows part of the reconstructed *Brain* image corresponding to the region within the white frame in Fig. 2.2(a). It is clear that with an undersampling ratio of 22.9%, the MRI image is reconstructed with only small distortion. Figure 2.2(d) shows an example of the sampling pattern generated directly from the proposed sampling function given by Eq. (2.7) with $a_F = 3.5$ and $\sigma_F = 0.134$, whose performance serves as a benchmark for the proposed spiral patterns. The corresponding reconstructed image is shown in Fig. 2.3(b), which contains less distortion than Fig. 2.3(a).

To compare the proposed sampling patterns with other practical sampling patterns, we also reconstruct the MRI image from samples taken from radial sampling pattern, logarithmic spiral sampling pattern and random phase-encodes undersampling pattern shown in Fig. 2.4(a), Fig. 2.4(b) and Fig. 2.4(c), respectively. The random phase-encodes undersampling is restricted to undersampling of the phase-encodes and fully sampled readouts and the sampling density scales according to a power of distance [23]. The corresponding reconstructed MRI images for the above sampling patterns are shown in Fig. 2.5(a), Fig. 2.5(b) and Fig. 2.5(c), respectively. All reconstructed MRI images show more low frequency interference and the image qualities are not as good as that of the proposed single-shot spiral sampling pattern.

Table 2.1 summarizes more extensive simulation results for the MRI test images reconstruction with different sampling patterns, where the number of measurements ranges from 5000 to 25000 (undersampling ratio from 7.63% to 38.12%). The quality of the reconstructed images is measured by the peak signal to noise ratio (PSNR) and the data are collected from an average of ten runs. The results of the sampling patterns generated directly from the proposed sampling functions serve as the benchmarks and among all the sampling patterns, the best result is highlighted

in bold font in each test set. The simulations again show that the proposed single-shot spiral sampling patterns consistently have better performance than other fast sampling patterns. The performance gain is $2 \sim 3$ dB at $J = 5000$ and $0.2 \sim 0.7$ dB at $J = 25000$ for both images. Furthermore, the difference in performance between the proposed single-shot spiral patterns and the sampling patterns generated from the proposed sampling density function is small.

In the second example, the proposed sampling method is applied to the acquisition and reconstruction of a set of natural images: *boat*, *Lena*, *Goldhill*, *baboon* and *Pentagon* with size 256×256 . The estimated parameter a for each images is estimated as: 2.65, 2.88, 2.32, 2.64, 2.27 and 2.05, respectively. Figure 2.6(b) shows a sampling pattern in the ordered DHT domain that contains 20000 sampling points generated from Eqn. (2.12) with $a_H = 3.5$ and $\sigma_H = 0.501$. Part of the reconstructed *boat* image corresponding to the region within the white frame in Fig. 2.6(a) is shown in Fig. 2.7(a), which shows that the reconstruction contains little distortion.

For comparison purposes, we also reconstruct the *boat* image from the samples taken from the radial sampling pattern and logarithmic spiral sampling pattern shown in Fig. 2.6(c) and Fig. 2.6(d), respectively. The number of measurements taken from both sampling patterns are the same as that of the proposed sampling pattern. Part of the corresponding reconstructed images are shown in Fig. 2.7(b) and Fig. 2.7(c), respectively. Again, both reconstructed images show more aliasing artifacts, which indicates that they are not as effective as the proposed sampling pattern.

Simulation results are summarized in Table 2.2, where the number of measurements ranges from 5000 to 25000 and the best results as the average of ten runs is also highlighted. For each test image, it is shown that the proposed variable density sampling achieves much better performance than logarithmic spiral patterns and radial patterns. The performance gain is $2 \sim 4$ dB at $J = 5000$ and $0.5 \sim 0.8$

dB at $J = 25000$. To verify that the proposed sampling pattern, which exploits the *a priori* information of natural images, achieves better performance than methods that do not exploit the *a priori* information, the simulation results using the Noiselet ensemble, SFE and SBHE under different number of measurements are also presented in Table 2.2. To acquire the image information, samples of the Noiselets, SFE and SBHE are taken randomly. The proposed sampling method achieves the best performance in all simulations. For illustrative purposes, Fig. 2.7(d) shows the reconstructed result for image *boat* using SBHE. Such comparison clearly shows the performance gain achieved by exploiting the *a priori* information.

The incoherence of the proposed sampling patterns can also be evaluated by using the proposed incoherence metric proposed in this thesis. We test three sampling patterns in the ordered DHT domain using the image “*Boat*” and take 5000 measurements. The incoherence metrics are 0.0034, 0.0062 and 0.0078 for the proposed variable density sampling pattern, radial sampling pattern and logarithmic spiral sampling pattern, respectively. The lowest metric value is yielded by the proposed variable density sampling pattern leading to the least aliasing interference, which, in turn, is in accordance with the best reconstruction performance.

Next, we show that the reconstruction performance is not sensitive to the parameters a_F or a_H in the sampling functions. Here, we test the reconstruction performance as the parameter a_H changes. Figure 2.8 shows the reconstruction results of all test images with 20000 number of measurements. Data is collected as the result of 20 runs. Each test image has different curves and textures, thus has different statistical model parameters. The sampling patterns are constructed with a_H ranging from 0.5 to 6. It shows that the sampling patterns lead to similar performance for all the images when a_H ranges from 2.5 to 4.5. The difference of performance measured by PSNR is within 0.4 dB. Thus, the image reconstruction is robust to variations over a_H . An empirical rule for the selection of a_H is $a_H = 1.3 a$.

If the estimation of a is not available, then set $a_H = 3.5$ is recommended since $a_H = 3.5$ lies in the middle of the flat region shown in Fig. 2.8. Note that the reconstruction performance tends to become worse as a_H increases. Since larger a_H means more low frequency samples are taken, the simulation shows that sampling only low frequency components is not a good strategy.

Figure 2.9 shows the simulation results of image recovery using min-TV. For illustrative purposes, only the following sampling schemes are considered: the proposed variable density sampling, logarithmic spiral sampling and SBHE [21]. The simulation results show that the proposed variable density sampling again achieves the best performance, which is more obvious when the sampling ratio is low. It can be concluded that the advantages of using the proposed variable density sampling does not depend on a specific reconstruction algorithm.

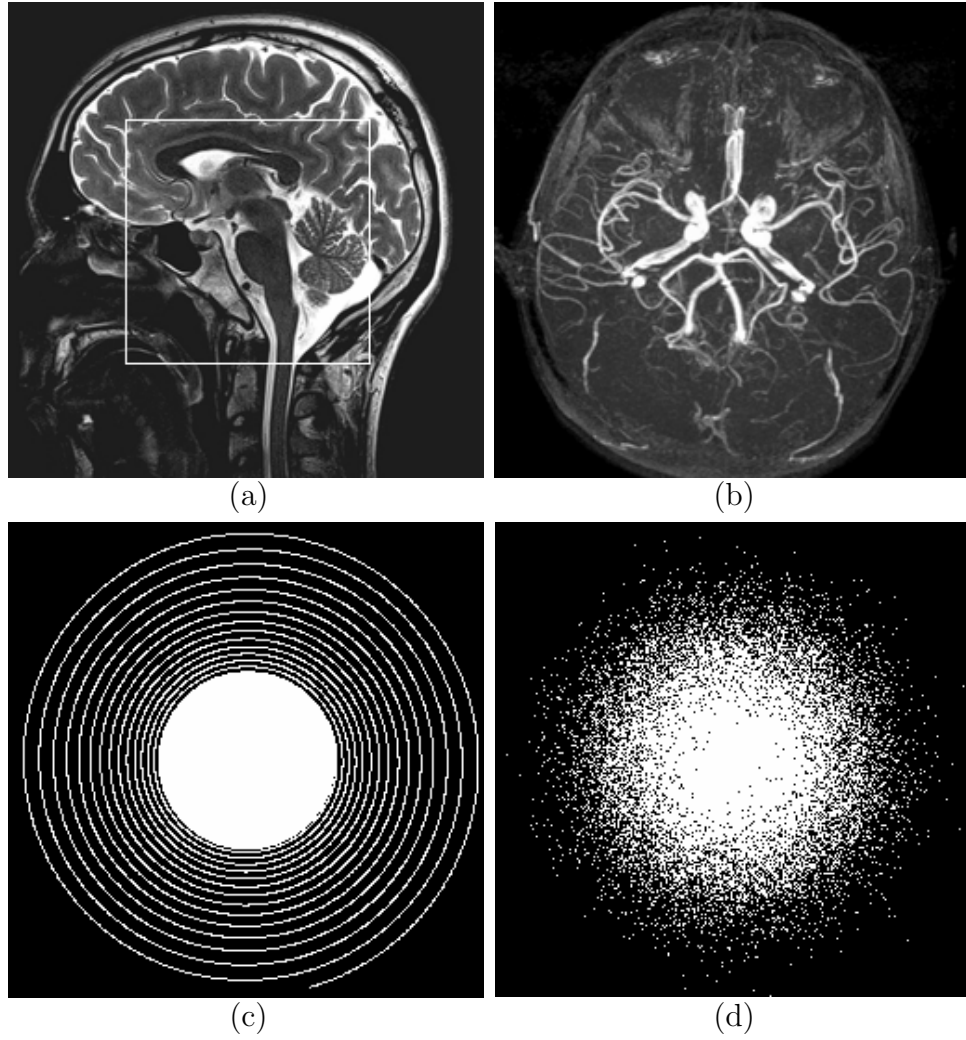


Figure 2.2: The original MRI images: (a) *Brain*; (b) *Angiography*. (c) Proposed single-shot spiral sampling pattern. (d) Proposed variable density sampling pattern. Each sampling pattern has a 22.9% undersampling ratio.

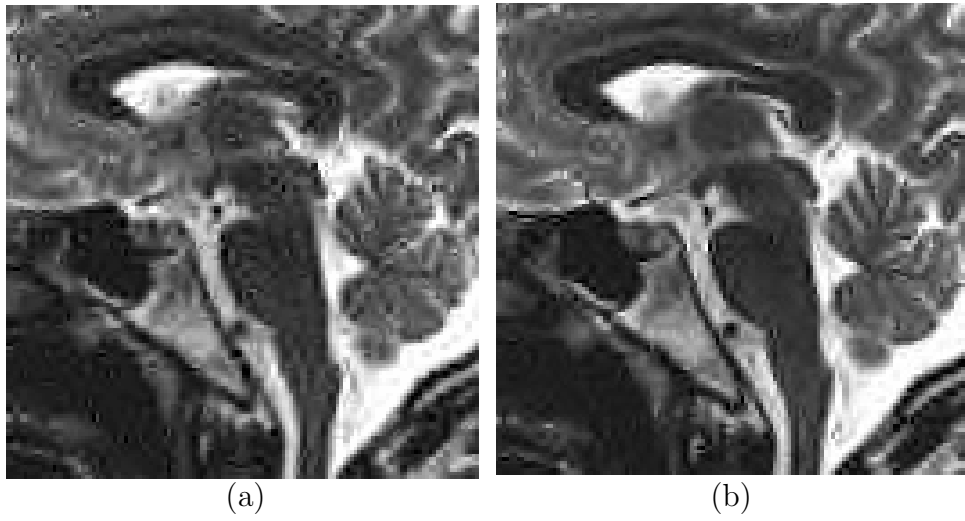


Figure 2.3: Part of the reconstructed image with (a) proposed spiral sampling pattern; (b) proposed variable density sampling pattern; See Table 2.1 for corresponding PSNR.

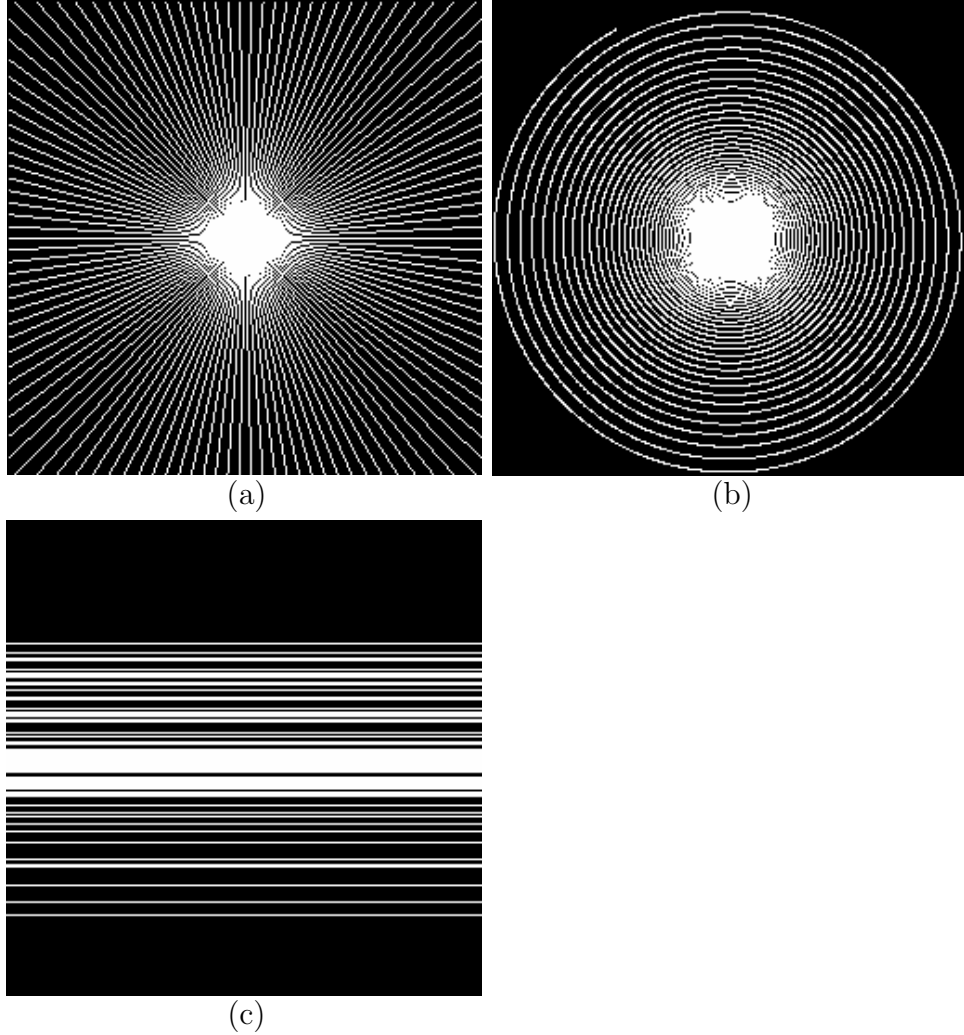


Figure 2.4: (a) Radial sampling pattern. (b) Logarithmic spiral pattern. (c) Random phase-encoded undersampling pattern. Each sampling pattern has a 22.9% undersampling ratio.

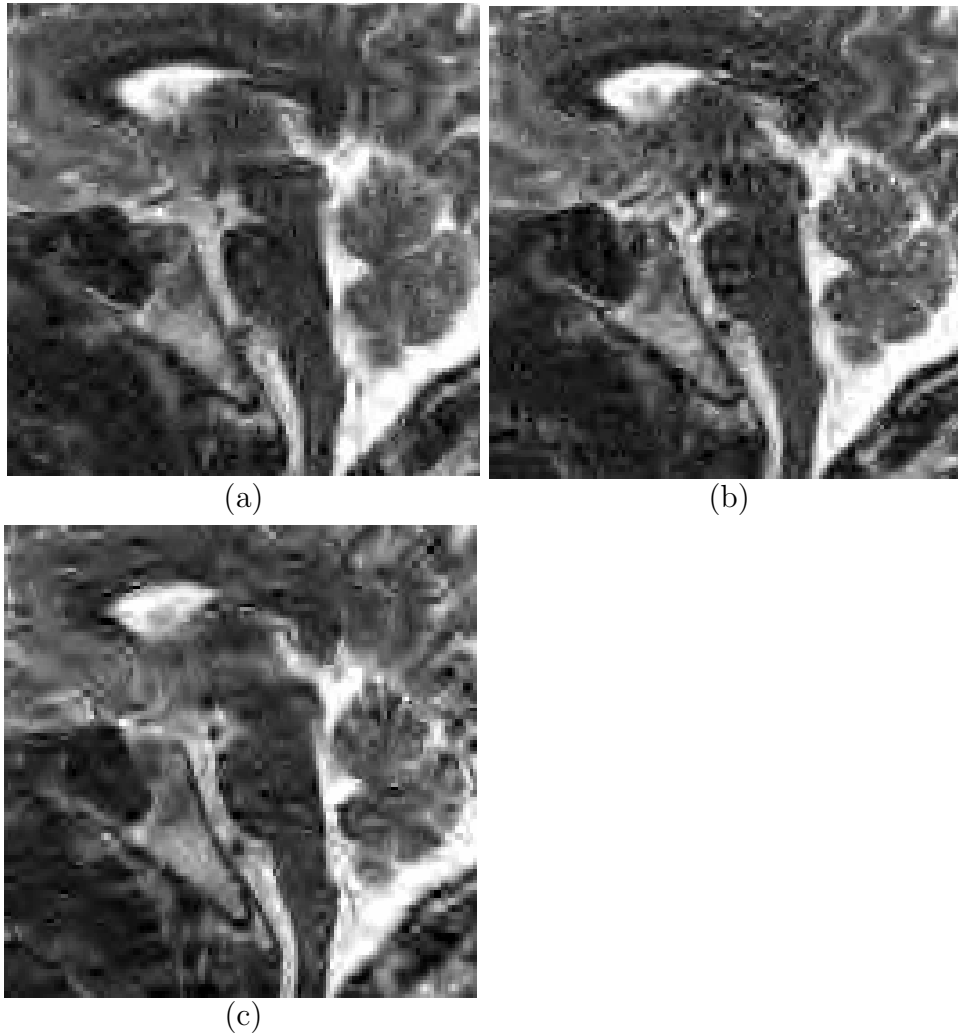


Figure 2.5: Reconstruction of (a) radial sampling pattern; (b) logarithmic spiral pattern. (c) random phase-encodes undersampling pattern. See Table 2.1 for corresponding PSNR.

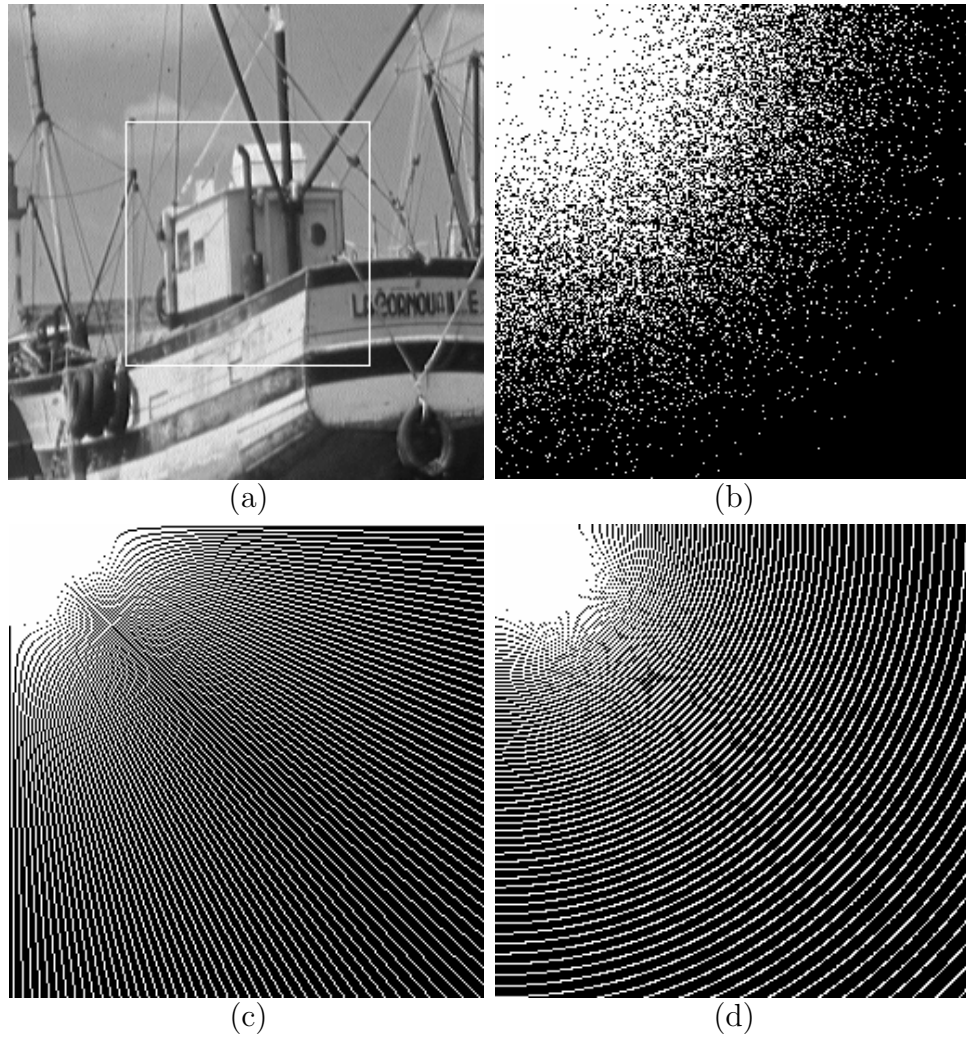


Figure 2.6: (a) The original image *Boat*. (b) Proposed variable density sampling pattern. (c) Radial sampling pattern. (d) Logarithmic spiral sampling pattern. Each sampling pattern has a 30.5% undersampling ratio.

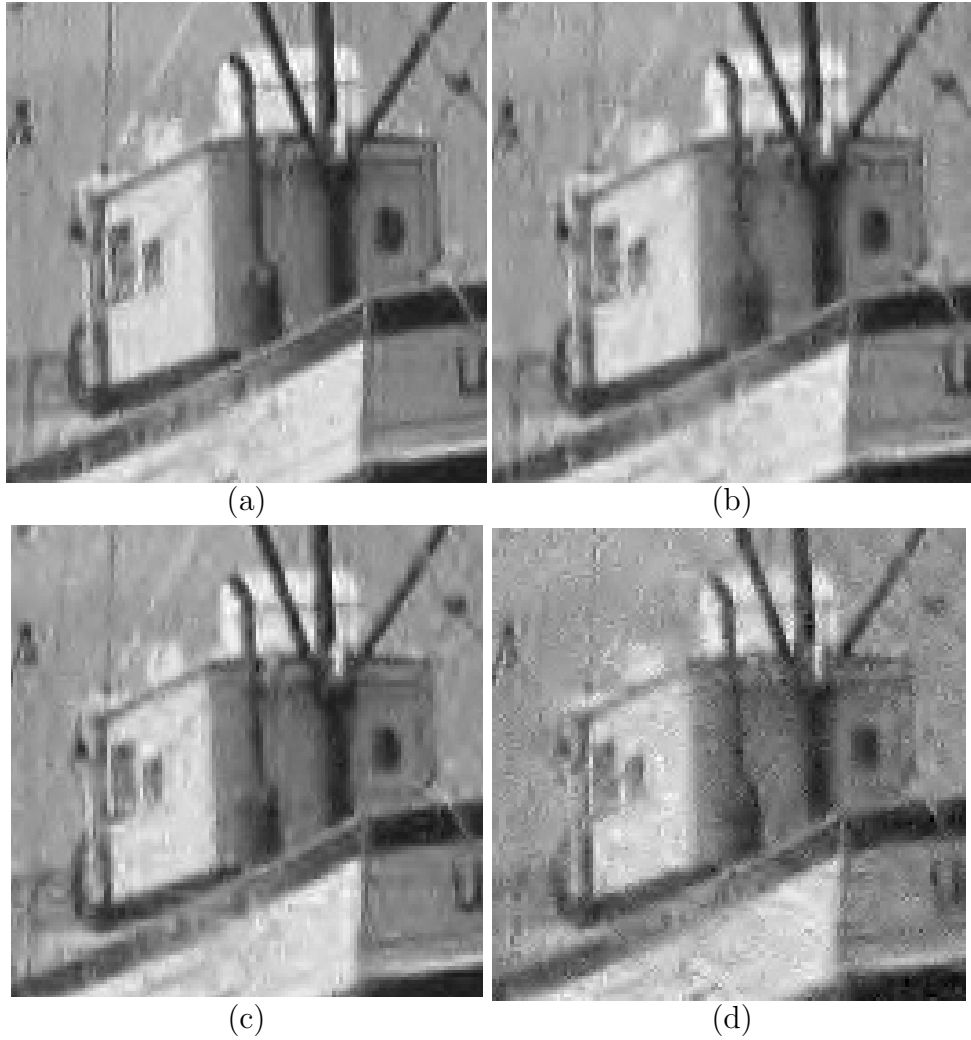


Figure 2.7: Part of the reconstructed image with (a) proposed variable density sampling pattern; (b) radial sampling pattern; (c) logarithmic spiral pattern; (d) SBHE. See Table 2.2 for corresponding PSNR.

Table 2.2: Reconstruction of images in ordered DHT domain. The performance is measured by PSNR (dB). “P. VD” is the proposed variable density sampling.

| No. | P. VD | Radial | Log-spiral | Noiselet | SFE | SBHE |
|-----------------|--------------|--------|------------|----------|-------|-------|
| <i>boat</i> | | | | | | |
| 5000 | 22.75 | 19.88 | 19.79 | 18.51 | 19.27 | 18.62 |
| 10000 | 24.93 | 22.93 | 22.77 | 20.78 | 21.39 | 20.74 |
| 15000 | 26.70 | 25.09 | 25.03 | 22.67 | 23.25 | 22.69 |
| 20000 | 28.36 | 26.96 | 26.95 | 24.19 | 24.93 | 24.56 |
| 25000 | 29.55 | 28.79 | 28.64 | 25.58 | 26.27 | 26.18 |
| <i>Lena</i> | | | | | | |
| 5000 | 25.51 | 21.28 | 21.51 | 20.14 | 21.25 | 20.05 |
| 10000 | 27.91 | 25.33 | 25.49 | 23.10 | 23.87 | 23.10 |
| 15000 | 29.77 | 28.24 | 28.04 | 25.06 | 25.77 | 25.45 |
| 20000 | 31.24 | 30.07 | 29.91 | 26.76 | 27.56 | 27.43 |
| 25000 | 32.57 | 31.82 | 31.54 | 28.48 | 29.17 | 29.01 |
| <i>Goldhill</i> | | | | | | |
| 5000 | 24.96 | 22.14 | 21.24 | 20.58 | 21.31 | 20.38 |
| 10000 | 27.09 | 25.14 | 24.80 | 22.89 | 23.36 | 22.81 |
| 15000 | 28.84 | 25.82 | 26.96 | 24.59 | 25.10 | 24.73 |
| 20000 | 30.18 | 27.30 | 28.67 | 25.98 | 26.59 | 26.52 |
| 25000 | 31.26 | 30.63 | 29.88 | 27.37 | 27.93 | 27.94 |
| <i>baboon</i> | | | | | | |
| 5000 | 22.47 | 21.09 | 20.93 | 19.59 | 20.16 | 19.48 |
| 10000 | 23.32 | 22.55 | 22.57 | 21.08 | 21.36 | 20.91 |
| 15000 | 24.31 | 23.46 | 23.64 | 22.12 | 22.33 | 22.01 |
| 20000 | 25.30 | 24.60 | 24.67 | 23.04 | 23.36 | 23.05 |
| 25000 | 26.40 | 25.92 | 25.82 | 23.88 | 24.31 | 24.15 |
| <i>pentagon</i> | | | | | | |
| 5000 | 24.78 | 22.59 | 22.69 | 21.37 | 21.95 | 21.32 |
| 10000 | 26.32 | 24.75 | 24.69 | 22.92 | 23.36 | 22.79 |
| 15000 | 27.61 | 26.32 | 26.19 | 24.33 | 24.54 | 24.17 |
| 20000 | 28.88 | 27.79 | 27.75 | 25.32 | 25.66 | 25.50 |
| 25000 | 29.86 | 28.13 | 28.97 | 26.22 | 26.87 | 26.77 |

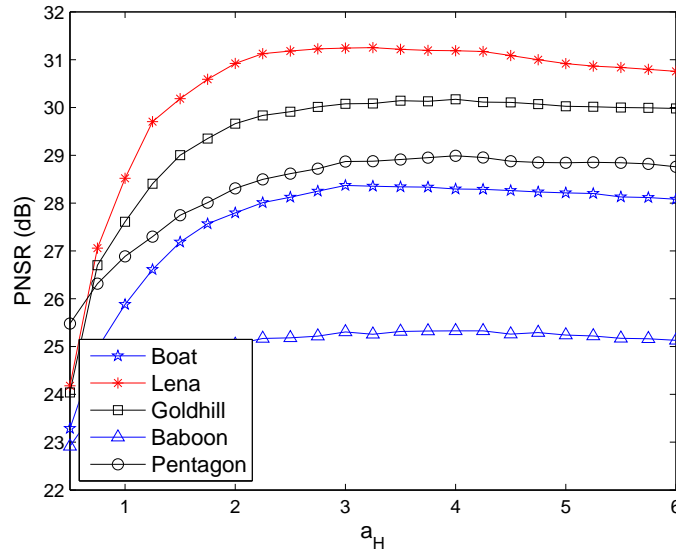


Figure 2.8: Reconstruction results of images from proposed sampling patterns generated by different a_H with 20000 number of measurements.

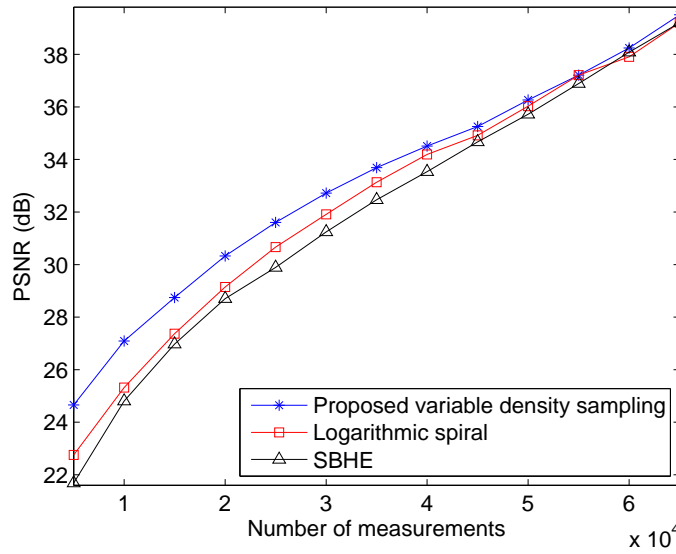


Figure 2.9: Reconstruction results for image “Boat” using min-TV algorithm with quadratic constraints.

Chapter 3

ADAPTIVE SUBSPACE COMPRESSIVE DETECTION FOR SPARSE SIGNALS

3.1 Motivation

We motivate the design of subspace compressive detectors by targeting the following application: detection of a known sparse signal with a data acquisition strategy where the objective is to reduce the number of measurements for a given detection performance. Here we assume an explicit subspace linear model for the sparse signal \mathbf{x} of length N . The K vectors of Ψ construct an $N \times K$ matrix $\mathbf{H} = [\underline{\psi}_{n_1}, \underline{\psi}_{n_2}, \dots, \underline{\psi}_{n_K}]$, where $n_i \in \{1, 2, \dots, N\}$ for $i = 1, \dots, K$. The signal \mathbf{x} is represented as $\mathbf{x} = \mathbf{H}\underline{\theta}$, where $\underline{\theta}$ is a $K \times 1$ vector with all non-zero entries. However, since a general data acquisition strategy is desirable, we do not assume that we have complete knowledge of \mathbf{x} at the time of acquisition. Signal templates are provided when making detection decisions. Without any other *a priori* information, it is also assumed that the signal energy is uniformly distributed over its entire subspace.

We first review the traditional approach that obtains measurements by directly sampling the received signal. Assume Nyquist sampling is achievable, then the detection problem is to distinguish between two hypotheses \mathcal{H}_0 and \mathcal{H}_1 :

$$\begin{aligned}\mathcal{H}_0 &: \mathbf{y} = \mathbf{w}, \\ \mathcal{H}_1 &: \mathbf{y} = \mathbf{x} + \mathbf{w},\end{aligned}\tag{3.1}$$

where $\mathbf{w} \sim \mathcal{N}(\mathbf{0}, \sigma^2 \mathbf{I}_N)$ is Gaussian noise. The probability of detection, denoted by P_d , is the probability of choosing \mathcal{H}_1 when \mathcal{H}_1 is true. The probability of false

alarm, denoted by P_f , is the probability of choosing \mathcal{H}_1 when \mathcal{H}_0 is true. According to the Neyman-Pearson (NP) criterion, the optimum decision strategy maximizes P_d while keeping P_f under a certain value [29]. It is well known that the optimal detector is the matched filter given by [29]:

$$t(\mathbf{y}) = \langle \mathbf{y}, \mathbf{x} \rangle. \quad (3.2)$$

$t(\mathbf{y})$ is a sufficient statistic which contains all the information relevant for the detection problem. It can be shown that the performance of the matched filter is given by [29]:

$$P_d = Q \left[Q^{-1}(P_f) - \sqrt{\frac{\mathbf{x}^T \mathbf{x}}{\sigma^2}} \right], \quad (3.3)$$

where $Q(x) \triangleq (2\pi)^{-\frac{1}{2}} \int_x^\infty e^{-x^2/2} dx$. Although the detection performance is optimal, this method would require fully sampled data, which puts high demanding requirements on sampling, post-processing and storage resources. Although such requirements can be lowered down by downsampling, the detection performance is generally not guaranteed.

The second approach which also provides a general data acquisition strategy is the compressive detector proposed in [25], which works directly on a reduced set of $M \leq N$ compressive measurements. The detection problem is to distinguish between two hypotheses \mathcal{H}_0 and \mathcal{H}_1 :

$$\begin{aligned} \mathcal{H}_0 & : \tilde{\mathbf{y}} = \Phi \mathbf{w}, \\ \mathcal{H}_1 & : \tilde{\mathbf{y}} = \Phi(\mathbf{x} + \mathbf{w}), \end{aligned} \quad (3.4)$$

where Φ is an $M \times N$ random measurement matrix with each entry taken from an i.i.d. random distribution. Without loss of generality, we assume that each entry of Φ obeys a zero-mean Gaussian distribution with variance $1/M$. The sufficient statistic is given by:

$$t(\tilde{\mathbf{y}}) = \tilde{\mathbf{y}}^T (\Phi \Phi^T)^{-1} \Phi \mathbf{x}, \quad (3.5)$$

and the performance of the compressive detector can be approximated as [25]:

$$P_d \approx Q \left[Q^{-1}(P_f) - \sqrt{M/N} \sqrt{\frac{\mathbf{x}^T \mathbf{x}}{\sigma^2}} \right]. \quad (3.6)$$

In the following, a derivation of (3.6) is provided below by invoking the central limit theorem. It can be shown that the performance of the compressive detector is:

$$P_d = Q \left[Q^{-1}(P_f) - \sqrt{\frac{\mathbf{x}^T \mathbf{P}_\Phi \mathbf{x}}{\sigma^2}} \right], \quad (3.7)$$

where

$$\mathbf{P}_\Phi = \Phi^T (\Phi \Phi^T)^{-1} \Phi. \quad (3.8)$$

We derive an approximation of (3.7) that has been presented in [25] by invoking the central limit theorem. Same approximation method is applied to the approximation of the proposed subspace compressive detection performance. Let $\mathbf{A} = \Phi \Phi^T$ and let Φ_j be the transpose of the j th row of Φ , then each entry of \mathbf{A} can be represented as: $\mathbf{A}_{ij} = \Phi_i^T \Phi_j$. The distribution of the diagonal entry \mathbf{A}_{ii} , for $i = 1, \dots, M$ is $\mathbf{A}_{ii} \sim (1/M) \chi_N^2$ with mean and variance:

$$\mathbb{E}(\mathbf{A}_{ii}) = N/M, \quad (3.9)$$

$$\text{var}(\mathbf{A}_{ii}) = 2N/M^2, \quad (3.10)$$

where χ_N^2 denoting a central chi-squared distribution with N degrees of freedom. If N is sufficiently large, the off-diagonal entries \mathbf{A}_{ij} , for $i \neq j$, can be approximated as a Gaussian variable with mean and variance:

$$\mathbb{E}(\mathbf{A}_{ij}) = 0, \quad (3.11)$$

$$\text{var}(\mathbf{A}_{ij}) = N/M^2. \quad (3.12)$$

Thus if M is also sufficiently large, \mathbf{A} can be approximated as: $\mathbf{A} \approx N/M \mathbf{I}_{M \times M}$, leading to the following approximation:

$$\mathbf{x}^T \mathbf{P}_\Phi \mathbf{x} \approx M/N \|\Phi \mathbf{x}\|_2. \quad (3.13)$$

It has been shown that, with high probability, the random measurement matrix Φ satisfies the restricted isometry property (RIP) and is proved to be a stable embedding of K -sparse signals for M sufficiently large [25, 26, 14]. That is,

$$(1 - \epsilon)\|\mathbf{x}\|_2 \leq \|\Phi\mathbf{x}\|_2 \leq (1 + \epsilon)\|\mathbf{x}\|_2, \quad (3.14)$$

for $\epsilon > 0$ sufficiently small. Thus, the detection performance can be approximated as [25]:

$$P_d \approx Q \left[Q^{-1}(P_f) - \sqrt{M/N} \sqrt{\frac{\mathbf{x}^T \mathbf{x}}{\sigma^2}} \right]. \quad (3.15)$$

It is clear that the detection performance depends on the signal energy that the detector can collect, which is approximately proportional to the number of measurements. Since $M/N \leq 1$, the compressive detector suffers from lower probability of detection with reduced number of measurements. As an example, the number of measurement which is 50% of the full sampled signal length would lead to a performance degradation equivalent to 3 dB loss in signal energy to noise ratio (ENR) defined as $\mathbf{x}^T \mathbf{x} / \sigma^2$.

To improve the detecting performance with compressive measurements, we exploit the fact that a sparse signal resides in a low dimension subspace and we can capture most of the signal energy with as few as K measurements just by projecting the signal into its own subspace. Furthermore, the information of the signal subspace can be inferred from known signal characteristics or learned from training data. To this end, we assume that at the time of acquisition, we know the signal subspace or we know the matrix \mathbf{H} . However, we should not assume that we can always obtain as many as K measurements. On one hand, K could be a pretty large number for a practical signal with large dimension. On the other hand, the number of measurements can be further constrained by limited hardware complexity, as in a parallel integration-dump structure, or constrained by limited acquisition time, such as in the detection of a high speed object by single-pixel camera [2, 3]. Thus,

we consider broad applications where only $M \leq K$ measurements are available. We design the subspace measurement matrix as follows:

$$\bar{\Phi} = \mathbf{G}(\mathbf{H}^T \mathbf{H})^{-1} \mathbf{H}^T, \quad (3.16)$$

where \mathbf{G} is an $M \times K$ random matrix with $M \leq K$ where each entry of \mathbf{G} is taken from an i. i. d. random distribution. The detection problem reduces then to distinguish between two hypotheses \mathcal{H}_0 and \mathcal{H}_1 :

$$\begin{aligned} \mathcal{H}_0 &: \bar{\mathbf{y}} = \bar{\Phi} \mathbf{w}, \\ \mathcal{H}_1 &: \bar{\mathbf{y}} = \bar{\Phi}(\mathbf{x} + \mathbf{w}). \end{aligned} \quad (3.17)$$

It is easy to show that the sufficient statistic is given by:

$$t(\bar{\mathbf{y}}) = \bar{\mathbf{y}}^T (\bar{\Phi} \bar{\Phi}^T)^{-1} \bar{\Phi} \mathbf{x} = \bar{\mathbf{y}}^T [\mathbf{G}(\mathbf{H}^T \mathbf{H})^{-1} \mathbf{G}^T]^{-1} \mathbf{G} \underline{\boldsymbol{\theta}}, \quad (3.18)$$

and the detector performance is then given by:

$$P_d = Q \left[Q^{-1}(P_f) - \sqrt{\frac{\mathbf{x}^T \mathbf{P}_{\bar{\Phi}} \mathbf{x}}{\sigma^2}} \right], \quad (3.19)$$

where

$$\mathbf{P}_{\bar{\Phi}} = \bar{\Phi}^T (\bar{\Phi} \bar{\Phi}^T)^{-1} \bar{\Phi}. \quad (3.20)$$

Note that as in CS, each measurement here is equally important in probability. To reveal the tradeoff between the detection performance and the number of measurements, we assume, without loss of generality, that \mathbf{H} is drawn from an orthonormal basis and each entry of \mathbf{G} follows a Gaussian distribution with zero mean and variance $1/M$. Then, $\mathbf{x}^T \mathbf{P}_{\bar{\Phi}} \mathbf{x}$ can be represented as:

$$\begin{aligned} \mathbf{x}^T \mathbf{P}_{\bar{\Phi}} \mathbf{x} &= \mathbf{x}^T \bar{\Phi}^T (\bar{\Phi} \bar{\Phi}^T)^{-1} \bar{\Phi} \mathbf{x} \\ &= \underline{\boldsymbol{\theta}}^T \mathbf{G}^T [\mathbf{G} \mathbf{G}^T]^{-1} \mathbf{G} \underline{\boldsymbol{\theta}}. \end{aligned} \quad (3.21)$$

Following the analysis described in the derivation of (3.6) with central limit theorem, we can obtain the following approximation $\mathbf{G}\mathbf{G}^T \approx K/M\mathbf{I}_{K \times K}$ for $K, M \gg 1$. Thus $\mathbf{x}^T \mathbf{P}_{\bar{\phi}} \mathbf{x}$ can be further approximated as:

$$\mathbf{x}^T \mathbf{P}_{\bar{\phi}} \mathbf{x} \approx (M/K) \underline{\theta}^T \mathbf{G}^T \mathbf{G} \underline{\theta}. \quad (3.22)$$

Let $\mathbf{D} = \mathbf{G}^T \mathbf{G}$ and let \mathbf{g}_j be the j th column of \mathbf{G} , then each entry of \mathbf{D} can be represented as: $\mathbf{D}_{ij} = \mathbf{g}_i^T \mathbf{g}_j$. Furthermore,

$$\underline{\theta}^T \mathbf{G}^T \mathbf{G} \underline{\theta} = \sum_{i=1}^K \sum_{j=1}^K \theta_i \mathbf{D}_{ij} \theta_j. \quad (3.23)$$

The diagonal entries \mathbf{D}_{ii} , for $i = 1, \dots, K$ follow a chi-squared distribution with mean and variance:

$$\mathbb{E}(\mathbf{D}_{ii}) = 1, \quad (3.24)$$

$$\text{var}(\mathbf{D}_{ii}) = 2/M. \quad (3.25)$$

If K is sufficiently large, the off-diagonal entries of \mathbf{D} can be approximated as a Gaussian variable with mean and variance:

$$\mathbb{E}(\mathbf{D}_{ij}) = 0, \quad (3.26)$$

$$\text{var}(\mathbf{D}_{ij}) = 1/M. \quad (3.27)$$

Thus, if M is large enough, to get an approximation of (3.23), we can ignore the off-diagonal entries of \mathbf{D} and approximate the diagonal entries as 1 reaching the following approximation:

$$\underline{\theta}^T \mathbf{G}^T \mathbf{G} \underline{\theta} \approx \sum_{i=1}^k \theta_i \mathbf{D}_{ii} \theta_i \approx \mathbf{x}^T \mathbf{x}. \quad (3.28)$$

Finally, the detector performance can be approximated as:

$$P_d \approx Q \left[Q^{-1}(P_f) - \sqrt{M/K} \sqrt{\frac{\mathbf{x}^T \mathbf{x}}{\sigma^2}} \right]. \quad (3.29)$$

The approximation of P_d by (3.29) also holds when ψ_i in Ψ has unit energy and are only approximately orthogonal to each other. Note that (3.29) is only a coarse approximation and a randomly selected matrix \mathbf{G} may lead to worse results than expected by (3.29), especially if $\underline{\theta}$ is located in the null space of \mathbf{G} . However, the sparsity K of many practical signals is not a trivial number and may be on the order of 10^2 or more [19]. Usually the number of measurements M is also much larger than 1. Thus, with high probability, the detection performance is closely concentrated around its expected performance. For a sequence of detection operations, one realization of \mathbf{G} can be selected for each detection to avoid the worst scenario.

Compared with (3.6), the proposed detector improves the detection performance with the same number of measurements by exploiting the signal subspace. The design of $\bar{\Phi}$ is to project the noisy data $\bar{\mathbf{y}}$ into the signal subspace first and then project the result onto random basis. By projecting the noisy data into signal subspace, there is no loss of signal energy. However, the noise power is significantly reduced. Thus, good detection performance is expected even with a small number of measurements. Furthermore, much like the compressive detector provides an universal detection scheme for signals in the N -dimensional space, the subspace compressive detector exploiting the linear signal model provides an universal detection scheme for all signals in the same subspace. The introduction of the random matrix \mathbf{G} makes the detector robust to magnitude variations over $\underline{\theta}$.

In (3.16), \mathbf{G} seems to be redundant if the number of measurement matches the signal sparsity. That is: $M = K$. However, from the hardware implementation aspect, a random matrix \mathbf{G} with size $M \times M$ is still desirable since adding of the random matrix \mathbf{G} leads to measurements equally important in probability. Thus, if any measurement goes wrong, it will not lead to severe performance degradation. Without \mathbf{G} , what is measured are the signal transform coefficients. Since failing to

measure a large coefficient may lead to wrong detection results, such transform based detection is not robust. Another advantage of introducing \mathbf{G} lies in its robustness to quantization which is inevitable in hardware implementation. If \mathbf{H} is drawn from an orthonormal basis, then each entry of $\bar{\Phi}$ belongs to the same Gaussian distribution. Thus, optimal quantization based on Gaussian distribution can be employed [51].

The design of the subspace compressive detector above was motivated for the detection of a known sparse signal. The performance improvement by exploiting additional signal information can be easily manifested by comparing with that of the compressive detector [25]. The main focus of this thesis, however, is the design of subspace compressive detectors for the detection of an unknown sparse signal. We assume that the information of signal subspace can be obtained as *a priori* or learned from the compressive measurements of training data [2].

3.2 Detection of Unknown Sparse Signal

3.2.1 Subspace Compressive Detection

In many practical applications, the signal to be detected is unknown or has unknown parameters. Clearly in such cases, a simple detector like a matched filter is not available. In the following, it is assumed that in the signal sparsity model, $\underline{\theta}$ is unknown but \mathbf{H} is available. We apply the design of subspace measurement matrix to the detection of an unknown sparse signal.

Let $\mathbf{a} = \bar{\Phi}\mathbf{H}\underline{\theta}$ and $\bar{\mathbf{C}} = \sigma^2\bar{\Phi}\bar{\Phi}^T$, where $\bar{\Phi}$ is the subspace measurement matrix designed according to (3.16). With the same hypothesis testing problem (3.17), the decision strategy is given by the generalized likelihood ratio test (GLRT) [29]:

$$L(\bar{\mathbf{y}}) = \frac{p(\bar{\mathbf{y}}; \hat{\mathbf{a}}, \mathcal{H}_1)}{p(\bar{\mathbf{y}}; \mathcal{H}_0)} \underset{\mathcal{H}_0}{\overset{\mathcal{H}_1}{\gtrless}} \gamma, \quad (3.30)$$

where $\hat{\mathbf{a}}$ is the maximum likelihood estimation (MLE) of \mathbf{a} under \mathcal{H}_1 . It is easy to

show that the probability density function (PDF) of $\bar{\mathbf{y}}$ under \mathcal{H}_0 is given by:

$$p(\bar{\mathbf{y}}; \mathcal{H}_0) = \frac{1}{(2\pi)^{\frac{M}{2}} \det^{\frac{1}{2}}(\bar{\mathbf{C}})} \exp\left[-\frac{1}{2}\bar{\mathbf{y}}^T \bar{\mathbf{C}}^{-1} \bar{\mathbf{y}}\right], \quad (3.31)$$

and the PDF of $\bar{\mathbf{y}}$ under \mathcal{H}_1 is given by:

$$p(\bar{\mathbf{y}}; \hat{\mathbf{a}}, \mathcal{H}_1) = \frac{1}{(2\pi)^{\frac{M}{2}} \det^{\frac{1}{2}}(\bar{\mathbf{C}})} \exp\left[-\frac{1}{2}(\bar{\mathbf{y}} - \hat{\mathbf{a}})^T \bar{\mathbf{C}}^{-1} (\bar{\mathbf{y}} - \hat{\mathbf{a}})\right]. \quad (3.32)$$

In (3.30), γ is a threshold chosen to achieve a desired probability of false alarm.

Thus, \mathcal{H}_1 is selected if $L(\bar{\mathbf{y}}) > \gamma$, otherwise \mathcal{H}_0 is chosen.

In (3.32), the MLE of \mathbf{a} can be obtained by solving the following equation:

$$\frac{\partial p(\bar{\mathbf{y}}; \mathbf{a}, \mathcal{H}_1)}{\partial \mathbf{a}} = 0, \quad (3.33)$$

which leads to:

$$\hat{\mathbf{a}} = \bar{\mathbf{y}}. \quad (3.34)$$

Then the sufficient statistic of the subspace compressive GLRT detector can be derived as:

$$t(\bar{\mathbf{y}}) = 2\ln L(\bar{\mathbf{y}}) = \frac{\bar{\mathbf{y}}^T (\bar{\Phi} \bar{\Phi}^T)^{-1} \bar{\mathbf{y}}}{\sigma^2} > \gamma'. \quad (3.35)$$

Not that

$$\bar{\mathbf{y}} \sim \begin{cases} N(\mathbf{0}, \sigma^2 \bar{\Phi} \bar{\Phi}^T) & : \text{under } \mathcal{H}_0 \\ N(\bar{\Phi} \mathbf{H} \underline{\theta}, \sigma^2 \bar{\Phi} \bar{\Phi}^T) & : \text{under } \mathcal{H}_1, \end{cases} \quad (3.36)$$

which leads to the distribution of $t(\bar{\mathbf{y}})$ as follows:

$$t(\bar{\mathbf{y}}) \sim \begin{cases} \chi_M^2 & : \text{under } \mathcal{H}_0 \\ \chi_M'^2(\lambda) & : \text{under } \mathcal{H}_1, \end{cases} \quad (3.37)$$

where χ_M^2 denoting a central chi-squared distribution with M degrees of freedom and $\chi_M'^2(\lambda)$ denotes a noncentral chi-squared distribution with M degrees of freedom and noncentrality parameter λ . It can be easily shown that the noncentrality parameter λ is given by:

$$\lambda = \frac{\underline{\theta}^T \mathbf{G}^T [\mathbf{G}(\mathbf{H}^T \mathbf{H})^{-1} \mathbf{G}^T]^{-1} \mathbf{G} \underline{\theta}}{\sigma^2}. \quad (3.38)$$

From the above analysis, we can obtain the detection performance for a given γ' as follows:

$$P_f = Q_{\chi_M^2}(\gamma'), \quad (3.39)$$

$$P_d = Q_{\chi_M'^2(\lambda)}(\gamma'), \quad (3.40)$$

where $Q_{\chi_M^2}$ is the right-tail probability of a chi-squared random variable with M degrees of freedom; $Q_{\chi_M'^2(\lambda)}$ is the right-tail probability of a noncentral chi-squared random variable with M degrees of freedom and noncentrality parameter λ [29].

Equations (3.39)-(3.40) do not give us an intuitive interpretation on how the number of measurements affects the detection performance. Note that if M is sufficiently large, $t(\bar{\mathbf{y}})$ can be approximated as a Gaussian random variable. Furthermore, if M also satisfies $M \gg \mathbf{x}^T \mathbf{P}_{\bar{\Phi}} \mathbf{x} / \sigma^2$, then the detection performance can be approximated as [29]:

$$P_d \approx Q \left[Q^{-1}(P_f) - \frac{\mathbf{x}^T \mathbf{P}_{\bar{\Phi}} \mathbf{x}}{\sigma^2} \sqrt{\frac{1}{2M}} \right] \quad (3.41)$$

$$\approx Q \left[Q^{-1}(P_f) - \sqrt{\frac{M}{2}} \frac{\mathbf{x}^T \mathbf{x}}{K \sigma^2} \right]. \quad (3.42)$$

Compared with (3.29), there is performance loss due to unknown $\underline{\theta}$ when $\mathbf{x}^T \mathbf{x} / \sigma^2 \leq 2M$.

3.2.2 Compressive Detection

Here we consider the extension of the compressive detector proposed in [25] to the detection of unknown sparse signals since it is instructive to compare its performance to that yielded by the subspace compressive detector. Since compressive detector does not exploit the signal structure, it provides the most universal measurement scheme. However, it is assumed that the information of signal subspace, which can be exploited to improve the detection performance, can be obtained when

making detection decision of the unknown sparse signals. In the following, the compressive GLRT detector is derived for the detection of an unknown sparse signal. We consider the measurement matrix Φ with the number of measurement M . Since for $M < K$, the signal subspace can not be exploited and the detection performance is intrinsically poor, we only consider the case $K \leq M \leq N$. In such cases, the unknown parameters $\underline{\theta}$ in the signal sparsity model can be estimated. The estimation of $\underline{\theta}$ then is used in the LRT, yielding the compressive GLRT detector that depends on the random projections $\tilde{\mathbf{y}}$. With the detecting problem (3.4), we proceed as follows.

Let $\mathbf{C} = \sigma^2 \Phi \Phi^T$ and $\mathbf{B} = \Phi \mathbf{H}$, the PDF of the measured data under \mathcal{H}_0 is:

$$p(\tilde{\mathbf{y}}; \mathcal{H}_0) = \frac{1}{(2\pi)^{\frac{M}{2}} \det^{\frac{1}{2}}(\mathbf{C})} \exp \left[-\frac{1}{2} \tilde{\mathbf{y}}^T \mathbf{C}^{-1} \tilde{\mathbf{y}} \right]. \quad (3.43)$$

The PDF of the measured data under \mathcal{H}_1 is:

$$p(\tilde{\mathbf{y}}; \hat{\underline{\theta}}, \mathcal{H}_1) = \frac{1}{(2\pi)^{\frac{M}{2}} \det^{\frac{1}{2}}(\mathbf{C})} \exp \left[-\frac{1}{2} (\tilde{\mathbf{y}} - \mathbf{B} \hat{\underline{\theta}})^T \mathbf{C}^{-1} (\tilde{\mathbf{y}} - \mathbf{B} \hat{\underline{\theta}}) \right]. \quad (3.44)$$

Then the compressive likelihood ratio is:

$$L(\tilde{\mathbf{y}}) = \frac{p(\tilde{\mathbf{y}}; \hat{\underline{\theta}}, \mathcal{H}_1)}{p(\tilde{\mathbf{y}}; \mathcal{H}_0)}, \quad (3.45)$$

where $\hat{\underline{\theta}}$ is the MLE of $\underline{\theta}$ obtained by solving the follow problem:

$$\frac{\partial p(\tilde{\mathbf{y}}; \underline{\theta}, \mathcal{H}_1)}{\partial \underline{\theta}} = 0. \quad (3.46)$$

It can be shown that:

$$\hat{\underline{\theta}} = (\mathbf{B}^T \mathbf{C}^{-1} \mathbf{B})^{-1} \mathbf{B}^T \mathbf{C}^{-1} \tilde{\mathbf{y}}. \quad (3.47)$$

The sufficient statistic is then given by:

$$t(\tilde{\mathbf{y}}) = 2 \ln L(\tilde{\mathbf{y}}) = \tilde{\mathbf{y}}^T \mathbf{C}^{-1} \mathbf{B} (\mathbf{B}^T \mathbf{C}^{-1} \mathbf{B})^{-1} \mathbf{B}^T \mathbf{C}^{-1} \tilde{\mathbf{y}} > \tilde{\gamma}, \quad (3.48)$$

Note that under \mathcal{H}_0 ,

$$\mathbf{B}^T \mathbf{C}^{-1} \tilde{\mathbf{y}} = \mathbf{B}^T \mathbf{C}^{-1} \Phi \mathbf{w} \sim \mathcal{N}(\mathbf{0}, \mathbf{B}^T \mathbf{C}^{-1} \mathbf{B}). \quad (3.49)$$

Under \mathcal{H}_1 ,

$$\mathbf{B}^T \mathbf{C}^{-1} \tilde{\mathbf{y}} = \mathbf{B}^T \mathbf{C}^{-1} \Phi(\underline{\theta} + \mathbf{w}) \sim \mathcal{N}(\mathbf{B}^T \mathbf{C}^{-1} \mathbf{B} \underline{\theta}, \mathbf{B}^T \mathbf{C}^{-1} \mathbf{B}). \quad (3.50)$$

Thus, the sufficient statistics follows the distributions:

$$t(\tilde{\mathbf{y}}) \sim \begin{cases} \chi_K^2 & : \text{under } \mathcal{H}_0 \\ \chi_K'^2(\lambda) & : \text{under } \mathcal{H}_1, \end{cases} \quad (3.51)$$

where the noncentrality parameter is:

$$\lambda = \frac{\mathbf{x}^T \Phi^T (\Phi \Phi^T)^{-1} \Phi \mathbf{x}}{\sigma^2}. \quad (3.52)$$

The detection performance is then given by:

$$P_f = Q_{\chi_K^2}(\tilde{\gamma}) \quad (3.53)$$

$$P_d = Q_{\chi_K'^2(\tilde{\lambda})}(\tilde{\gamma}), \quad (3.54)$$

As will be illustrated in the simulations, with less number of measurements, the subspace compressive GLRT detector outperforms the compressive GLRT detector which does not exploit signal structure at data acquisition.

3.3 Detection with Narrowband interference

3.3.1 Subspace Compressive Detection

In many scenarios, the signals are contaminated not only by additive Gaussian noise, but also are corrupted by narrowband interference (NBI), which makes the detection problem more challenging. The subspace compressive detection method proposed can be naturally extended into NBI mitigation. Instead of using a notch filter at the analog front end or using adaptive algorithms to post-process the measurement data [63, 64], we try to mitigate the NBI at the measurement stage. That is, by designing appropriate measurement matrix, we project the incoming signal onto NBI null subspace so that NBI can be totally filtered out [65].

Consider the interference modeled by $\mathbf{Z} = \mathbf{S}\varphi$ where \mathbf{S} is an $N \times J$ matrix whose columns span the interference subspace $\langle \mathbf{S} \rangle$ and $\varphi \in \mathcal{R}^J$ is the interference coefficient vector with $J \ll N - K$. It is assumed that \mathbf{S} is available but φ is unknown. Note that even when the NBI subspace is unknown, we can estimate it from random compressive measurements via CS approaches since the NBI usually has sparse representation in the DFT domain or DCT domain.

With the existence of NBI, the detection of a sparse signal needs to distinguish between two hypotheses \mathcal{H}_0 and \mathcal{H}_1 :

$$\begin{aligned}\mathcal{H}_0 & : \mathbf{y}' = \mathbf{S}\varphi + \mathbf{w}, \\ \mathcal{H}_1 & : \mathbf{y}' = \mathbf{H}\underline{\theta} + \mathbf{S}\varphi + \mathbf{w}.\end{aligned}\tag{3.55}$$

Using subspace compressive measurements, it is desirable to design a measurement matrix that on the one hand cancels out the interference and on the other hand exploits the fact that the signal-of-interest lies in a known subspace spanned by the columns of \mathbf{H} . It turns out that by letting the projection matrix be

$$\check{\Phi} = \mathbf{G}(\check{\mathbf{H}}^T \check{\mathbf{H}})^{-1} \check{\mathbf{H}}^T = \mathbf{G}(\mathbf{H}^T \mathbf{P}_S^\perp \mathbf{H})^{-1} \mathbf{H}^T \mathbf{P}_S^\perp\tag{3.56}$$

where $\check{\mathbf{H}} = \mathbf{P}_S^\perp \mathbf{H}$ and $\mathbf{P}_S^\perp = \mathbf{I}_N - \mathbf{S}(\mathbf{S}^T \mathbf{S})^{-1} \mathbf{S}^T$, both goals are jointly achieved in the projection stage [36]. Note that \mathbf{P}_S^\perp is the orthogonal projection matrix for the NBI null space. \mathbf{G} is, as before, an $M \times K$ random matrix whose entries are drawn from an i.i.d. distribution. Thus, the hypothesis problem reduces to:

$$\begin{aligned}\mathcal{H}_0 & : \check{\mathbf{y}} = \check{\Phi}(\mathbf{S}\varphi + \mathbf{w}), \\ \mathcal{H}_1 & : \check{\mathbf{y}} = \check{\Phi}(\mathbf{H}\underline{\theta} + \mathbf{S}\varphi + \mathbf{w}).\end{aligned}\tag{3.57}$$

Note that under \mathcal{H}_1 , $\check{\mathbf{y}}$ reduces to: $\check{\mathbf{y}} = \check{\Phi}(\mathbf{H}\underline{\theta} + \mathbf{w})$. Thus, the NBI is eliminated at the measurement stage. It is necessary to point out that the design of the subspace measurement matrices according to (3.56) incorporates the principle of zero-forcing

equalizer [66, 67]. The interference, if present, are completely eliminated by projecting the received signal onto the interference null space. Then the received signal is again projected onto the desired signal subspace to reduce the noise effect.

In the following, we focus on the detection of an unknown sparse signal with NBI mitigation. When the signal coefficient $\underline{\theta}$ is unknown, a GLRT detector can be derived following a similar approach as in Sec. 3.2, whose sufficient statistics is given by:

$$t(\check{\mathbf{y}}) = \frac{\check{\mathbf{y}}^T (\check{\Phi} \check{\Phi}^T)^{-1} \check{\mathbf{y}}}{\sigma^2} > \gamma. \quad (3.58)$$

The detection performance with unknown coefficients $\underline{\theta}$ is given by:

$$\begin{aligned} P_f &= Q_{\chi_M^2}(\gamma) \\ P_d &= Q_{\chi_M'^2(\lambda)}(\gamma), \end{aligned}$$

where the noncentrality parameter λ is:

$$\lambda = \frac{\underline{\theta} \mathbf{G}^T (\mathbf{G} (\mathbf{H}^T \mathbf{P}_S^\perp \mathbf{H})^{-1} \mathbf{G}^T)^{-1} \mathbf{G} \underline{\theta}}{\sigma^2}. \quad (3.59)$$

There is signal energy loss when projecting the received signal onto the null space of the interference. Performance loss can be expected compared with the case when there is no interference present. In Section 3.5, extensive simulations are performed to elaborate these performance differences.

3.3.2 Compressive Detection

Note that if the compressive measurement are obtained without exploiting any signal structure, the contribution of the interference can still be canceled out on condition that we know the interference subspace [68]. In the following, we extend the interference cancelation method proposed in [68] to the detection of an unknown sparse signal with NBI mitigation. The comparison with subspace compressive detector developed above will be presented in the simulations section.

Following the procedure proposed in [68], obtaining the data for detection takes in two steps. In the first step, compressive measurements are obtained by matrix Φ with each entry taken from an i.i.d. random distribution. In the second step, the compressive measurements are projected onto space orthogonal to the NBI components by a linear operator $\tilde{\mathbf{P}}$. Let $\mathbf{F} = \Phi\mathbf{S}$, we first obtain $\mathbf{E} \in \mathcal{R}^{M \times (M-S)}$ as an orthonormal basis for the null space of \mathbf{F}^T by singular value decomposition (SVD) [69]. Then $\tilde{\mathbf{P}}$ is designed as follows:

$$\tilde{\mathbf{P}} = (\mathbf{E}^T \mathbf{E})^{-1} \mathbf{E}^T. \quad (3.60)$$

$\tilde{\mathbf{P}}$ can successfully remove the contributions of the interference and the detection problem can be formulated as:

$$\begin{aligned} \mathcal{H}_0 &: \tilde{\mathbf{y}} = \tilde{\mathbf{P}}\Phi(\mathbf{S}\varphi + \mathbf{w}), \\ \mathcal{H}_1 &: \tilde{\mathbf{y}} = \tilde{\mathbf{P}}\Phi(\mathbf{H}\Theta + \mathbf{S}\varphi + \mathbf{w}) \end{aligned} \quad (3.61)$$

Note that under \mathcal{H}_1 , $\tilde{\mathbf{y}}$ reduces to $\tilde{\mathbf{y}} = \tilde{\mathbf{P}}\Phi(\mathbf{H}\Theta + \mathbf{w})$. Let $\tilde{\mathbf{C}} = \sigma^2 \Phi \tilde{\mathbf{P}} (\Phi \tilde{\mathbf{P}})^T$, $\tilde{\mathbf{B}} = \Phi \tilde{\mathbf{P}} \mathbf{H}$ and assume $M - S > K$. Then following a similar procedure as in Sec. 3.2, a sufficient statistics can be derived as:

$$t(\tilde{\mathbf{y}}) = 2\ln L(\tilde{\mathbf{y}}) = \tilde{\mathbf{y}}^T \tilde{\mathbf{C}}^{-1} \tilde{\mathbf{B}} (\tilde{\mathbf{B}}^T \tilde{\mathbf{C}}^{-1} \tilde{\mathbf{B}})^{-1} \tilde{\mathbf{B}}^T \tilde{\mathbf{C}}^{-1} \tilde{\mathbf{y}} > \tilde{\gamma}, \quad (3.62)$$

The detection performance then can be derived from the distribution of $t(\tilde{\mathbf{y}})$ as follows:

$$\begin{aligned} P_f &= Q_{\chi_K^2}(\tilde{\gamma}) \\ P_d &= Q_{\chi_K'^2(\tilde{\lambda})}(\tilde{\gamma}), \end{aligned}$$

where the noncentrality parameter is:

$$\lambda = \frac{\mathbf{x}^T (\tilde{\mathbf{P}}\Phi)^T ((\tilde{\mathbf{P}}\Phi)(\tilde{\mathbf{P}}\Phi)^T)^{-1} \tilde{\mathbf{P}}\Phi \mathbf{x}}{\sigma^2}. \quad (3.63)$$

The performance of the compressive GLRT detector with NBI mitigation will be investigated in the simulation part along the comparison to subspace GLRT detector.

3.4 Discussion

For the proposed adaptive subspace compressive detectors, information of signal subspace can be obtained from the compressive measurements of training signals. In this section, we address two implementation issues of the proposed adaptive subspace compressive detectors for practical applications. The first one discusses how to retrieving signal subspace information via CS approaches. The second one focuses on the effect of measurement waveform quantization on detection performance.

3.4.1 Signal Subspace Estimation using Compressive Measurements

The information of signal subspace is required to construct the subspace measurement matrix. In some cases, we can have *a priori* information of the signal subspace. For example, an image object to be detected can be well approximated by a linear combination of a few of the coarsest wavelet components. As another example, a received OFDM radio signal only occupies a limited frequency band, thus can be sparsely repressed by a few of known DFT atoms [33]. More frequently, the subspace information can be obtained from a reduced set of compressive measurements from the training data via CS approaches. It should be pointed out that the use of training signals is widely employed in the context of signal detection. Adaptive detectors rely on the training signal to estimate the detector parameters before the detection stage [70, 71, 72, 73].

For the signal \mathbf{x} which can be approximated as a K -sparse model on a known basis Ψ , we are interested in locating the K vectors of Ψ relevant to the signal \mathbf{x} . These K relevant vectors that expand the signal subspace are used to define the matrix \mathbf{H} . CS reconstruction algorithm, such as matching pursuit (MP), orthogonal matching pursuit (OMP) and basis pursuit denoising (BPDN) algorithm can be readily applied to retrieve the K relevant vectors [13, 16].

Matching Pursuit algorithm was initially introduced in [74] for signal reconstruction and later extended for signal detection in [15, 2, 65]. Given the basis $\Psi \in \mathcal{R}^{N \times N}$, the i.i.d. random measurement matrix $\Phi \in \mathcal{R}^{M \times N}$ and the compressive measurements $\mathbf{y} = \Phi \mathbf{x}$, the MP algorithm aims to extract K column vectors of the composite dictionary $\mathbf{U} = \Phi \Psi$ that are most correlated to the measurement vector \mathbf{y} . Those vectors, in turn, are related to the K elements in the basis Ψ that spans the signal subspace $\langle \mathbf{H} \rangle$. It was shown that far fewer measurements are required to extract most of the significant signal components than for exact sparse signal reconstruction using MP [15]. OMP is similar to MP in that at each iteration, it chooses the column of \mathbf{U} that is most strongly correlated with the measurements. However, it avoids choosing the same column repeatedly by subtracting all the contribution of the selected column from the measurements. With only K iterations, the algorithm is able to exact the K sparse components of \mathbf{x} [16]. Note that in the application at hand, the measurement vector is the projection of the signal-of-interest plus noise, thus it is contaminated with colored noise. Therefore, whitening of the measurement is required before signal subspace estimation via MP or OMP.

Although MP and OMP algorithms are computationally efficient, they are not robust to the noise and the result is not satisfactory when SNR is low. An alternative adopted approach for signal subspace estimation that explicitly takes noise effect into account is the BPDN algorithm [13]. The BPDN algorithm proposed is an extension of the Basis Pursuit (BP) algorithm [13] suitably modified for the reconstruction of noisy signals. The BPDN algorithm unifies sparse signal reconstruction and a denoising operation into a single task by solving an optimization problem. Formally, given a noisy random projection \mathbf{y}_n , a measurement matrix Φ and a basis Ψ , BPDN finds the sparse vector $\boldsymbol{\xi}$ that solves the constrained minimization problem [13, 18]:

$$\hat{\boldsymbol{\xi}} = \arg \min_{\boldsymbol{\xi}} \|\Phi \Psi \boldsymbol{\xi} - \mathbf{y}_n\|_2^2 + \lambda \|\boldsymbol{\xi}\|_1, \quad (3.64)$$

where $\mathbf{y}_n = \Phi \Psi \boldsymbol{\xi} + \mathbf{w}$, $\|\boldsymbol{\xi}\|_1 = \sum_i |\xi_i|$ and $\lambda \leq \|2(\Phi \Psi)^T \mathbf{y}_n\|$ [18]. As for MP and

OMP algorithms, whitening of the measurement is required before signal subspace estimation via BPDN. Taking this fact into account, the optimization problem given by (3.64) may be suitably modified to introduce the whitening operation yielding:

$$\hat{\boldsymbol{\xi}} = \arg \min_{\boldsymbol{\xi}} \|\mathbf{V}\Phi\Psi\boldsymbol{\xi} - \mathbf{V}\mathbf{y}_w\|_2^2 + \lambda\|\boldsymbol{\xi}\|_1, \quad (3.65)$$

where $\mathbf{y}_w = \Phi(\Psi\boldsymbol{\xi} + \mathbf{w})$, \mathbf{V} is chosen such that $\mathbf{V}^T\mathbf{V} = (\Phi\Phi^T)^{-1}$ and \mathbf{y}_w denotes the random projection of the received signal at the estimation stage.

Given the solution to the optimization problem (3.65), if the signal sparsity K is known, then we can estimate the locations of the K significant signal components by locating K entries of $\hat{\boldsymbol{\xi}}$ with the largest magnitudes. These K entries correspond to the K column-vectors in the basis $\Psi = [\psi_1, \psi_2, \psi_3, \dots, \psi_N]$ that spans the subspace where the signal-of-interest lies. Assembling those K N -dimensional vectors as a $N \times K$ matrix, we obtain the estimate of \mathbf{H} as $\hat{\mathbf{H}}$. We are interested in searching for the subspace components that contains a large fraction of the signal energy. Simulation experiments in section 3.5 show that we can always achieve partial sparsity recovery via CS approaches from a limited set of compressive measurements which is insufficient for signal recovery.

For a practical signal that can be approximated by a K -sparse model, we can estimate its subspace with size K , and then design the projection matrix for the proposed adaptive detector as:

$$\hat{\Phi} = \mathbf{G}(\hat{\mathbf{H}}^T\hat{\mathbf{H}})^{-1}\hat{\mathbf{H}}^T, \quad (3.66)$$

However, constructing $\hat{\mathbf{H}}$ as an $N \times K$ matrix for detection purposes is only justified if the underlying K sparse signal has its energy uniformly distributed in its subspace. In practice, the coefficients of compressible signals that can be approximated by sparse models decays rapidly following a power-law. Thus, not each subspace component is equally important. For detection purposes, when the number of measurements is constrained by $M < K$, we only need to exploit the signal subspace

where SNR is high. To design a practical detector, only the M most significant signal components need to be considered. That is, in the solution of (3.65), only M entries with the largest magnitude are selected. When constructing $\hat{\Phi}$, a random matrix \mathbf{G} with size $M \times M$ is employed. If the subspace estimation is accurate, this method guarantees that the energy contained by the M most significant signal components will be collected. If M is a tunable parameter, then its optimal value depends on the SNR. For SNR sufficiently low, an optimal M should be less than K .

3.4.2 Optimal Quantization for the Subspace Projection

The compressive measurement only requires a reduced number of measurements needed for a desired detection performance, leading to simplified hardware design. One approach to obtain the compressive measurement is via a parallel analogy projection where the analog received signal is projected onto analog measurement waveforms in parallel [54]. Each analog measurement waveforms matches to one row of the measurement matrix. However, in many practical applications, it is difficult to generate arbitrary analog measurement waveforms, thus requiring the quantization of the measurement matrix to very limited levels. In the worst cases, as in the detection of wideband radio signals or in the detection of visual objects, the measurement waveforms have to be quantized to only 2 levels $\{-1, 1\}$ or 3 levels $\{-1, 0, 1\}$ for easy analog hardware implementations [3, 36].

The quantization of the measurement waveform may lead to no performance loss for compressive detectors if each entry of the measurement matrix is taken from an i.i.d. Bernoulli distribution. However, the entry of subspace compressive measurement matrix contains the information of signal subspace and may takes on arbitrary levels. Quantization of the measurement matrix may lead to performance loss for the proposed subspace compressive detectors. To reduce the performance loss, an optimal bit allocation method called Lloyd-Max method be employed. The

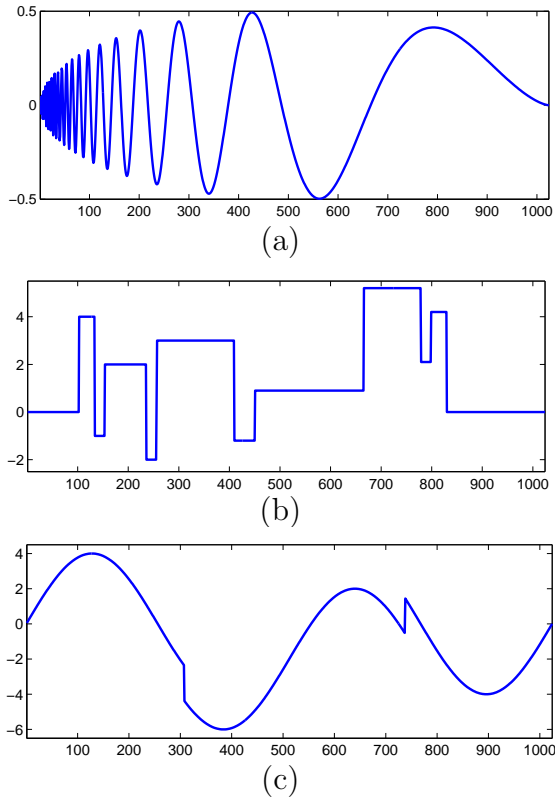


Figure 3.1: Test signal: (a) Doppler, (b) Bumps, (c) HeaviSine. They are sparse in the Daubechies-8, Haar and Daubechies-8 wavelet basis, respectively. The length of the signals is 1024.

Lloyd-Max method minimizes the quantization noise by exploiting the fact that each entry of the subspace projection matrix follows the same Gaussian distribution [51]. The performance loss due to measurement waveform quantization will be investigated by numerical simulations in Sec.3.5. However, whenever signal subspace information is available, the subspace compressive detectors are preferred. Although there may be performance loss, quantized measurement still preserves partial signal subspace information and the quantized subspace compressive detectors still outperform the compressive detectors [75].

3.5 Simulations

In this section, the performance of the proposed subspace compressive detectors are evaluated through extensive simulations. We focus on the detection of unknown sparse signals. Comparisons with conventional GLRT detectors and the compressive GLRT detectors are also illustrated. It is observed that the simulation results validate the theoretical performance analysis. However, to simplify the illustrations, the results of theoretic analysis are not shown.

Both standard test signals, Doppler, Bumps and HeaviSine, and randomly generated test signals are employed for evaluation purposes. The standard test signals, which are widely used in sparse signal analysis, are shown in Fig.3.1, where the length of all the signals is $N = 1024$ [76]. To obtain their subspace matrices \mathbf{H} , the Doppler signal is approximated by a linear combination of $K = 111$ components in a Daubechies-8 wavelet basis. Similarly, the Bumps signal is approximated by a linear combination of $K = 77$ components in a Haar basis. The HeaviSine signal is also approximated by a linear combination of $K = 48$ components in a Daubechies-8 basis. Thus, the signal subspace matrices are then constructed from the K corresponding sparse atoms. For all the simulations we define the energy to noise ratio (ENR) as $\text{ENR} = \frac{\mathbf{x}^T \mathbf{x}}{\sigma^2}$ and the signal to noise ratio (SNR) as $\text{SNR} = \frac{\mathbf{x}^T \mathbf{x}}{N\sigma^2}$.

In the first simulation, the proposed subspace compressive detector is applied to the detection of an unknown signal lying in a known subspace. Doppler signal is employed and it is assumed that we known the signal subspace matrix obtained from its sparse approximation. However, with no other *a priori* information, it is assumed that the signal energy is uniformly distributed in its subspace. For known signal length N and signal sparsity K , the number of measurements for subspace compressive detection is $M_s = 77 \approx 0.7K$ and the number of measurements for compressive detection is $M_c = 0.5N = 512$. A Gaussian random matrix $\mathbf{G} \in \mathcal{R}^{M_s \times K}$ and a Gaussian random matrix $\Phi \in \mathcal{R}^{M_c \times N}$ are generated at random for subspace

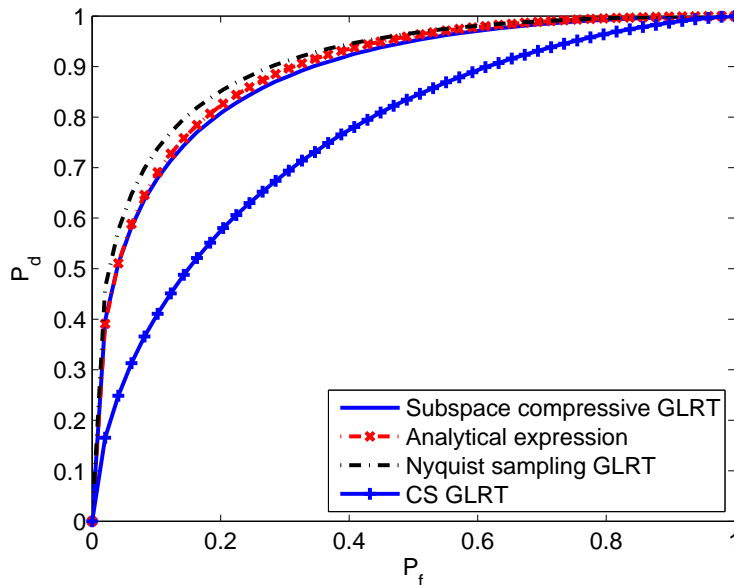


Figure 3.2: Detection of unknown Doppler signal with known subspace. The simulation parameters are set as: $N = 1024$, $K = 111$, $M_s = 77$, $M_c = 512$, $\text{ENR} = 15$ dB.

compressive detection and for compressive detection, respectively. At $\text{ENR} = 15$ dB, the performance of the detectors for different P_f is shown in Fig. 3.2 where each simulation result is the average of 10^6 runs for different noise realizations. It is clear that with far fewer measurements, subspace compressive detection improves the detection performance by exploiting the subspace information. For comparison purposes, the simulation results of detection by a conventional GLRT detector which is constructed based on the signal linear model and requires Nyquist sampling is also shown in Fig. 3.2 [29]. The performance gap between the conventional GLRT detector and the subspace compressive detector is much smaller than the performance gap between the subspace compressive detector and the compressive detector. Approximate performance of the subspace compressive detection given by the analytical expression (3.42) are also presented, which demonstrates the approximation (3.42) are quite accurate at estimating the detection performance.

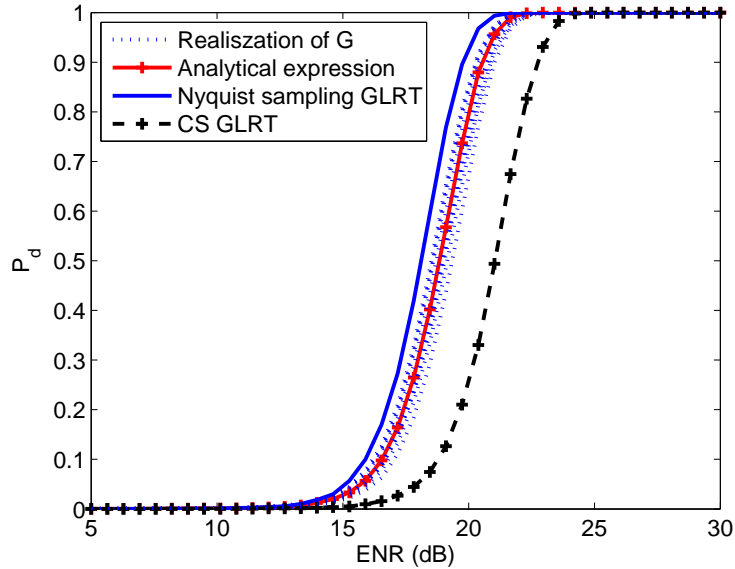


Figure 3.3: Detection of unknown Doppler signal with known subspace. The simulation parameters are set as: $N = 1024$, $K = 111$, $M_s = 77$, $M_c = 512$, $P_f = 10^{-4}$.

At $P_f = 10^{-4}$, simulation results of the proposed subspace compressive detectors with varying ENR are shown in Fig. 3.3. To show the diversity caused by different realizations of matrix \mathbf{G} , the detection performance of 10 subspace compressive detectors, each with a different realization of \mathbf{G} , are provided. It shows that all the results are closely clustered around their expected performance. For a given P_d , subspace compressive detectors on average have about 2 ~ 3 dB performance gains in ENR over compressive detection. To further illustrate the ability of the subspace compressive measurement matrix to collect the signal energy, Figure 3.4 shows the histogram of the ratio of $\mathbf{x}^T \mathbf{P}_{\bar{\mathbf{g}}} \mathbf{x}$ over $\mathbf{x}^T \mathbf{x}$ for 1000 realizations of random matrix \mathbf{G} . Again, it shows that all the results are clustered around their expected value 0.7. More than 75% of the realization have ratio within $1 \pm 10\%$ of the expected value and only 14.8% are below 90% of the expected value. Thus, for practical applications, with high probability, the approximation (3.42) is valid.

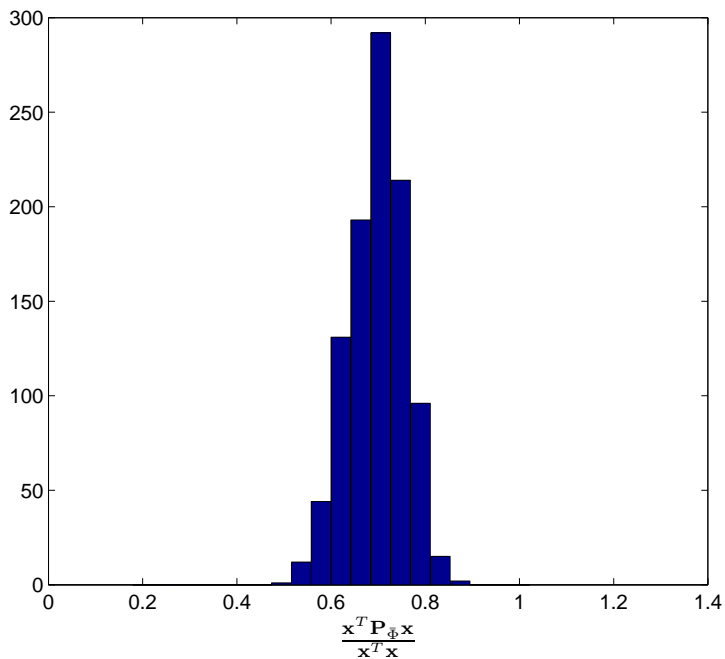


Figure 3.4: Ratio of $\mathbf{x}^T \mathbf{P}_{\hat{\phi}} \mathbf{x}$ over $\mathbf{x}^T \mathbf{x}$ for different realization of \mathbf{G} .

In the third simulation, the performance of the proposed subspace compressive GLRT detector with narrowband interference mitigation is evaluated. The Bumps signal is employed and its subspace matrix has dimension $N = 1024$ and $K = 77$. The narrowband interference \mathbf{z} is given by $\mathbf{z} = \mathbf{S}\varphi$, where $\mathbf{S} \in \mathcal{R}^{1024 \times 20}$. Each entry of \mathbf{S} and φ is drawn from an i.i.d. normal distribution. The number of measurements for subspace compressive detection is $M_s = 54 \approx 0.7K$ and the number of measurements for compressive detection is $M_c = 0.5N = 512$. At ENR = 15 dB, the simulation result of the proposed subspace compressive GLRT detector is compared with that of the compressive GLRT detector with interference rejection, as shown in Fig. 3.5. It shows that the proposed subspace compressive detector with interference mitigation improves the detection performance with fewer measurements by exploiting more signal information. Compared with the case when there is no NBI, the performance loss for subspace compressive detection with NBI

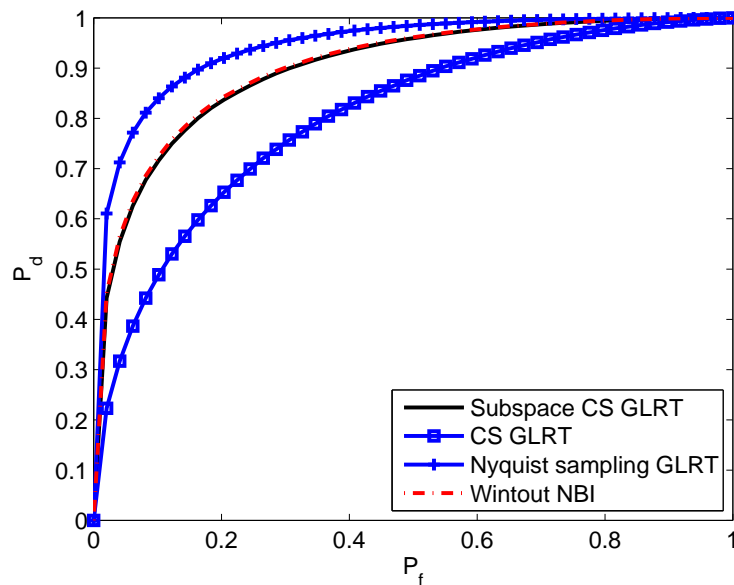


Figure 3.5: Performance of subspace compressive GLRT detector with interference rejection. The number of measurements are $M_s = 54$ and $M_c = 512$.

mitigation is very small. Although the compressive detector can successfully filter out the interference components, its inefficiency at collecting the desired signal energy leads to less probability of detection. Furthermore, the proposed subspace compressive GLRT detection has competitive performance compared to that yielded by the matched subspace GLRT detector which also requires Nyquist sampling [30].

Next, the capability of the BPDN algorithm to extract sparse signal subspace information from compressive measurements is investigated. From the compressive measurements, we try to obtain an estimation of the signal subspace which contains most of the signal energy. We evaluate the performance of the BPDN algorithm by calculating the ratio of the signal energy residing in the estimated signal subspace over the total signal energy. For comparison purposes, we also investigate the performance of the BPDN for signal reconstruction. A signal is considered to be successfully reconstructed if the reconstruction error is less than 1% of the signal's

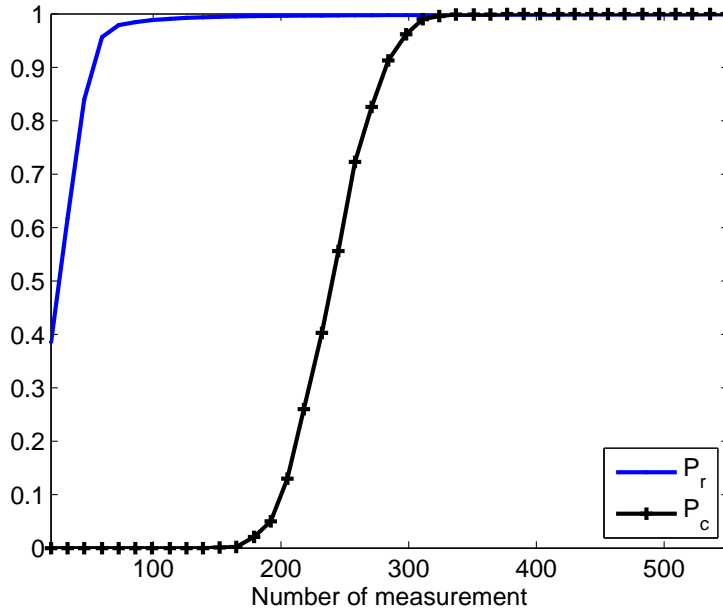


Figure 3.6: Signal subspace estimation and signal reconstruction by modified BPDN algorithm. P_r is the ratio of the signal energy residing in the estimated signal subspace over the total signal energy; P_c is the probability of perfect reconstruction.

energy, i.e., $(\mathbf{x} - \hat{\mathbf{x}})^T(\mathbf{x} - \hat{\mathbf{x}})/\mathbf{x}^T\mathbf{x} < 0.01$, where $\hat{\mathbf{x}}$ is the estimated signal. The Heavisine signal, whose estimated sparsity is $K = 48$, is employed here. The estimated signal subspace also has dimension 1024×48 . At $\text{SNR} = 20$ dB, the results are shown in Fig. 3.6 where each point of the curves is obtained by averaging over 1000 trials. As shown in Fig. 3.6, to obtain an estimated signal subspace which contains most of the signal energy, the number of measurements required is about one third for perfect signal reconstruction. This corroborates that far fewer measurements are needed for partial sparsity recovery than for signal reconstruction. Very similar results are obtained when the Doppler and Bumps signals are used for test.

In the next simulation, we try to follow a more practical application scenario where the subspace of the unknown sparse signal is unknown and has to be estimated from compressive measurements of training signals. A subspace compressive GLRT

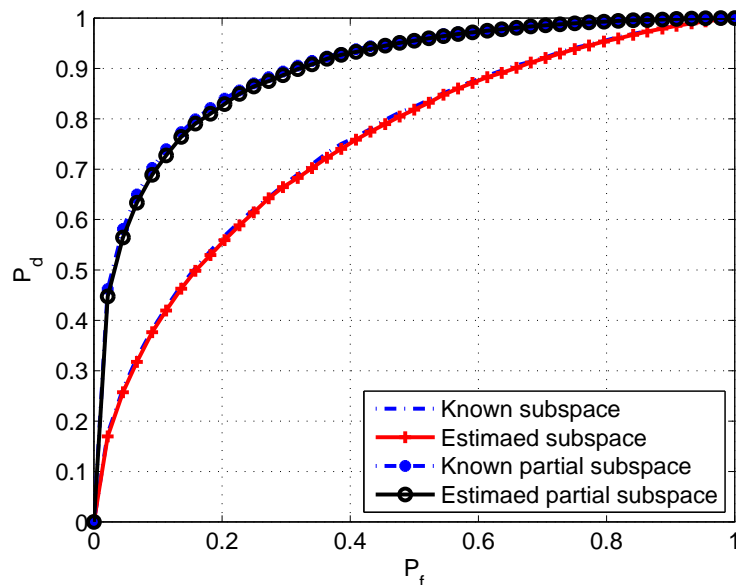


Figure 3.7: Performance of BPDN + subspace compressive GLRT detector. In one method, signal subspace with dimension 49 is estimated; In another case, signal subspace with dimension 33 is estimated.

detector is then constructed based on the estimated signal subspace. We assume we know the signal sparsity K and consider the number of measurements for detection less than K . The HeaviSine signal is again employed here and the ENR is set as $\text{ENR} = 16$ dB. 200 training signals are used and for each training signal, $4K$ measurements are made. The modified BPDN algorithm is used to estimate the signal subspace from the averaged noisy measurements. Then $M_s = 33 \approx 0.7K$ subspace compressive measurements are obtained for signal detection. We consider two cases. In the first case, an estimated signal subspace matrix with full size $N \times K$ is obtained and the simulation results are compared to the case to that yielded by the subspace compressive GLRT detector where \mathbf{H} is assumed to be known. In the second case, only M_s significant signal components are estimated. The results are also compared to the detection where the most M_s significant signal components are known. At each P_f , 10^4 realizations of the simulation scenario are used to compute P_d . Figure 3.7 depicts the resulting detection probabilities. As can be

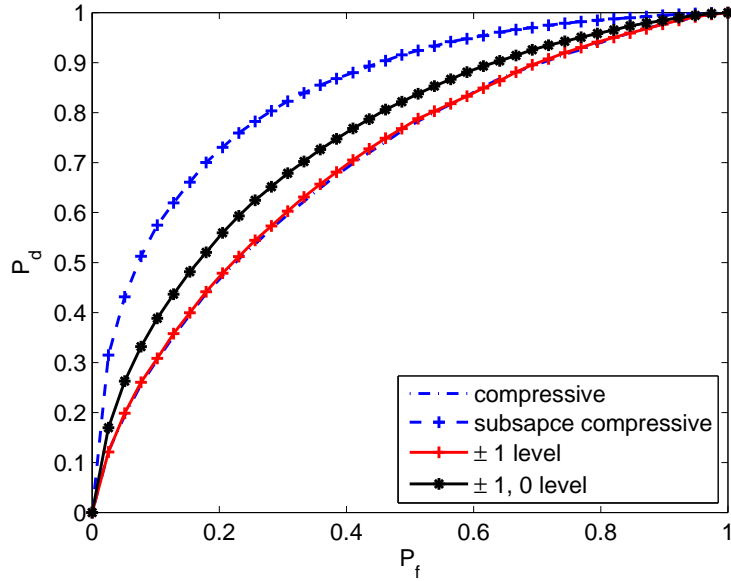


Figure 3.8: Quantization on the detection performance.

seen, the modified BPDN algorithm can effectively estimate the signal structure yielding a performance close to the ideal case of known signal subspace. Although the signal subspace estimation will have some error, the detector will work well if the estimated signal subspace captures most of the signal energy. Since the energy of the HeaviSine signal is not uniformly distributed along its signal space and its coefficients decay rapidly, simulation results show that estimating only M_s components lead to better detection performance than that of estimating the entire signal subspace.

In the last simulation, the effect of waveform quantization on the detection performance is investigated. We consider a general case. The sparse signal \mathbf{x} under consideration is given by: $\mathbf{x} = \mathbf{H}\underline{\theta}$, where each entry of \mathbf{H} and $\underline{\theta}$ is drawn from an i.i.d. normal distribution. \mathbf{H} is assumed known and its dimension is 2000×200 . The number of subspace compressive measurements is $M_s = 160$. A subspace measurement matrix is first constructed based on \mathbf{H} and then quantized to two levels $\{\pm 1\}$ or three levels $\{\pm 1, 0\}$. The quantization of the measurement matrix follows

the Lloyd-Max method which minimizes the quantization noise [51]. At ENR = 15 dB, the results are shown in Fig.3.8 and compared with the non-quantized case. It can be seen that quantization leads to perceivable performance loss with less quantization level leading to more performance loss. For comparisons purposes, we also show the detection performance of a compressive detection with the number of measurements $M_c = 1000$. For the compressive detection, each entry of the measurement matrix is drawn from an i.i.d. Bernoulli distribution. It is observed that the subspace compressive detector whose measurement matrix is quantized to two levels, obtains almost the same performance as the compressive detector, but with only about one sixth of the number of measurements.

Chapter 4

ADAPTIVE COMPRESSIVE DETECTION FOR PILOT ASSISTED ULTRA-WIDEBAND IMPULSE RADIO

4.1 System Design

4.1.1 Model of Received UWB Signal

Consider a peer-to-peer I-UWB communication system where binary symbols are conveyed by a stream of ultra-short pulses. The transmitted signal $z(t)$ over a burst transmission of N_d symbols can be expressed as:

$$z(t) = \sum_{n=0}^{N_d N_f - 1} a_n b_{\lfloor n/N_f \rfloor} \sqrt{E} g(t - nT_f - c_n T_c), \quad (4.1)$$

where $g(t)$ is an unit energy signal pulse with a time duration T_g on the order of sub-nano second. Pulses of $g(t)$ are modulated by pulse amplitude modulation (PAM) and are repeated over N_f consecutive frames to transmit a binary symbol. Here $b_{\lfloor n/N_f \rfloor} \in \{\pm 1\}$ denotes the binary symbol to be transmitted where $\lfloor x \rfloor$ denotes the largest integer less than or equal to x and represents the index of the data symbol to be transmitted in the n th frame. The time duration of a frame is T_f and thus a symbol period is $T_s = N_f T_f$. Furthermore, each frame is divided into N_c chips with a chip duration T_c leading to $T_f = N_c T_c$. The energy of the transmitted pulse is denoted by E and thus the energy needed to transmit one bit is $E_b = N_f E$.

For the proposed UWB signaling, direct sequence (DS) spread spectrum coding and time-hopping (TH) coding are adopted [39, 77]. In (4.1), $a_n \in \{\pm 1\}$ is the pseudorandom (PN) spread spectrum code and c_n is the PN time-hopping (TH)

code assumed to be uniformly distributed in $[0, 1, \dots, N_c - 1]$. This DS-TH UWB signaling scheme has the advantage that the spectrum of the transmitted signal is smooth. It can be shown that the spectrum of the transmitted signal is given by

$$\Gamma_{zz}(f) = \frac{2E}{T_f} |\mathcal{G}(f)|^2, \quad (4.2)$$

where $\mathcal{G}(f)$ is the Fourier transform of $g(t)$. This avoids spectrum spikes that can cause coexistence problems [78].

Due to the large bandwidth of transmitted pulses, the I-UWB channel contains resolvable delay bins and can thus be characterized by a tapped-delay model as [38, 39, 40]:

$$h(t) = \sum_{l=0}^{L-1} \alpha_l \delta(t - \tau_l), \quad (4.3)$$

where L is the number of propagation paths and α_l and τ_l are, respectively, the amplitude and the delay associated with the l th path; $\delta(t)$ denotes the delta function. Although the number of channel paths could be large, we consider here sparse channels where a few carefully selected paths contain most of the channel energy. Wideband high-frequency UWB channels can be modeled as sparse channels since many resolvable delay bins do not carry significant power due to the large transmission bandwidth [42]. In [43], it is observed that the UWB channel is sparse if the signal bandwidth is > 2 GHz and if the small-scale fading is modeled as Rayleigh. The frequency selectivity presented in UWB channels also leads to pulse distortion over each path. This effect can be accounted for by modeling $h(t)$ with more paths [42]. Even so, it is observed that the sparsity of UWB channels is still preserved [38, 42]. Furthermore, to avoid intersymbol interference (ISI) and intrasymbol interference, it is assumed that $T_c > T_g + T_d$ where T_d is the maximum excess delay of the multipath channel [79]. It is also assumed that the channel remains invariant over $t_s = N_d N_f T_f$ seconds for a burst transmission.

The received signal is corrupted by zero-mean, additive white Gaussian noise (WGN) with a two-sided power spectral density $N_0/2$. The noisy received signal then goes through an ideal bandpass filter with one-sided bandwidth B and central frequency F_c to eliminate the out-of-band noise. Therefore B is set such that the desirable signal passes through the bandpass filter without any distortion. Within a transmission burst, the received signal at the output of the bandpass filter is given by:

$$\tilde{r}(t) = \int_0^{t_s} h(t - \tau)z(\tau)d\tau + \tilde{w}(t), \quad (4.4)$$

where $\tilde{w}(t)$ is a zero-mean Gaussian random process with an autocorrelation function given by:

$$R_{\tilde{w}}(\tau) = BN_0\text{sinc}(B\tau)\cos(2\pi F_c\tau). \quad (4.5)$$

Note that $R_{\tilde{w}}(\tau)$ is approximately equal to zero for $|\tau| \geq T_d + T_g$ if $B \gg 1/(T_d + T_g)$. Hence, noise samples separated by more than $T_d + T_g$ are assumed to be statistically independent [79]. Note that in (4.4) we made an implicit assumption that the effects of transmitter antenna and receiver antenna have been appropriately incorporated in the pulse $p(t)$ [80].

4.1.2 Receiver Structure

To avoid the use of ultra-fast ADCs, the proposed UWB receiver projects the filtered signal onto a set of measurement waveforms in the analog domain where each waveform corresponds to a row vector of a measurement matrix. The receiver structure is shown in Fig.4.1 where the random projection of the received UWB signal is implemented by a bank of mixer-integrators. The outputs of the mixer-integrators are the inner product of the received signal and the measurement waveforms. The receiver knows the transmitter PN sequences a_n and c_n , and we assume synchronization with the received pulses [77].

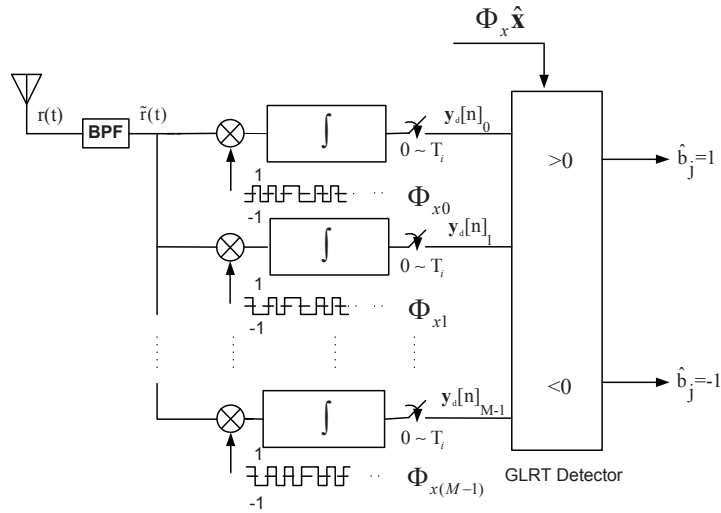


Figure 4.1: Proposed I-UWB Receiver for subspace compressive detection.

The integration interval, T_i , of the mixer-integrators satisfies $T_g + T_d > T_i \geq T_g$. For the received signal in the n th frame, the integration of the mixer-integrators begins at time $t = c_n T_c + (n - 1) T_f$. After T_i seconds, the outputs of the mixer-integrators are sampled to obtain projected measurements and the mixer-integrators are then reset and ready for the next set of measurements. For representation purposes, $\mathbf{x} \in \mathcal{R}^{N \times 1}$ is defined as the digitized noise-free received signal $h(t) * g(t)$ within the measurement interval T_i , where $*$ denotes convolution. An underlying sampling frequency F_s is also implied and as in critical Nyquist sampling, the underlying sampling frequency F_s satisfies $F_s = 2B$. Given the integration interval T_i , the length of \mathbf{x} is thus $N = T_i F_s$. However, it should be clear that only the projected results go through the ADCs.

Note that less sampling rate can be achieved by following the traditional CS measurement approaches where compressive measurements are obtained by projecting the received UWB signal onto a purely random basis without exploiting any *a priori* information about the structure of the received UWB signal [49]. However, the compressive measurements directly employed for UWB symbol detection are

not efficient at gathering the energy of the received UWB signal, thus suffering from much performance degradation. In this thesis, subspace compressive detectors are proposed for UWB symbol detection by exploiting the fact that the received UWB signal has a sparse representation and resides in a low-dimensional subspace. Therefore, one can capture most of the signal energy with a few measurements just by projecting the received UWB signal into its own subspace [30]. More precisely, by designing a measurement projection matrix tailored to the UWB signal subspace, the UWB signal energy can be captured more efficiently, and at the same time, the effect of noise and interference can be greatly mitigated. Thus, desired detection performance can be achieved with far fewer measurements. As a result, the hardware implementation is simplified.

To design the subspace compressive measurement matrix that can efficiently capture the UWB signal energy, channel estimation is needed. To this end, much like conventional digital communication systems that rely on pilot symbols for channel estimation and synchronization, the proposed UWB system employs a pilot symbol assisted modulation scheme for UWB signal subspace estimation and channel side information acquisition [81]. Thus, each transmission burst includes N_p pilot symbols that are not data modulated and N_s data symbols that are modulated by transmitted symbols leading to a total number of $N_d = N_p + N_s$ symbols in one burst. Furthermore, the pilot symbols are further divided into two groups. The first group contains N_{p1} pilot symbols used to estimate the UWB signal subspace while the second group contains N_{p2} pilot symbols used to provide side information about the UWB channel to generate detection templates. For all pilot symbols, the symbol to be transmitted b_j is fixed at 1, i.e., $b_j = 1$ for $0 \leq i \leq N_p N_f - 1$. For the data symbols, $b_j = \pm 1$ is assumed to be drawn independently with equal probability.

Correspondingly, within a transmission burst, the symbol detection of the proposed subspace compressive UWB receiver comprises three stages. In the first

stage, a set of compressive measurements are acquired to obtain a coarse estimation of the signal subspace and a random projection matrix with each entry taken from a Bernoulli distribution is employed. Then a subspace compressive measurement matrix is designed based on the estimated signal subspace. With the designed subspace compressive measurement matrix, the second stage collects the UWB channel side information. Then, in the third stage, the received symbols are demodulated based on the template generated from the second stage.

4.2 Design of subspace measurement operator

4.2.1 Sparsity Dictionary

To design a subspace measurement operator, the received signal subspace has to be estimated. In this thesis, CS based reconstruction algorithms are adapted to estimate the subspace of sparse UWB signal. Compressive measurements for subspace estimation are obtained from pilot symbols. We first address the design of a sparsity dictionary tailored to the application at hand to sparsely represent the received UWB signal. Since the wireless UWB channel is sparse in the time domain, a dictionary Ψ_c can be suitably designed such that the received I-UWB signal becomes sparse in this dictionary [38, 2]. Note that the received UWB signal can be expressed as a linear combination of delayed versions of the transmitted waveform $g(t)$ modulated by the UWB path amplitudes. Therefore, the dictionary Ψ_c can be constructed so that each element of Ψ_c , denoted by Ψ_{cj} , is a time-shifted version of the transmitted pulse $g(t)$. More precisely, the j th element of the dictionary is defined as [2]:

$$\Psi_{cj}(t) = g(t - j\xi), \quad (4.6)$$

where $\xi > 0$ is a time shift between consecutive pulses. Let Ψ_u be the sampled version of Ψ_c and let $\xi = 1/F_s$, then the j th column vector of Ψ_u is designed as

$$\Psi_{uj}(n) = g(n/F_s - j/F_s), n = 0, 1, \dots, F_s T_i - 1. \quad (4.7)$$

Ψ_u is further adjusted by normalization on its column vectors.

The total number of paths of a UWB channel can be quite large, leading to a dense representation of the received signal on the designed dictionary Ψ_u . However, a large number of these paths have small amplitudes that can be considered as negligible, leading to a sparse channel model that still introduces multipath diversity but with far fewer parameters. Thus, only the K paths with the largest path gains are considered to give the received UWB signal a sparse representation and, at the same time, capture a great percentage of the received UWB signal energy. Consequently, the received UWB signal can be approximated as $\mathbf{x} \approx \mathbf{H}_u \underline{\theta}_u$, where $\underline{\theta}_u$ is a $K \times 1$ all non-zero vector and the $N \times K$ matrix \mathbf{H}_u is constructed from the K relevant column vectors of Ψ_u .

4.2.2 Estimation of Signal Subspace

Note that the received UWB signal can be thought of as residing in the K -dimensional subspace spanned by the column vectors of the $N \times K$ matrix \mathbf{H}_u . Our objective is to obtain an estimation of the signal subspace which contains most of the signal energy from a reduced set of compressive measurements of the received UWB pilots. It is equivalent to the estimation of the most significant UWB channel paths. Since we are only interested in searching for the most significant channel bins that contain a large fraction of the channel energy, or equivalently, partial sparsity recovery of the received UWB signal, the number of compressive measurements needed is far fewer than that predicted by complete channel recovery thus leading to less demanding ADC resources [15, 34, 35]. However, the required number of measurements may still be too demanding in hardware. As can be observed from Fig.4.1, the proposed I-UWB receiver has only M parallel mixer-integrators and thus for each transmitted pulse, only M measurements can be obtained. Due to the constraints on the receiver size and power consumption, M should be relatively small and may not be sufficient for a reliable channel estimation. To overcome this

problem, a complete set of random measurements for partial sparsity recovery are obtained over multiple pilots. Let M_e be the number of measurements needed for UWB subspace estimation where it is assumed that M_e is a multiple of M and can be represented as $M_e = DM$. Furthermore, it is also assumed that the pilot number N_{p1} is a multiple of D and can be represented as $N_{p1} = DN_{\bar{p}}$. Then for partial sparsity recovery, a random matrix $\Phi_e \in \mathcal{R}^{M_e \times N}$ is employed by the receiver where each entry of Φ_e is drawn from an i.i.d. Bernoulli distribution. To distribute a complete set of measurements onto D pilots, Φ_e is further divided row-wise into D sections as represented below:

$$\Phi_e = [\Phi_0^T | \Phi_1^T | \Phi_2^T \dots \Phi_{D-1}^T]^T, \quad (4.8)$$

where each Φ_i , for $i = 0, 1, \dots, D - 1$ is a $M \times N$ random matrix. For the first group of pilot symbols, Φ_0 is used to correlate with first $N_{\bar{p}}$ pilot signals; Φ_1 is used to correlate with the second $N_{\bar{p}}$ pilot signals, and so on. The compressive measurements multiplied by the PN code in one frame are represented as:

$$\mathbf{y}_{p1}[n] = \Phi_{\lfloor \frac{n}{N_{\bar{p}}N_f} \rfloor} \left[\mathbf{x} + a_n \mathbf{w}[n] \right], \quad n = 0, \dots, N_{p1}N_f - 1, \quad (4.9)$$

where $N_{\bar{p}} = N_{p1}/D$. The measurement vector $\mathbf{y}_{p1}[n]$ is an M -dimensional vector containing the outputs of the M mixer-integrators during the n th frame. Note that the same projection matrix is used for $N_f N_{\bar{p}}$ consecutive received pilot signals. In (4.9), $\mathbf{w}[n]$ is the digitized noise within the measurement interval of the n th frame and is assumed to be WGN with variance $N_0 B$. However, it should be clear that only the measurements $\mathbf{y}_{p1}[n]$ are sampled and digitized.

Based on the compressive measurements $\mathbf{y}_{p1}[n]$, the signal subspace can be estimated. To this end, $\{\mathbf{y}_{p1}[n]\}$ is reorganized as $N_{\bar{p}}N_f$ vectors with size $M_e \times 1$,

for $n = 0, 1, 2, \dots, N_f N_{p1} - 1$, as shown below:

$$\tilde{\mathbf{y}}_0 = \begin{bmatrix} \mathbf{y}_{p1}[0] \\ \mathbf{y}_{p1}[N_{\tilde{p}}N_f] \\ \vdots \\ \mathbf{y}_{p1}[(D-1)N_{\tilde{p}}N_f] \end{bmatrix}, \quad (4.10)$$

$$\tilde{\mathbf{y}}_1 = \begin{bmatrix} \mathbf{y}_{p1}[1] \\ \mathbf{y}_{p1}[N_{\tilde{p}}N_f + 1] \\ \vdots \\ \mathbf{y}_{p1}[(D-1)N_{\tilde{p}}N_f + 1] \end{bmatrix}, \quad (4.11)$$

...

and

$$\tilde{\mathbf{y}}_{N_{\tilde{p}}N_f-1} = \begin{bmatrix} \mathbf{y}_{p1}[N_{\tilde{p}}N_f - 1] \\ \mathbf{y}_{p1}[2N_{\tilde{p}}N_f - 1] \\ \vdots \\ \mathbf{y}_{p1}[DN_{\tilde{p}}N_f - 1] \end{bmatrix}. \quad (4.12)$$

Represented digitally, these compressive measurements can be easily averaged to reduce the noise effect leading to:

$$\bar{\mathbf{y}}_{p1} = \frac{1}{N_{\tilde{p}}N_f} \sum_{i=0}^{N_{\tilde{p}}N_f-1} \tilde{\mathbf{y}}_i. \quad (4.13)$$

Given Φ , Ψ_u and the averaged compressive measurements $\bar{\mathbf{y}}_{p1}$, the signal subspace can be estimated by suitably adapting a CS reconstruction algorithm to find the basis elements of a sparse signal. In this work, we use the Basis Pursuit Denoising (BPDN) algorithm which solves the following optimization problem [13, 18, 8]:

$$\hat{\underline{\theta}} = \arg \min_{\underline{\theta}} \|\mathbf{U}\Phi\Psi_u\underline{\theta} - \mathbf{U}\bar{\mathbf{y}}_{p1}\|_2^2 + \lambda\|\underline{\theta}\|_1, \quad (4.14)$$

where $\mathbf{U} \in \mathcal{R}^{M \times M}$ is a whitening operator defined such that $\mathbf{U}\mathbf{U}^T = (\Phi\Phi^T)^{-1}$. BPDN algorithm is a robust CS reconstruction algorithm which balances the tasks

of seeking a sparse solution and minimizing the measurement noise [13]. With noisy measurements, BPDN leads to better subspace estimation than other CS reconstruction algorithms like Matching Pursuit (MP) or orthogonal Matching Pursuit (OMP) at the expense of slightly higher computation [74, 16]. The resultant solution $\hat{\theta}$ gives an estimation of the signal structure. If we know that most of the UWB channel energy is concentrated on K significant paths, we can then locate the K entries of $\hat{\theta}$ with the largest magnitude values. The locations of those K entries are related to the K column vectors in Ψ_u that spans the received UWB signal. Assembling those K N -dimensional vectors as a $N \times K$ matrix, we obtain $\hat{\mathbf{H}}_u$, the estimate of \mathbf{H}_u .

4.2.3 Design of Subspace Compressive Measurement Matrices

Given $\hat{\mathbf{H}}_u$, we can proceed to design a subspace compressive measurement matrix Φ_x (the projection operator) with size $M \times N$ for subsequent detection stages. This matrix is employed to project the second group of pilot symbols and all the transmitted data symbols. As will be observed in Sec. 4.3, the detection performance of the proposed UWB receiver depends on the term:

$$\varsigma = \mathbf{x}^T \Phi_x^T (\Phi_x \Phi_x^T)^{-1} \Phi_x \mathbf{x} \leq \mathbf{x}^T \mathbf{x}, \quad (4.15)$$

where ς is the energy that the projection operator Φ_x can collect. Thus, designing Φ_x should exploit the fact that we want to collect as much energy as possible from the received UWB signal.

Since we are interested in the design of a low-power consumption receiver, the number of parallel measurement paths M is in general smaller than K . Therefore, instead of locating K vectors in the optimal solution of (4.14), only M most significant paths are extracted leading to $\hat{\mathbf{H}}_u$ constructed with only M column vectors. Then the subspace compressive projection matrix is constructed as [31]:

$$\Phi_x = \mathbf{G}(\hat{\mathbf{H}}_u^T \hat{\mathbf{H}}_u)^{-1} \hat{\mathbf{H}}_u^T, \quad (4.16)$$

where \mathbf{G} is an $M \times M$ random matrix with each entry drawn from an i.i.d. Gaussian distribution. If the estimation of the UWB channel is accurate, it can be shown that ς is always equal to the energy contained by the most significant M paths. Note that by designing Φ_x as in (4.16), the noisy received signal is projected into an estimated signal subspace first, and the result is then randomly projected onto random vectors. By projecting the noisy data into the estimated signal subspace, most of the desired signal energy is preserved. However, the noise power is significantly reduced. Thus, a good detection performance is expected even with a small number of measurements.

At first glance, \mathbf{G} seems to be redundant in the construction of Φ_x . However, adding \mathbf{G} to (4.16) has the following advantages. First, as in CS sampling framework, each measurement is equally important. Thus, if any path in the parallel architecture shown in Fig. 4.1 should fail, the detection performance will not be heavily effected, which is a desirable feature from a hardware implementation aspect. Second, since each measurement has the same dynamic range, selection of the appropriate ADCs becomes easier. Another important feature of the proposed method is that since each entry of Φ_x belongs to the same zero-mean Gaussian distribution, optimal quantization via the Lloyd-Max algorithm will be effective leading to less performance loss due to waveform quantization in the hardware implementation [51].

To simplify the hardware implementation, it is desirable to quantize Φ_x to binary, because the resulting high bandwidth binary analog waveform is much easier to generate than a higher resolution version. Thus, the binary measurement matrix is given by:

$$\Phi_x = Q_b[\mathbf{G}(\hat{\mathbf{H}}_u^T \hat{\mathbf{H}}_u)^{-1} \hat{\mathbf{H}}_u^T] \quad (4.17)$$

where $Q_b[\]$ denotes the quantization of the measurement matrix to binary levels. Quantization leads to inevitable performance degradation. The Lloyd-Max method minimizes the quantization noise by exploiting the fact that each entry of the original subspace projection matrix follows the same Gaussian distribution [51].

4.3 Symbol Demodulation

For the proposed subspace compressive receivers, symbol demodulation is similar to the autocorrelation receivers. However, the signal template is in digital form leading to ease of noise reduction via template averaging. The proposed UWB detector for symbol demodulation is discussed below.

4.3.1 Test Statistic for Compressive UWB Signal Detection

During the second group of the pilot symbols, the received signal is projected onto binary sequences corresponding to rows of Φ_x . The subspace compressive measurements multiplied by the PN code during this stage are represented as:

$$\mathbf{y}_{p2}[n] = \Phi_x \mathbf{x} + a_{n+\Delta N} \Phi_x \mathbf{w}[n + \Delta N], \quad (4.18)$$

where $n = 0, 1, \dots, N_{p2}N_f - 1$ and $\Delta N = N_{p1}N_f$. By averaging $\mathbf{y}_{p2}[n]$ over multiple frames, the side information of the UWB channel can be obtained and used as the template for symbol demodulation.

In the data demodulation stage, the subspace compressive measurements multiplied by the PN code for the j th data modulated symbol are given by:

$$\mathbf{y}_{d[j]}[n] = b_j \Phi_x \mathbf{x} + a_{n+\tilde{\Delta}N} \Phi_x \mathbf{w}[n + \tilde{\Delta}N], \quad (4.19)$$

where $n = 0, 1, \dots, N_f - 1$, $\tilde{\Delta}N = (N_p + j)N_f$ and $j = 0, 1, \dots, N_s - 1$. As it will be shown shortly, by employing a GLRT detector, b_j can be demodulated from the measurement $\mathbf{y}_{d[j]}[n]$.

Assume that the data bits $\{1, -1\}$ are transmitted with equal probability. Without loss of generality, the detection of the j th symbol b_j is discussed. To simplify the notations, the index j is suppressed when appropriate. Based on the subspace compressive measurements, two hypotheses must be distinguished:

$$\begin{aligned} \mathcal{H}_0 & : \mathbf{y}_d[n] = -\Phi_x \mathbf{x} + a_{n+\tilde{\Delta}N} \Phi_x \mathbf{w}[n + \tilde{\Delta}N], \quad (b_j = -1), \\ \mathcal{H}_1 & : \mathbf{y}_d[n] = \Phi_x \mathbf{x} + a_{n+\tilde{\Delta}N} \Phi_x \mathbf{w}[n + \tilde{\Delta}N], \quad (b_j = 1), \end{aligned}$$

with $n = 0, 1, \dots, N_f - 1$. Let $\chi = \Phi_x \mathbf{x}$ and $\hat{\chi}$ be the maximum likelihood estimation (MLE) of χ , then the likelihood ratio test for this detection problem is given by:

$$L(\mathbf{y}_d) = \frac{p(\mathbf{y}_d; \hat{\chi}, \mathcal{H}_1)}{p(\mathbf{y}_d; \hat{\chi}, \mathcal{H}_0)} \underset{\mathcal{H}_0}{\underset{\mathcal{H}_1}{\geq}} 1. \quad (4.20)$$

where $p(\mathbf{y}_d; \hat{\chi}, \mathcal{H}_1)$ and $p(\mathbf{y}_d; \hat{\chi}, \mathcal{H}_0)$ are the probability density function (PDF) of the projected data under \mathcal{H}_1 and \mathcal{H}_0 , respectively. Here \mathbf{y}_d is defined as: $\mathbf{y}_d = [\mathbf{y}_d[0], \mathbf{y}_d[1], \dots, \mathbf{y}_d[N_f - 1]]^T$. In (4.20), $\hat{\chi}$ is obtained from the subspace compressive measurements of the second group of the pilot signals as follows:

$$\hat{\chi} = \frac{1}{N_{p2}N_f} \sum_{n=0}^{N_{p2}N_f-1} \mathbf{y}_{p2}[n] = \Phi_x \mathbf{x} + \Phi_x \bar{\mathbf{w}}_p, \quad (4.21)$$

where

$$\bar{\mathbf{w}}_p = \frac{1}{N_{p2}N_f} \sum_{n=0}^{N_{p2}N_f-1} a_{n+\Delta N} \mathbf{w}[n + \Delta N], \quad (4.22)$$

is an $N \times 1$ WGN vector with variance $N_0 B / (N_{p2} N_f)$.

It can be easily shown that under \mathcal{H}_0 , the PDF of the projected UWB signal within one symbol is:

$$p(\mathbf{y}_d; \hat{\chi}, \mathcal{H}_0) = \frac{1}{(2\pi)^{\frac{MN_f}{2}} \det^{\frac{N_f}{2}}(\mathbf{C})} \exp \left[-\frac{1}{2} \sum_{n=0}^{N_f-1} (\mathbf{y}_d[n] + \hat{\chi})^T \mathbf{C}^{-1} (\mathbf{y}_d[n] + \hat{\chi}) \right], \quad (4.23)$$

where $\mathbf{C} = N_0 B \Phi_x \Phi_x^T$. While under \mathcal{H}_1 , the PDF of the projected UWB signal is:

$$p(\mathbf{y}_d; \hat{\chi}, \mathcal{H}_1) = \frac{1}{(2\pi)^{\frac{MN_f}{2}} \det^{\frac{N_f}{2}}(\mathbf{C})} \exp \left[-\frac{1}{2} \sum_{n=0}^{N_f-1} (\mathbf{y}_d[n] - \hat{\chi})^T \mathbf{C}^{-1} (\mathbf{y}_d[n] - \hat{\chi}) \right]. \quad (4.24)$$

After some simplifications, an equivalent test statistic is obtained following the likelihood ratio test in (4.20):

$$\begin{aligned} t(\mathbf{y}_d) &= \frac{\ln L(\mathbf{y}_d)}{2N_f} \\ &= (\Phi_x \mathbf{x} + \Phi_x \bar{\mathbf{w}}_p)^T (N_0 B \Phi_x \Phi_x^T)^{-1} (b_j \Phi_x \mathbf{x} + \Phi_x \bar{\mathbf{w}}_d), \end{aligned}$$

where

$$\bar{\mathbf{w}}_d = \frac{1}{N_f} \sum_{n=0}^{N_f-1} a_{n+\tilde{\Delta}N} \mathbf{w}[n + \tilde{\Delta}N]$$

is an $N \times 1$ WGN vector with variance N_0B/N_f . The estimation of b_j turns out to be the sign of the test statistic, i.e.:

$$\hat{b}_j = \text{sgn}(t(\mathbf{y}_d)). \quad (4.25)$$

4.3.2 Performance Evaluation

Given a channel realization and the quantized subspace measurement matrix, the performance of the proposed subspace compressive GLRT UWB detector can be evaluated as follows. Without loss of generality, let $b_j = 1$ be the transmitted symbol. The subspace compressive UWB detector generates an error when $t(\mathbf{y}_d)|_{b_j=1} < 0$. To facilitate the performance analysis, the measurements are whitened first, hence the test statistic $t(\mathbf{y}_d)$ can be rewritten as:

$$t(\mathbf{y}_d) = (\mathbf{U}_x \Phi_x \mathbf{x} + \mathbf{U}_x \Phi_x \bar{\mathbf{W}}_p)^T (\mathbf{U}_x \Phi_x \mathbf{x} + \mathbf{U}_x \Phi_x \bar{\mathbf{w}}_d).$$

where \mathbf{U}_x is an $M \times M$ whitening matrix such that $\mathbf{U}_x^T \mathbf{U}_x = (N_0B \Phi_x \Phi_x^T)^{-1}$. Define $\mathbf{z} = \mathbf{U}_x \Phi_x \mathbf{x}$, $\mathbf{w}'_p = \mathbf{U}_x \Phi_x \bar{\mathbf{w}}_p$ and $\mathbf{w}'_d = \mathbf{U}_x \Phi_x \bar{\mathbf{w}}_d$, then $t(\mathbf{y}_d)$ reduces to:

$$t(\mathbf{y}_d) = (\mathbf{z} + \mathbf{w}'_p)^T (\mathbf{z} + \mathbf{w}'_d). \quad (4.26)$$

Based on (4.26), an approximate expression for the bit error rate (BER) can be derived under the Gaussian assumption as follows. By the central limit theorem, for $M \gg 1$, $\mathbf{w}'_p{}^T \mathbf{w}'_d$ is approximately Gaussian with zero mean and variance $\frac{M}{N_p 2 N_f^2}$. When $M \gg 1$, it is also valid to assume $\mathbf{w}'_p{}^T \mathbf{w}'_d$, $\mathbf{w}'_p{}^T \mathbf{z}$ and $\mathbf{w}'_d{}^T \mathbf{z}$ as independent Gaussian random variables. Then, it can be shown that the mean of $t(\mathbf{y}_d)$ is given by:

$$\overline{t(\mathbf{y}_d)} = \mathbf{z}^T \mathbf{z}. \quad (4.27)$$

Furthermore, the variance of $t(\mathbf{y}_d)$ is given by:

$$\text{VAR}(t(\mathbf{y}_d)) = \frac{(N_{p2} + 1)|\mathbf{z}|^2}{N_{p2}N_f} + \frac{M_d}{N_{p2}N_f^2}. \quad (4.28)$$

Thus, for a given projection matrix Φ_x and a UWB channel realization, $h(t)$, the BER is given by:

$$P|_{h, \Phi_x} = Q \left[\left(\left(\frac{N_{p2} + 1}{N_{p2}N_f} \right) \frac{1}{|\mathbf{z}|^2} + \frac{M}{N_{p2}N_f^2|\mathbf{z}|^4} \right)^{-\frac{1}{2}} \right]. \quad (4.29)$$

Note that the detection performance depends on the signal to noise ratio and the signaling parameters. Although less obvious, the detection performance also depends on the sparsity of the UWB channel.

4.4 Discussion

4.4.1 Parameter Selection and Hardware Implementation

As can be seen from (4.29), a large number of frames N_f and a large number of pilots N_{p2} reduce the received signal noise leading to a better BER. Although less evident in (4.29), the number of pilots N_{p1} and the number of pilot compressive measurements M_e for signal subspace estimation also affect the performance of signal detection. A larger N_{p1} leads to less noise in the measurements and, in turn, a more reliable signal subspace estimation is achieved. Likewise, more measurements M_e contain more salient information about the underlying signal leading to a more accurate subspace estimation. Consequently, the capability of the receiver to collect the desired signal energy is improved leading to a better detection performance. Note that $|\mathbf{z}|^2$ represents the desired signal energy the detector can capture, which is closely related to the accuracy of the subspace estimation. The number of measurements M_e should be sufficiently large to be able to reliably estimate the signal subspace. As a rule of thumb, we find that the compressive measurements M_e should be about $3 \sim 4 \times K$ to achieve robust subspace estimation. However,

increasing N_f , N_{p2} and N_{p1} also reduces the achievable data rate and increases the system overhead. A large M_e also requires that N_{p1} should be sufficiently large.

An optimal value of M depends on the signal to noise ratio (SNR). For SNR sufficiently large, better detection performance can be achieved with larger M . However, M in practice is constrained by the hardware limits and thus can not be arbitrary large. To get satisfactory detection performance, M should be a significant portion of the channel sparsity K . The filter bandwidth B , the pulse energy E and the mixer integration time T_i also have direct effects on the captured signal energy $\mathbf{z}^T \mathbf{z}$. As stated above, the filter bandwidth B should be selected as small as possible to reduce the introduced noise, but large enough to bring negligible distortion to the received signal. Furthermore, as expected, increasing the pulse energy E improves the BER. However, the pulse energy should be chosen to satisfy the US Federal Communications Commission (FCC) power spectrum regulations [1]. The measurement interval T_i should be chosen such that a significant portion of the received signal energy is collected. An unnecessarily large T_i only deteriorates the detector performance as more noise is introduced with no or little gain on the captured energy [82]. In [83], it is suggested that the optimum integration time in a noisy environment is approximately twice the RMS delay spread of the channel. See [82, 83, 84] for more discussion on the integration time.

The proposed UWB receivers have practical hardware implementations, which makes low-cost and low-power I-UWB communication system feasible. The proposed receiver is composed of a wideband filter at the front end, M high-speed wideband analog mixers, M wideband binary sequence generators and M low-speed ADCs. Wideband filtering technology is relatively mature [85]. High-speed analog mixers suitable for UWB communication are also available. See [86, 87, 88, 89] for more details on wideband mixers. Wideband binary sequence generator can be implemented by high-speed shift registers with flip-flops, which could potentially lead

to low-power integrated circuits. Refer to [53, 52, 90] and the references therein for more details on high-speed wideband binary sequence generators. Note that cutting-edge technology shows that even multi-bit waveform generator at GS/s is feasible [50]. Current research also shows that it is promising to design simple GHz wideband analog waveform generators (AWG) through optical techniques [91, 92, 93].

4.4.2 Comparison with Other Receivers

With the same hardware architecture, a compressive receiver can be built where the projection matrix denoted as Φ_c in this case is constructed such that each entry of the projection matrix belongs to an i.i.d. Bernoulli distribution. Although the measurement follows the traditional CS approaches, in this case Φ_c does not exploit signal structure and is not efficient at collecting the signal energy. It can be shown Φ_c leads to the collected energy $\varsigma \approx \frac{M}{N} \mathbf{x}^T \mathbf{x}$. For M small, ς is much less than $\mathbf{x}^T \mathbf{x}$ leading to poor detection performance. In the simulation section, we will compare the detection performance of the proposed detector with that yielded by a compressive detector adapted for I-UWB symbol detection [49]. The sufficient statistic of the compressive detector is given by:

$$\varrho = \alpha^T (\Phi_c \Phi_c^T)^{-1} \beta, \quad (4.30)$$

where

$$\alpha = \frac{1}{N_p N_f} \sum_{n=0}^{N_p N_f - 1} \Phi_c(\mathbf{x} + a_n \mathbf{w}[n]) \quad (4.31)$$

is a noisy template obtained from received pilot symbols and

$$\beta = \frac{1}{N_f} \sum_{n=0}^{N_f - 1} \Phi_c(\mathbf{x} + a_{n+\check{\Delta}N} \mathbf{w}[n + \check{\Delta}N]) \quad (4.32)$$

is the average of the received signals in a symbol interval where $\check{\Delta}N = N_p N_f$. The estimated symbol is $\hat{b} = \text{sgn}(\varrho)$.

A natural extension of the proposed approach emerges if the random matrix \mathbf{G} is replaced by an identity matrix leading to a projection matrix designed as:

$$\Phi_t = (\hat{\mathbf{H}}_u^T \hat{\mathbf{H}}_u)^{-1} \hat{\mathbf{H}}_u^T, \quad (4.33)$$

It can be shown that Φ_t has equal capability to collect the signal energy as the proposed subspace projection matrix Φ_x . The UWB receiver based on Φ_t is called transform based receiver [37]. The transform based receiver has two disadvantages. The measurement matrix actually measures the UWB path strengths. Due to the fast decaying of the path amplitudes over the time axis, not every measurement is equally important. Failure to measure a large path strength will lead to high probability of detection error. Thus, the receiver is not robust to hardware failures. Second, simulation results in Sec. 4.5 show that the transform based receiver is also less robust to waveform quantization leading to worse detection performance.

The proposed receivers have similar hardware architecture to SRake receivers. Note that both the proposed receivers and SRake receivers rely on the information of significant channel paths to collect the desired signal energy. Just as the proposed receivers, SRake receivers also employ parallel integrate-and-dump structure, thus high-speed mixers are also needed. However, instead of generating binary sequences, local pulse templates are generated to match the received pulses. Although generating an ultra-shot pulse could be easy, generating a pulse that fits the FCC transmission spectrum is not trivial. To generate the pulse with the desired power spectrum, the employment of more complex hardware is required, which makes the implementations of parallel local pulse generators challenging [94, 95, 96]. Instead, in our design, the local pulse generators are replaced with binary sequence generators which can be implemented in integrated circuits, thus making a low-cost, low-power design possible. More importantly, the proposed receivers can use the same set of hardware for channel estimation and symbol detection.

For comparison purposes, an SRake receiver tailored to the proposed signaling scheme is introduced below. It is assumed that the underlying SRake receiver has the ability to estimate the significant UWB paths via CS approaches, as in our proposed receiver. Thus, N_p pilot symbols are employed to get an estimation of the UWB channel $\hat{\mathbf{h}}$. The measurement and the estimation approach is the same as in our proposed subspace compressive detection. The sufficient statistic of the SRake receiver is:

$$\pi = \zeta^T \nu, \quad (4.34)$$

where ζ is a noisy template obtained from the channel estimation and is given by:

$$\zeta = \Psi_u \hat{\mathbf{h}}, \quad (4.35)$$

and ν is the average of the received signal in a symbol interval given by:

$$\nu = \frac{1}{N_f} b \sum_{n=0}^{N_f-1} \mathbf{x} + a_{n+\check{\Delta}N} \mathbf{w}[n + \check{\Delta}N]. \quad (4.36)$$

The estimated symbol is $\hat{b} = \text{sgn}(\pi)$.

Obviously, a full-resolution GLRT detector relying on Nyquist sampling can lead to the best detection performance. However, the requirement of high-speed ADCs makes a low-cost and low-power implementation impossible. In the comparative study in Sec. 4.5, the performance of full-resolution GLRT detector serves as a benchmark for the proposed detectors. The sufficient statistic of the full-resolution GLRT detector is given by [97]:

$$\omega = \gamma^T \nu, \quad (4.37)$$

where γ is a noisy template obtained by averaging the received pilot symbols given by:

$$\gamma = \frac{1}{N_p N_f} \sum_{n=0}^{N_p N_f - 1} \mathbf{x} + a_n \mathbf{w}[n]. \quad (4.38)$$

The estimated symbol is $\hat{b} = \text{sgn}(\omega)$.

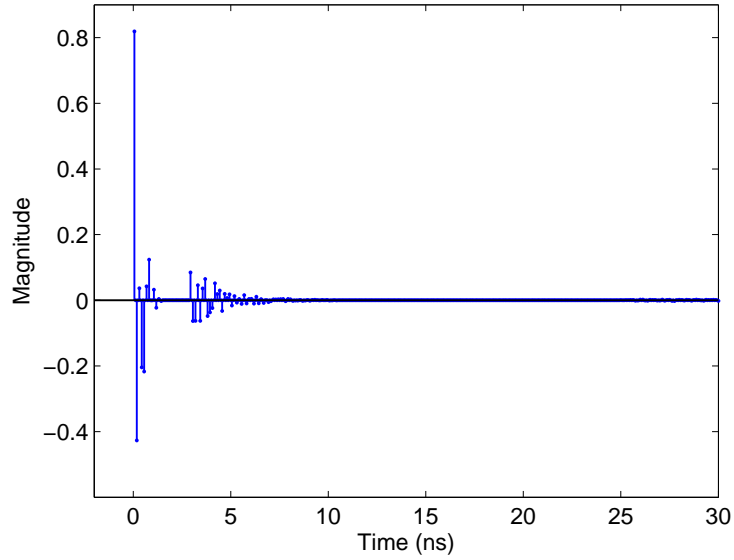


Figure 4.2: A channel realization of CM-7 sparse in the time domain [1].

4.5 Simulations

In this section, the performance of the subspace compressive GLRT I-UWB detector is evaluated through extensive simulations. The UWB channel model used for simulation is the IEEE 802.15.4a CM-7, industrial light of sight (LOS) channel [1]. The root-mean-square (RMS) delay spread of the CM-7 channel is around $T_{rms} = 10$ ns. The maximal excess delay of the channel is set to $T_{med} = 40$ ns and unit energy of the channel is assumed. The channel impulse response is based on the Saleh-Valenzuela (SV) model where the channel bins arrive in clusters and the most significant bin arrives first representing the LOS path [98]. A realization of CM-7 channel is depicted in Fig. 4.2, where two clusters of multipath components are shown. As can be seen in Fig. 4.2, the channel has only a few significant paths and its power delay profile (PDP) is not monotonic, but rather sparse. Although there are two clusters, the magnitudes of the bins in the second cluster are much smaller than those in the first cluster and we can estimate the channel sparsity K at around 15. See [1] for more details on the channel characteristics.

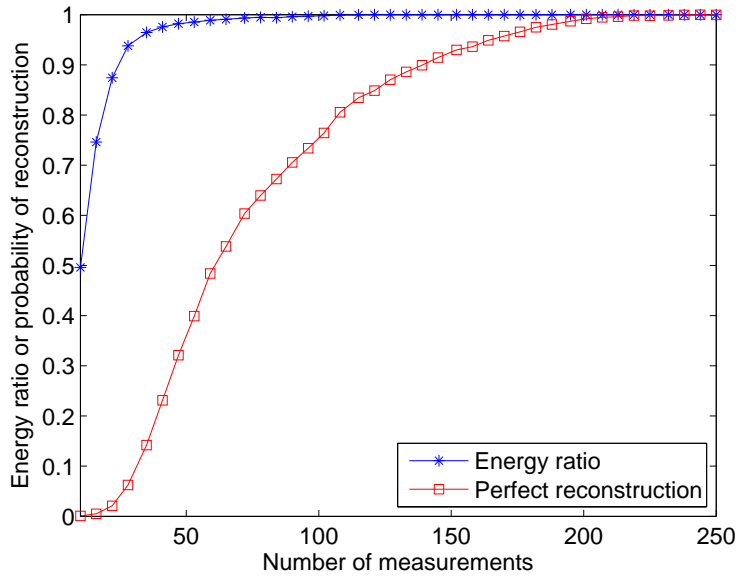


Figure 4.3: Performance of UWB subspace estimation algorithm with different number of measurements.

The transmitted pulse $g(t)$ is the second derivative of a Gaussian pulse with a central frequency of 3 GHz and pulse duration $T_g \approx 0.35$ ns [99]. For the front-end filter, the filter bandwidth B is 8 GHz. For simulation purposes, the underlying sampling frequency F_s for the random digital sequence is then set to 16 GHz. The received UWB signals are contaminated with additive white Gaussian noise with variance N_0 . To avoid excessive additive noise, the integration time is set to $T_i = 16$ ns. Note that T_i here is smaller than T_{med} and is only around $1.5 \times T_{rms}$. However, this time interval contains most of the desired signal energy. Correspondingly, the length of the received signal is $N = T_i * F_s = 256$.

4.5.1 UWB Subspace Estimation

First, we investigate the ability of the modified BPDN algorithm given by (4.14) to estimate the UWB signal subspace from random measurements contaminated with additive Gaussian noise. For the purpose of signal subspace estimation, the noisy received UWB signal is projected onto binary random waveforms. We

evaluate the performance of the BNDN algorithm by calculating the ratio of the signal energy residing in the estimated signal subspace over the total signal energy. For comparison purposes, we also compute the probability of successful reconstruction yielded by BPDN algorithm with different number of measurements. A reconstruction is considered successful if $(\mathbf{x} - \hat{\mathbf{x}})^T(\mathbf{x} - \hat{\mathbf{x}})/\mathbf{x}^T\mathbf{x} < 0.01$, where $\hat{\mathbf{x}}$ is the reconstructed signal. For ease of comparison, all the paths whose magnitudes are less than 5% that of the largest path are omitted and then the estimated signal subspace is of size 256×16 . Figure 4.3 shows the simulation results where $\text{SNR} = 17.9$ dB with SNR defined as $\text{SNR} = \mathbf{x}^T\mathbf{x}/(NN_0B)$ [29]. Each simulation result is the average over 1000 channel realizations. As shown in Fig. 4.3, high probability of perfect reconstruction is not achievable at such low SNR until the number of measurements is over 200. However, with as few as 50 measurements, the proposed subspace estimation algorithm can effectively determine the locations of the most significant signal components and, therefore, the estimated signal subspace contains most of the UWB signal energy. Thus, BPDN can be effectively used as UWB signal subspace estimator requiring a small number of random measurements.

4.5.2 Symbol Detection with Binary Measurement Waveform

We evaluate the detection performance of the proposed subspace compressive UWB receivers before and after waveform binarization. The I-UWB signaling parameters are set as follows: $N_{p1} = 40$, $N_{p2} = 2$, $N_f = 5$, $N_c = 16$, $T_c = 25$ ns and $T_f = 400$ ns. The targeted data rate is approximately 500 Kb/s. One thousand channel realizations are used and for each channel realization, 1000 symbols are transmitted. It is assumed that one pulse transmission leads to $M = 16$ measurements. However, a set of 64 measurements are required for the signal subspace estimation, thus one complete set of measurements for channel estimation are distributed to 4 pilots. The average of 10 sets of compressive measurements are employed by the modified BPDN algorithm to estimate the signal subspace. As

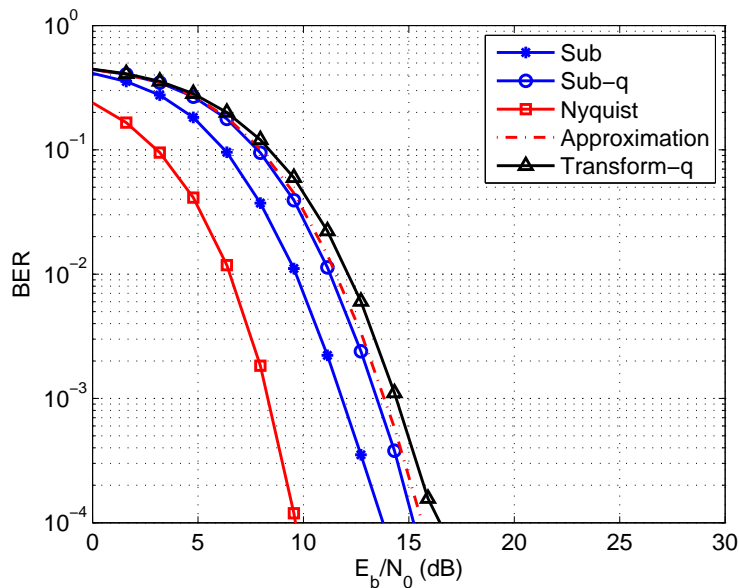


Figure 4.4: Performance of subspace compressive GLRT UWB detectors. “Sub” is the proposed receiver; “Sub-q” is the proposed receiver with binary measurement waveform; “Nyquist” is the full-resolution digital receiver; “Approximation” is the Gaussian approximation; “Transform-q” is the transform based receiver with quantized binary measurement waveform.

stated previously, the number of subspace compressive measurements is $M = 16$ for the GLRT symbol detection. Note that this number is only 6.25% of the data length, which means the sampling rate is only 6.25% of the original Nyquist sampling rate. Since only $M = 16$ measurements can be made, we estimate 16 most significant subspace components or channel paths in order to capture most of the received signal energy.

Measured by the BER, the detection performance of the proposed receivers as a function of E_b/N_0 is shown in Fig. 4.4. Compared with the case when no quantization is made, the measurement waveform quantized to only two levels leads to graceful degradation with only 1.5 dB loss in SNR at $\text{BER} = 10^{-4}$. However, the hardware implementation is much simplified. Compared with the transform based receiver with measurement waveforms also quantized to two levels, the detection

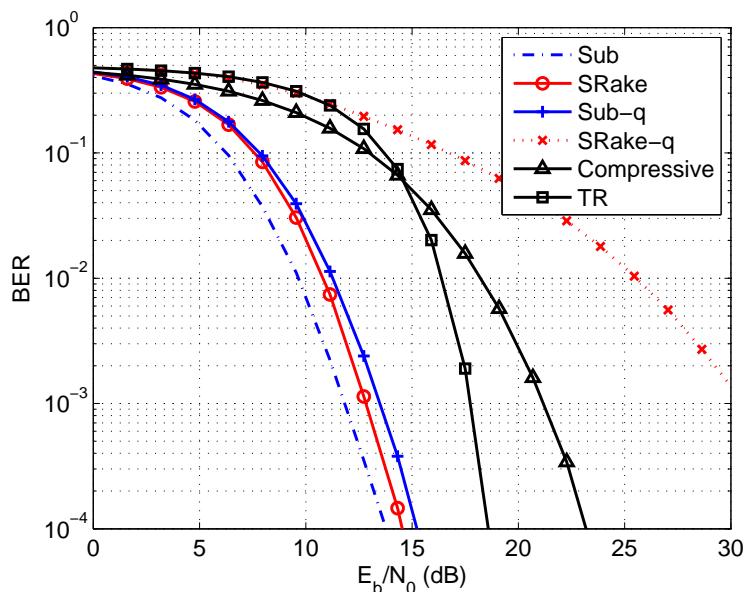


Figure 4.5: Comparison with different receivers. “SRake” is the SRake receiver; “SRake-q” is the SRake receiver with binary measurement waveform; “Compressive” is the compressive receiver; “TR” is the transmitted reference receiver.

performance of our proposed receiver has about 1.2 dB gain at $\text{BER} = 10^{-4}$. Thus, the proposed receiver is more robust against waveform quantization. The simulation results of the proposed receiver are also compared with those given by the analytic expression given by (4.29) based on the Gaussian assumption. As can be seen in Fig. 4.4, the approximation of the BER based on the Gaussian assumption is quite accurate which validates the approximation for the derivation of (4.29).

Figure 4.4 also shows the simulation results of the traditional full-resolution GLRT detector relying on Nyquist sampling, which serves as a benchmark for the proposed detector. For a fair comparison, we set the number of pilot symbols as $N_p = 42$ for the full-resolution digital detector. Simulation results show that the subspace compressive GLRT detector without quantization only has about 4 dB loss at $\text{BER} = 10^{-4}$, which shows that with a much lower sampling rate subspace random projection is an efficient way to capture the signal energy leading to good

detection performance. With relatively high SNR, the BPDN algorithm is effective at estimating the signal subspace, which in turn improves the detection performance of the subspace compressive I-UWB detector.

Comparisons of the proposed subspace compressive receivers with SRake receiver [43], compressive receiver and transmitted reference receiver [45] are shown in Fig. 4.5. Again for fair comparison, we set the number of pilot symbols as $N_p = 42$ for both the SRake receiver and the compressive detector. Based upon the channel estimation, the SRake receiver not only utilizes the information of path delays, but also the estimated path gains. However, for the BER range 10^{-3} to 10^{-4} , the SNR is still too low to get a reliable estimation of the path amplitudes. Thus, SRake receiver does not lead to better detection performance than that of the proposed subspace compressive receiver, as shown in Fig. 4.5. The proposed subspace compressive receiver without waveform quantization has 0.6 dB gain over SRake receiver at BER= 10^{-4} . The SRake receiver has about 1 dB gain over the quantized subspace compressive receiver. However, the quantized subspace compressive receiver is easier to implement in hardware. If the pulse template of the SRake receiver is also quantized to binary levels via optimal quantization, then the useful signal information is almost wiped out, which can be verified by the receiver's poor detection performance shown in Fig. 4.5.

Figure 4.5 also shows that the proposed quantized detector substantially outperforms the compressive GLRT detector that does not exploit the signal structure. Since the measurements are already in the digital form in the proposed receiver, noise reduction can be easily implemented by averaging the noisy measurements. Thus, in the interesting BER range, the proposed receiver also outperforms the transmitted reference receiver whose performance degrading occurs due to the employment of a noisy templet for symbol demodulation.

Since the measurement waveform with binary levels is the most suitable for

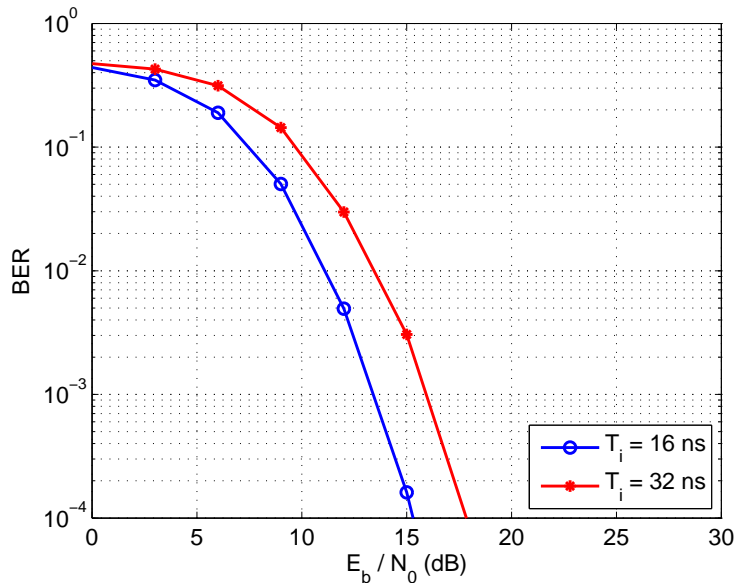


Figure 4.6: Performance of subspace compressive GLRT UWB detector with $T_i = 16$ ns and $T_i = 32$ ns.

hardware implementation, the rest of the simulations will focus on symbol detection with such binary measurement waveforms. In the second simulation, we show the effect of the integration time T_i on the performance of the subspace compressive GLRT I-UWB detectors. Figure 4.6 shows the simulation results for $T_i = 16$ ns and $T_i = 32$ ns with binary measurement waveforms, respectively. As can be observed in Fig. 4.6, $T_i = 16$ ns leads to better performance for UWB symbol detection. An integration time larger than 16 ns does not gain much signal energy, but results in collecting much more noise which degrades the detection performance. This observation is expected since the channel under study is a UWB LOS channel where most of the significant channel bins come within T_{rms} after the first bin, as seen in Fig. 4.2. Thus, a small T_i is more suitable for such channels. However, if T_i is too small, the detector is not able to collect the signal diversity introduced by the multipath UWB channel. It can be shown that the choice of $T_i = 16$ ns is in accordance with the guideline proposed in [83].

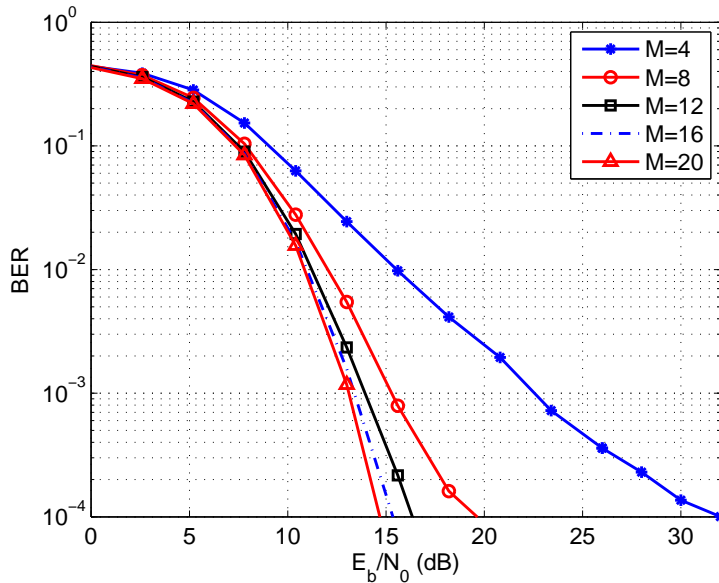


Figure 4.7: Performance of subspace compressive GLRT UWB detector with different number of measurements.

In the third simulation, the effects of the number of compressive measurements M on the system performance are evaluated. We consider $M = 4, 8, 12, 16$ and 20 , respectively, with $T_i = 16$ ns. The simulation results are depicted in Fig. 4.7. As expected, as the number of measurements increases, the performance of the proposed detector increases. However, due to the sparsity of the UWB channel, the channel energy concentrates on a few significant delays. Subsequently, only a few measurements are needed, around 10 for this simulation. As shown in Fig. 4.7, for more than 12 measurements the performance gain becomes insignificant.

4.5.3 Circuit Nonideality

Our proposed measurement scheme for UWB symbol detection is similar to the RMPI architecture which is claimed to be robust to circuit nonidealities [6]. The simulations presented below confirm such observations. In the following simulations, we investigate how the CMOS circuit delay and switching behavior affect the detection performance. Here, we assume that the CMOS gates have

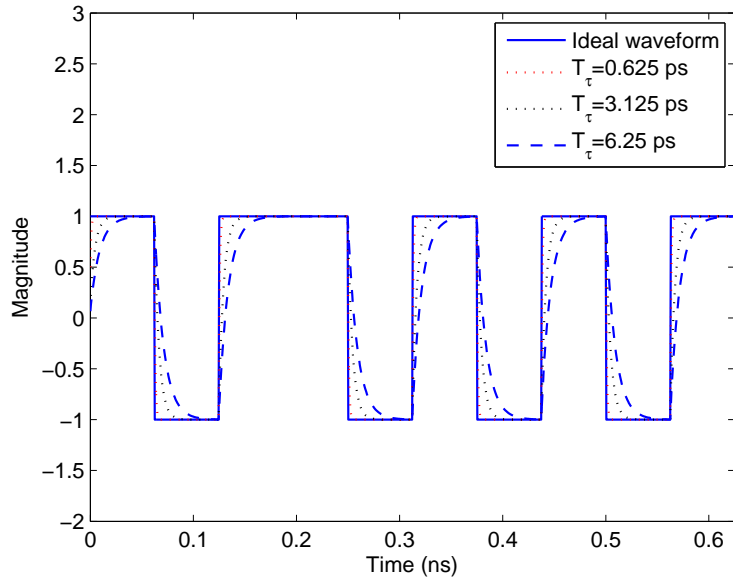


Figure 4.8: Measurement waveform with different delay time. No delay is assumed for the ideal waveform.

simple resistance and capacitance (RC) loads. Thus, the measurement waveforms rise and fall exponentially in transition. To characterize such switching behavior, we use the time delay T_τ defined as the time between the 50% points of the magnitude of the input and output waveforms [100]. Figure 4.8 illustrates how the time delay distorts the shape of a binary measurement waveform, where the nominal period of one bit is 62.5 ps with an underlying frequency of 16 GHz. The simulation results for several values of T_τ are shown in Fig. 4.8. To simulate the continuous waveform, 200 samples are taken for each period. This shows that a time delay which is 5% to 10% of the bit period already causes severe waveform distortions.

Simulation results for symbol detection with delayed measurement waveforms are shown in Fig. 4.9, where the time delay of $T_\tau = 0.625$ ps, 3.125 ps, 6.25 ps and 9.375 ps are investigated. It can be observed that the UWB symbol detection performance degrades gracefully with larger time delay. With the time delay as large as $T_\tau = 6.25$ ps or equivalently 10% of one bit period, the detection performance

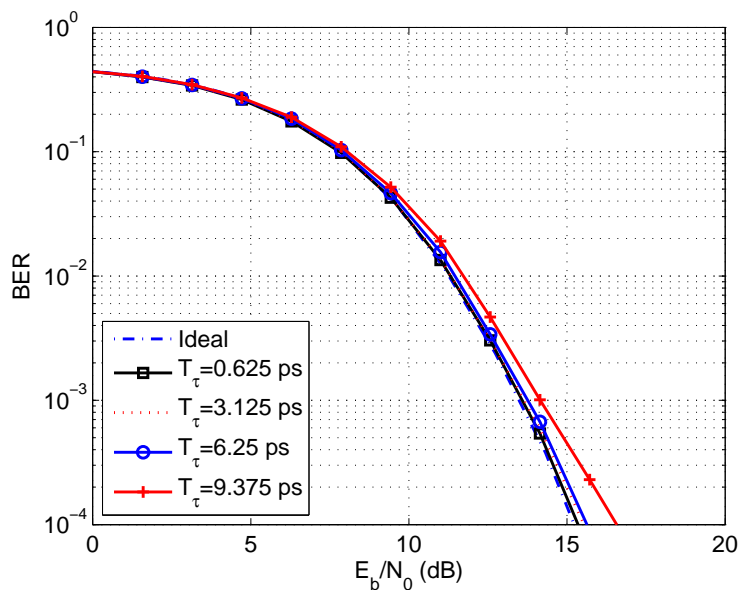


Figure 4.9: Performance of subspace compressive GLRT UWB detector with delayed measurement waveforms.

only degrades about 0.5 dB at $\text{BER} = 10^{-4}$.

Clock timing error is inevitable in practical CMOS circuits. In the last simulation, we investigate the effect of clock timing error on the UWB symbol detection where the measurement waveform time delay also exists. Figure 4.10 shows the simulation results where the clock timing error is modeled as a random variable uniformly distributed within $[-\eta, \eta]$. The cases where $\eta = 6.25$ ps, 12.5 ps and 18.75 ps are investigated, which corresponds to 10%, 20% and 30% of the bit period, respectively. It is also assumed that the delay time of the circuit is $T_\tau = 3.125$ ps or 5% of the bit period. Again, it is observed that the UWB symbol detection performance degrades gracefully with larger clock timing errors. The performance of the UWB GLRT detector actually depends on the capability of the measurement waveforms to exploit the received signal energy. Moderate deviation from the ideal waveforms, however, does not significantly impair their ability to collect the received signal energy. Thus, the proposed UWB receivers are robust both to circuit delay

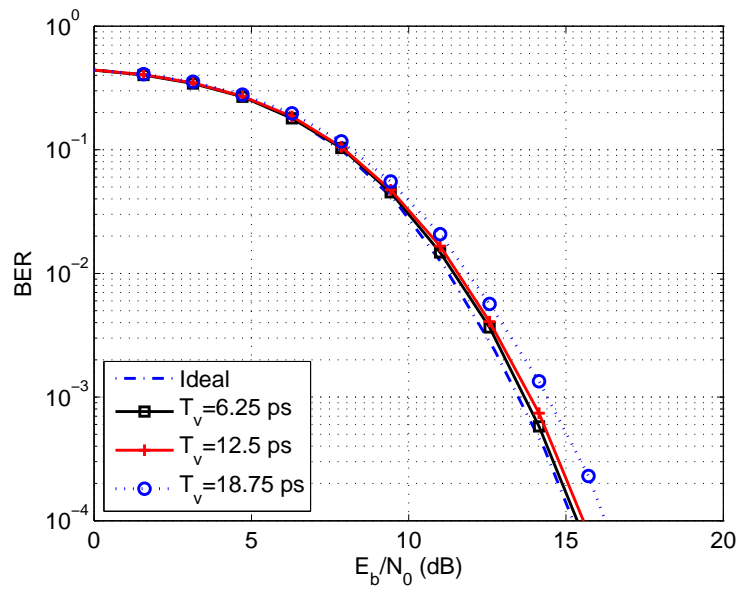


Figure 4.10: Performance of subspace compressive GLRT UWB detector under timing error and measurement waveforms delay.

and timing error.

Chapter 5

SUMMARY

In this thesis, we have expanded the research on compressed sensing in three directions. Firstly, an variable density sampling method is proposed for efficient natural image acquisition. By reducing the number of measurement needed, the proposed method leads to simple hardware implantation or less measurement time. Second, by exploring the structure of sparse signals, improved detection performance is achieved with less compressive measurements. The proposed detection method is robust against waveform quantization and is also robust against hardware failure. Third, CS based subspace compressive detection is applied to the design of novel I-UWB receivers, which avoids the use of ultra-fast ADCs. For simple implementations, quantized subspace measurement waveforms with two levels are proposed for practical UWB receivers. The proposed measurement scheme is shown to be robust to circuit nonidealities. In the following, we summarize our contributions and also point out future research directions.

5.1 Variable Density Sampling

We have proposed a family of variable density sampling patterns for compressive sampling of natural images in the DFT, DCT and ordered DHT domain. Compared with other compressive sampling scheme, the proposed sampling method is simple, fast and suitable for a wide range of applications such as in [2, 101].

The proposed variable density sampling patterns are based on a reliable statistical model of natural images in the sparse wavelet domain. Based on the subband

incoherent sampling, the proposed sampling patterns try to maximize the incoherence between the measurement ensemble and the sparsity basis. The proposed sampling pattern is generated from the variable density sampling function by blue noise dithering. The sampling pattern having blue noise characteristics are faithful to the variable density sampling function and leads to lower coherence. Compared with sampling methods that do not exploit any “*a priori*” information of natural images, the proposed sampling method has much better performance. Furthermore, the “*a priori*” information needed in this thesis is general and no extensive data training for parameter estimation is needed.

A significant difference of our proposed method from other sampling patterns that also exploit some “*a priori*” information of natural images is that our proposed sampling pattern, while retaining a simply form, is not heuristically constructed, but based on the statistical model drawn from empirical data. Thus, not only there is analytical justifications, but in practice, the proposed sampling pattern achieves much better performance than other sampling schemes. Furthermore, the proposed sampling method is robust to the “*a priori*” information we can obtain. The proposed metric, along with extensive simulation study, shows that the proposed sampling pattern leads to the least coherent interference. Simulations show that the proposed sampling scheme is effective for compressed sensing of images conforming to the proposed wavelet model.

Although this thesis focuses on the compressive sampling of 2D images, the method of sampling patterns can be extended to 1D and 3D signals if the corresponding statistical wavelet model still hold. We need to point out that if the underlying signals can be properly modeled by some other statistical model, then based on incoherent sampling principles, an appropriate sampling density function other than the sampling density functions proposed here can be designed. Future

research work includes designing sampling patterns for signals with a variety of sparsity models. Future research plan also includes exploiting the dependance between sparse components in image reconstruction to further improve the quality of the reconstructed image.

5.2 Compressive Detection for Sparse Signal

In this thesis, subspace compressive detection is proposed for the detection of sparse signals within the framework of compressed sensing. By exploiting the a *priori* information of signal subspace, subspace compressive detection greatly reduces the number of measurements needed for a desired detection performance. The subspace compressive measurement scheme first projects the received signal onto signal subspace and then projects it to a random basis with a reduced dimension. By projecting the received signal onto signal subspace, there is no loss of signal energy, but the noise is greatly reduced. By projecting the signal onto random basis, we obtain a measurement scheme which is universal for all signals residing in the same subspace. Although there is performance diversity with different realization of the random basis \mathbf{G} , the performance diversity is small if the number of measurements $M_s \gg 1$.

In this thesis, we focus on the detection of unknown sparse signals. The signal subspace information can be obtained by CS reconstruction algorithms from a reduced number of compressive measurements from training signals. It is shown that the number of measurements needed to extract sufficient information for detection purposes is far fewer than that requires for perfect signal reconstruction. The proposed subspace compressive detection is adaptive in the sense that the measurement scheme is adaptive to the signal structure. Furthermore, the design of the subspace compressive measurement scheme can be easily extended to the detection of unknown sparse signal with NBI mitigation.

Theoretic analysis of the performance for the proposed subspace compressive detectors is provided. Extensive simulations have illustrated the effectiveness of the proposed detectors. Compared with traditional GLRT detector and the compressive detector, the number of measurement needed is greatly reduced. The proposed detectors are suitable for applications where the number of measurements is stringent due to the hardware constraints. In this thesis, we also consider the practical hardware implementations and evaluate the effect of measurement waveform quantization on the detection performance. It is shown that the quantization have only limited effect on the detection performance. Even with quantized measurement waveform, subspace compressive detection still shows improvements over the compressive detection.

Future research will focus on the application of the proposed subspace compressive detectors to wide band signal detection. We will also try to design optimal quantization method for the subspace measurement matrix for the best detection performance.

5.3 Compressive Detection for Impulse Ultra-wideband

In this thesis, we apply CS based subspace compressive detection to the design of novel I-UWB receivers, which avoids the use of ultra-fast ADCs. With a limited number of noisy random measurements from the training symbols, the BPDN algorithm is employed to estimate the sparsity model of the I-UWB signals in multipath UWB channels. The proposed I-UWB receivers then exploit the sparsity of the I-UWB signals in the construction of a measurement projection matrix which is efficient at collecting the received UWB signal energy. Thus, satisfactory detection performance is achieved with far fewer measurements. Furthermore, for simple implementations, quantized subspace measurement waveforms with two levels are proposed for practical UWB receivers. The proposed measurement scheme is shown to be robust to circuit nonidealities.

Pilot assisted I-UWB signaling with DS-TH coding is proposed for the subspace compressive I-UWB communications. Theoretical analysis of the performance of the proposed subspace compressive I-UWB communication is provided. The roles of the key parameters in the proposed communication scheme, such as the number of measurements and the integration time are analyzed in detail. Compared with autocorrelation receivers, the proposed receiver can better exploit the repetition of the signaling and leads to better detection performance. Extensive simulation results show the effectiveness of the proposed communication schemes.

Future research will focus on the prototype implementation of the proposed I-UWB receivers. We will also extend the proposed subspace compressive I-UWB communications to multi-user access and narrowband interference mitigation. Optimal assignment of the signaling parameters will be investigated. Although only PAM signaling is considered in this thesis, the results can be readily extended to pulse position modulation (PPM).

BIBLIOGRAPHY

- [1] A. F. Molisch, K. Balakrishnan, C. Chong, S. Emami, A. Fort, J. Karedal, J. Kunisch, H. Schantz, U. Schuster, and K. Siwiak, "Ieee 802.15.4a channel model - final report," Tech. Rep., IEEE 802.15 TG4a, <http://www.ieee802.org/15/pub/TG4a.html>, 2006.
- [2] J. L. Paredes, G. R. Arce, and Z. Wang, "Ultra-wideband compressed sensing: channel estimation," *IEEE J. STSP*, vol. 1, no. 3, pp. 383–395, Oct. 2007.
- [3] M. Duarte, M. Davenport, D. Takhar, J. Laska, T. Sun, K. Kelly, and R. Baraniuk, "Single-pixel imaging via compressive sampling," *IEEE Signal Process. Mag.*, vol. 25, no. 2, pp. 83–91, Mar. 2008.
- [4] E. Candés and J. Romberg, "Practical signal recovery from random projections," in *Proc. Wavelet Applications in Signal and Image Processing XI, SPIE*, 2004.
- [5] Emmanuel Candés, "Compressive sampling," *Int. Congress of Mathematics*, vol. 3, pp. 1433–1452, 2006.
- [6] E. J. Candes and M. B. Wakin, "An introduction to compressive sampling," *IEEE Signal Process. Mag.*, vol. 25, no. 2, pp. 21–30, Mar. 2008.
- [7] D.L Donoho and X. Huo, "Uncertainty principles and ideal atomic decomposition," *IEEE Trans. Inform. Theory*, vol. 47, no. 7, pp. 2845–2862, Nov. 2001.
- [8] E. Candés, J. Romberg, and T. Tao, "Stable signal recovery from incomplete and inaccurate measurements," *Comm. Pure Appl. Math.*, vol. 59, no. 8, pp. 1207–1223, Aug. 2006.
- [9] D. Donoho, "Compressed sensing," *IEEE Trans. Inf. Theory*, vol. 52, no. 4, pp. 1289–1306, Apr. 2006.
- [10] J. Lindenstrauss W. Johnson, "Extensions of lipschitz maps into a hilbert space," *Contemp. Math*, vol. 26, pp. 186–206, 1984.

- [11] R. Baraniuk, M. Davenport, R. DeVore, and M. Wakin, “A simple proof of the restricted isometry property for random matrices,” *Constructive Approximation*, vol. 28, no. 3, pp. 253–263, Dec. 2008.
- [12] E. Candés, J. Romberg, and T. Tao, “Robust uncertainty principles: Exact signal reconstruction from highly incomplete frequency information,” *IEEE Trans. Inf. Theory*, vol. 52, no. 2, pp. 489–509, Feb. 2006.
- [13] S. S. Chen, D. L. Donoho, and M. A. Saunders, “Atomic decomposition by Basis Pursuit,” *SIAM SCI. Comput.*, vol. 20, no. 1, pp. 33–61, Aug. 1998.
- [14] E. Candés and T. Tao, “Decoding by linear programming,” *IEEE Trans. Inf. Theory*, vol. 51, no. 12, pp. 4203–4215, Dec. 2005.
- [15] M. Duarte, M. Davenport, M. Wakin, and R. Baraniuk, “Sparse signal detection from incoherent projections,” in *Proc. IEEE ICASSP*, Toulouse, France, May 2006.
- [16] J. Tropp and A. Gilbert, “Signal recovery from random measurements via orthogonal matching pursuit,” *IEEE Trans. Inf. Theory*, vol. 53, no. 12, pp. 4655–4666, Dec. 2007.
- [17] M. Duarte, M. Wakin, and R. Baraniuk, “Fast reconstruction of piecewise smooth signals from random projections,” in *Proc. SPARS Workshop*, Nov. 2005.
- [18] S. J. Kim, K. Koh, M. Lustig, S. Boyd, and D. Gorinevsky, “A method for large-scale ℓ_1 -regularized least squares,” *IEEE J. STSP*, vol. 1, no. 4, pp. 606–617, Dec. 2007.
- [19] E. Candés and J. Romberg, “Sparsity and incoherence in compressive sampling,” *Inverse Problems*, vol. 23, no. 3, pp. 969–985, 2007.
- [20] M. Elad, “Optimized projections for compressed sensing,” *IEEE Trans. Signal Process.*, vol. 55, no. 12, pp. 5695–5702, Dec. 2007.
- [21] L. Gan, T. T. Do, and T. D. Tran, “Fast compressive imaging using scrambled block Hadamard ensemble,” Preprint, 2008.
- [22] M. Lustig, D. Donoho, and J. M. Pauly, “Sparse MRI: The application of compressed sensing for rapid MR imaging,” *Mag. Reson. in Med.*, vol. 58, no. 6, pp. 1182–1195, Dec. 2007.
- [23] C. Schröder, P. Börnert, and B. Aldefeld, “Spatial excitation using variable-density spiral trajectories,” *J. Mag. Reson. Imag.*, vol. 18, no. 1, pp. 136–141, 2003.

- [24] Y. Q. Shi and H. Sun, *Image and video compression for multimedia engineering*, CRC press, 1999.
- [25] M. Davenport, M. Wakin, and R. Baraniuk, “Detection and estimation with compressive measurements,” Tech. Rep., Dept. of ECE, Rice University, 2006.
- [26] M. Davenport, M. Duarte, M. Wakin, J. Laska, D. Takhar, K. Kelly, and R. Baraniuk, “The smashed filter for compressive classification and target recognition,” in *Proc. Comput. Imag. V at SPIE Electron. Imag.*, San Jose, CA, Jan. 2007.
- [27] J. Haupt and R. D. Nowak, “Compressive sampling for signal detection,” in *Proc. IEEE ICASSP*, Honolulu, HI, Apr. 2007.
- [28] M. Duarte, M. Davenport, M. Wakin, J. Laska, D. Takhar, K. Kelly, and R. Baraniuk, “Multiscale random projections for compressive classification,” in *Proc. IEEE ICIP*, San Antonio, TX, Sept. 2007.
- [29] S. M. Kay, *Fundamentals of Statistical Signal Processing-Detection Theory*, vol. 2, Prentice Hall PTR, 1998.
- [30] L. L. Scharf and B. Friedlander, “Matched subspace detectors,” *IEEE Trans. Signal Process.*, vol. 42, no. 8, pp. 2146–2157, Aug. 1994.
- [31] Z. Wang, G. R. Arce, and B. M. Sadler, “Subspace compressive detection for sparse signals,” in *Proc. ICASSP*, Las Vegas, NV, Mar. 2008.
- [32] Z. Wang and G. R. Arce, “Variable density compressed image sampling,” *IEEE Trans. Image Process*, to appear.
- [33] Z. Yu, S. Hoyos, and B. M. Sadler, “Mixed-signal parallel compressed sensing and reception for cognitive radio,” in *Proc. IEEE ICASSP*, Las Vegas, NV, Mar. 2008.
- [34] A. K. Fletcher, S. Rangan, and V. K. Goyal, “Necessary and sufficient conditions on sparsity pattern recovery,” Submitted to *IEEE Trans. Information Theory*, available at: <http://arxiv.org/abs/0804.1839>.
- [35] M. Akcakaya and V. Tarokh, “Noisy compressive sampling limits in linear and sublinear regimes,” in *Proc. Conf. Inform. Sci. & Sys.*, Princeton, NJ, Mar. 2008.
- [36] Z. Wang, G. R. Arce, B. M. Sadler, J. L. Paredes, and S. Hoyos an Z. Yu, “Compressed UWB signal detection with narrowband interference mitigation,” in *Proc. ICUWB*, Hannover, Germany, Sept. 2008.

- [37] B. Friedlander and B. Porat, “Performance analysis of transient detectors based on a class of linear data transforms,” *IEEE Trans. Inf. Theory*, vol. 38, no. 2, pp. 665–673, Mar. 1992.
- [38] Jeffrey H. Reed, *An Introduction to Ultra Wideband Communication Systems*, Prentice Hall Communications Engineering and Emerging Technologies Series. Prentice Hall, 2005.
- [39] M. Z. Win and R. A. Scholtz, “Ultra-wide bandwidth time-hopping spread-spectrum impulse radio for wireless multiple-access communications,” *IEEE Trans. Commun.*, vol. 48, no. 4, pp. 679–691, Apr. 2000.
- [40] L. Yang and G. B. Giannakis, “Ultra-wideband communications: An idea whose time has come,” *IEEE Signal Process. Mag.*, vol. 21, no. 6, pp. 26–54, Nov. 2004.
- [41] V. Lottici, A. D’Andrea, and U. Mengali, “Channel estimation for ultra-wideband communications,” *IEEE J. selected areas commun.*, vol. 20, no. 9, pp. 1638–1645, Dec. 2002.
- [42] A. F. Molisch, “Ultrawideband propagation channels-theory, measurement, and modeling,” *IEEE Trans. Veh. Tech.*, vol. 54, no. 5, pp. 1528–1545, Sept. 2005.
- [43] D. Cassioli, M. Z. Win, F. Vatalaro, and A. F. Molisch, “Low complexity Rake receivers in Ultra-wideband channels,” *IEEE Trans. Wireless Commun.*, vol. 6, no. 4, pp. 1265–1275, Apr. 2007.
- [44] R. T. Hoctor and H. W. Tomlinson, “Delay-hopped transmitted-reference RF communications,” in *Proc. UWBST*, Baltimore, MD, May 2002, pp. 265–270.
- [45] Y. Chao and R. A. Scholtz, “Ultra-wideband transmitted reference systems,” *IEEE Trans. Veh. Tech.*, vol. 54, no. 5, pp. 1556–1569, Sep. 2005.
- [46] J. D. Choi and W. E. Stark, “Performance of ultra-wideband communications with suboptimal receivers in multipath channels,” *IEEE JSAC*, vol. 20, no. 9, pp. 1754–1766, Dec. 2002.
- [47] D. L. Goeckel and Q. Zhang, “Slightly frequency-shifted reference ultra-wideband UWB radio: TR-UWB without the delay element,” in *Proc. MIL-COM*, Atlantic City, NJ, Oct. 2005.
- [48] W. Gifford and M. Win, “On transmitted-reference UWB communications,” in *Proc. Asilomar Conf. Signals Systems and Computers*, Pacific Grove, CA, Nov. 2004.

- [49] Z. Wang, G. R. Arce, J. L. Paredes, and B. M. Sadler, “Compressed detection for Ultra-wideband impulsive radio,” in *Proc. 8th IEEE Intl. Workshop SPAWC*, Helsinki, Finland, Jun. 2007.
- [50] X. Wu, P. Palmers, and M. S. J. Steyaert, “A 130 nm CMOS 6-bit full Nyquist 3 GS/s DAC,” *IEEE J. Solid-State Circuits*, vol. 43, no. 11, pp. 2396–2403, Nov. 2008.
- [51] P. Vary and R. Martin, *Digital Speech Transmission Enhancement, Coding and Error Concealment*, WILEY, 2005.
- [52] M. Mishali and Y. C. Eldar, “From theory to practice: Subnyquist sampling of sparse wideband analog signals.,” Preprint, http://arxiv.org/PS_cache/arxiv/pdf/0902/0902.4291v2.pdf, 2009.
- [53] J. Laska, S. Kirolos, M. Duarte, T. Ragheb, R. Baraniuk, and Y. Massoud, “Theory and implementation of an analog-to-information converter using random demodulation,” in *Proc. IEEE ISCAS*, New Orleans, LA, May 2007.
- [54] S. Hoyos and B. M. Sadler, “Ultra-wideband analog-to-digital conversion via signal expansion,” *IEEE Trans. Veh. Technol.*, vol. 54, no. 5, pp. 1609–1622, Sep. 2005.
- [55] S. Hoyos, B. M. Sadler, and G. R. Arce, “Broadband multicarrier communication receiver based on analog to digital conversion in the frequency domain,” *IEEE Trans. Wireless Commun.*, vol. 5, no. 3, pp. 652–661, Mar. 2006.
- [56] Z. Yu, S. Hoyos, and B. M. Sadler, “Mixed-signal parallel compressed sensing and reception for cognitive radio,” in *Proc. IEEE ICASSP*, Las Vegas, NV, Mar. 2008.
- [57] S. Mallat, *A Wavelet tour of signal processing*, Academic Press, 1998.
- [58] S. G. Chang, B. Yu, and M. Vetterli, “Adaptive wavelet thresholding for image denoising and compression,” *IEEE Tran. Image Process.*, vol. 9, no. 9, pp. 1532–1546, Sep. 2000.
- [59] J. K. Romberg, H. Choi, and R. G. Baraniuk, “Bayesian tree-structured image modeling using wavelet-domain hidden Markov models,” *IEEE Trans. Image Process.*, vol. 10, no. 7, pp. 1056–1068, Jul. 2001.
- [60] J. L. Prince and J. M. Links, *Medical imaging signals and systems*, Pearson Prentice Hall, 2006.

- [61] S-J Kim M. Lustig and J. M. Pauly, “A fast method for designing time-optimal gradient waveforms for arbitrary k-space trajectories,” *IEEE TMI*, vol. 27, no. 6, pp. 866–873, Jun. 2008.
- [62] N. P. Pitsianis, D. J. Brady, A. Portnoy, X. Sun, T. Suleski, M. A. Fiddy, M. R. Feldman, and R. D. Tekolste, “Compressive imaging sensors,” in *Proc. SPIE*, 1999, vol. 6232.
- [63] J. Wang and W. T. Tung, “Narrowband interference suppression in time-hopping impulse radio ultra-wideband communications,” *IEEE Trans. Commun.*, vol. 54, no. 6, pp. 1057–1067, Jun. 2006.
- [64] Y. D. Alemseged and K. Witrisal, “Modeling and mitigation of narrowband interference for transmitted-reference UWB systems,” *IEEE J. STSP*, vol. 1, no. 3, pp. 456–469, Oct. 2007.
- [65] Z. Wang, G. R. Arce, B. M. Sadler, J. L. Paredes, and X. Ma, “Compressed detection for pilot assisted ultra-wideband impulse radio,” in *Proc. ICUWB*, Singapore, Sept. 2007.
- [66] John G. Proakis, *Digital Communications*, Mc Graw Hill, 4 edition, 2000.
- [67] X. Wang and H. V. Poor, “Blind equalization and multiuser detection in dispersive CDMA channels,” *IEEE Trans. Commun.*, vol. 46, no. 1, pp. 91–103, Jan. 1998.
- [68] M. A. Davenport, P. T. Boufounos, and R. G. Baraniuk, “Compressive domain interference cancellation,” in *Proc. SPARS*, Saint-Malo, France, Apr. 2009.
- [69] T. K. Moon and W. C. Stirling, *Mathematical methods and algorithms for signal processing*, Prentice Hall, 2000.
- [70] T. F. Ayoub and A.M. Haimovich, “Modified GLRT signal detection algorithm,” *IEEE Trans. Aerospace and Electronic Systems*, vol. 36, no. 3, pp. 810–818, Jul. 2000.
- [71] Shawn Kraut, Louis L. Scharf, and L. Todd McWhorter, “Adaptive subspace detectors,” *IEEE Trans. Signal Process.*, vol. 49, no. 1, pp. 1–16, Jan 2001.
- [72] R. S. Raghavan, N. Pulsone, and D. J. McLaughlin, “Performance of the GLRT for adaptive vector subspace detection,” *IEEE Trans. on Aerospace and Electronic Systems*, vol. 32, no. 4, pp. 1473–1487, Oct. 1996.
- [73] E. J. Kelly, “An adaptive detection algorithm,” *IEEE Trans. Aerospace and Electronic Systems*, vol. AES-22, pp. 115–127, Jan 1986.

- [74] S. Mallat and Z. Zhang, “Matching pursuits with time-frequency dictionaries,” *IEEE Trans. Signal Process.*, vol. 41, no. 12, pp. 3397–3415, Dec 1993.
- [75] Z. Wang, G. R. Arce, B. M. Sadler, and J. L. Paredes, “Colored random projections for compressed sensing,” in *Proc. IEEE ICASSP*, Honolulu, HI, Apr. 2007.
- [76] J. Haupt and R. Nowak, “Signal reconstruction from noisy random projections,” *IEEE Trans. Inf. Theory*, vol. 52, no. 9, pp. 4036–4048, Sept. 2006.
- [77] Z. Xu and B. M. Sadler, “Multiuser transmitted reference ultra-wideband communication systems,” *IEEE JSAC*, vol. 24, no. 4, pp. 766–772, Apr. 2006.
- [78] P. Liu, Z. Xu, and B. M. Sadler, “Narrowband interference suppression of an MTR-UWB transceiver,” in *Proc. IEEE Radio and Wireless Symposium*, San Diego, CA, Jan. 2006.
- [79] T. Q. S. Quek and M. Z. Win, “Analysis of UWB transmitted-reference communication systems in dense multipath channels,” *IEEE J. Inf. Theory*, vol. 23, no. 9, pp. 1863–1874, Sep. 2005.
- [80] R. J. Cramer, R. A. Scholtz, and M. Z. Win, “Evaluation of an ultra-wideband propagation channel,” *IEEE Trans. Antennas Propag.*, vol. 50, no. 5, pp. 561–570, May 2002.
- [81] L. Yang and G. B. Giannakis, “Optimal pilot waveform assisted modulation for ultrawideband communications,” *IEEE Trans. Wireless Commun.*, vol. 3, no. 4, pp. 1236–1249, Jul. 2004.
- [82] S. Dubouloz, M. Pelissier, B. Denis, M. Sambuq, and L. Ouvry, “Energy characteristics of UWB channel models applied to system design,” in *Proc. ICUWB*, ETH Zurich, Switzerland, Sept. 2005.
- [83] M. Pausini and G. J. M. Janssen, “On the narrowband interference in transmitted reference UWB receivers,” in *Proc. ICUWB*, Sept. 2005, pp. 571–575.
- [84] Y. Chao, “Optimal integration time analysis for ultra-wideband correlation receivers,” in *Proc. Asilomar Conference on Signals, Systems, and Computers*, Pacific Grove, CA, Nov. 2004.
- [85] D. Kurita and K. Li, “Super uwb bandpass filter,” *IEICE Electron. Express*, vol. 4, no. 9, pp. 300–305, May 2007.
- [86] M. Tsai and H. Wang, “A 0.3-25-ghz ultra-wideband mixer using commercial 0.18-um CMOS technology,” *IEEE Microw. Wireless Compon. Lett.*, vol. 14, no. 11, pp. 522–524, Nov. 2004.

- [87] C. Kienmayer, M. Tiebout, W. Simburger, and A. L. Scholtz, "A low-power low-voltage nmos bulk-mixer with 20 GHz bandwidth in 90 nm CMOS," in *Proc. IEEE ISCAS*, Vancouver, Canada, May 2004.
- [88] B. Razavi, "A 60-GHz CMOS receiver front-end," *IEEE J. Solid-State Circuits*, vol. 41, no. 1, pp. 17–22, Jan. 2006.
- [89] C. Kuo, B. Huang, C. Kuo, K. Lin, and H. Wang, "A 1035 GHz low power bulk-driven mixer using 0.13 μ m CMOS process," *IEEE Microw. Wireless Compon. Lett.*, vol. 18, no. 7, pp. 455–457, July 2008.
- [90] E. Laskin and S. P. Voinigescu, "A 60 mW per Lane, 4 \times 23-Gb/s 2⁷-1 prbs generator," *IEEE J. Solid-State Circuits*, vol. 41, no. 10, pp. 2198–2208, Oct. 2006.
- [91] J. Azana, N. K. Berger, B. Levit, and B. Fischer, "Broadband arbitrary waveform generation based on microwave frequency upshifting in optical fibers," *J. Lightwave Tech.*, vol. 24, no. 7, pp. 2663–2675, Jul. 2006.
- [92] M. Abtahi, J. Magne, M. Mirshafiei, L. A. Rusch, and S. LaRochelle, "Generation of power-efficient FCC-complaint UWB waveforms using FBGs: analysis and experiment," *J. Lightweight Tech.*, vol. 26, no. 5, pp. 628–635, Mar. 2008.
- [93] W. Jiang et al., "A monolithic InP-based photonic integrated circuit for optical arbitrary waveform generation," in *Proc. OFC/NFOEC*, San Diego, CA, Feb. 2008.
- [94] X. Luo, L. Yang, and G. B. Giannakis, "Designing optimal pulse-shapers for ultra-wideband radios," *J. Comm. Networks*, vol. 5, no. 4, pp. 344–353, Dec. 2003.
- [95] G. Lu, P. Spasojevic, and L. Greenstein, "Antenna and pulse designs for meeting UWB spectrum density requirements," in *Proc. IEEE Conf. UWB System. Tech.*, Reston, VA, Nov. 2003.
- [96] S. Ciolino, M. Ghavami, and H. Aghvami, "Wavelet-based ultra wideband pulse generator circuits," *IET Commun.*, vol. 2, no. 5, pp. 642–649, May 2008.
- [97] S. Hoyos, B. M. Sadler, and G. R. Arce, "Monobit digital receivers for ultrawideband communications," *IEEE Trans. Wireless Commun.*, vol. 4, pp. 1337–1344, Jul. 2005.

- [98] A. A. Saleh and R. A. Valenzuela, “A statistical model for indoor multipath propagation,” *IEEE J. Selected Areas Commun.*, vol. 5, no. 2, pp. 128–137, Feb. 1987.
- [99] S. Hoyos and B. M. Sadler, “Frequency-domain implementation of the transmitted-reference ultra-wideband receiver,” *IEEE Trans. Microwave and Tech.*, vol. 54, no. 4, pp. 1745–1753, Apr. 2006.
- [100] R. J. Baker, H. W. Li, and D. D. Boyce, *CMOS circuit design, layout, and simulation*, IEEE PRESS, 1998.
- [101] P. Ye, J. L. Paredes, G. R. Arce, Y. Wu, C. Chen, and D. W. Prather, “Compressive confocal microscopy,” in *Proc. IEEE ICASSP*, Taiwan, 2009.